UNIVERSITÀ DEGLI STUDI DI MILANO

PhD in Biomolecular Pharmacological Sciences, Experimental and Clinical – XXXVI cycle

Dipartimento di Scienze Farmacologiche e Biomolecolari
"Rodolfo Paoletti"

CROSS-DISEASE ANALYSIS OF MOLECULAR AND CELLULAR MECHANISMS IN KIF5A-ASSOCIATED NEURODEGENERATIVE DISORDERS

SSD: BIO/13

PhD candidate:

Marta Cozzi

R12917

Supervisor: Prof. Angelo Poletti

Co-supervisor: Dr. James N. Sleigh

Coordinator: Prof. Giuseppe Danilo Norata

Academic Year 2022/2023

Table of contents

List of abbreviations

ACTR: actin-related protein

AD: Alzheimer's disease

ALS: amyotrophic lateral sclerosis

AMC: 7-amino-4-methyl coumarin

AMPA: α-amino-3-hydroxy-5-methylisoxazole-4-propionate

APP: amyloid precursor protein

ARC: activity-regulated cytoskeleton-associated protein

ATG: autophagy-related

BAG: Bcl2-associated athanogene co-chaperone

BDNF: brain-derived neurotrophic factor

BSA: bovine serum albumin

C9ORF72: chromosome 9 open reading frame 72

CAMK2α: Ca^{2+}/calmodulin-dependent kinase 2α

CAPZ: capping actin protein

CASA: chaperone-assisted selective autophagy

ChAT: choline acetyltransferase

CHX: cycloheximide

CMA: chaperone-mediated autophagy

CMT: Charcot-Marie-Tooth disease

D: day

DAPI: 4',6-diamidino-2-phenylindole

DCTN: dynactin subunit

DISC1: disrupted in schizophrenia 1

DMEM: Dulbecco's modified Eagle medium

DNAI: dynein axonemal intermediate chain

DPYSL2/CRMP2: dihydropyrimidinase like 2

DTT: dithiothreitol

DYNC1H1: dynein cytoplasmic 1 heavy chain 1

DYNLL: dynein light chain LC8-type

EF-1α: elongation factor-1α

ER: endoplasmic reticulum

ESCRT: endosomal sorting complex required for transport

EV: empty vector

fALS: familial ALS

FBS: foetal bovine serum

FMR1/FMRP: fragile X messenger ribonucleoprotein 1

FRAP: fluorescence recovery after photobleaching

FTD: frontotemporal dementia

G3BP1: G3BP stress granule assembly factor 1

GABA: γ-aminobutyric acid

$GABA_AR$: GABA type A receptor

GABARAP: $GABA_AR$-associated protein

GABARAPL: $GABA_AR$-associated protein-like

GAP43: growth associated protein 43

GAPDH: glyceraldehyde-3-phosphate dehydrogenase

GluR2: glutamate receptor 2

GOF: gain of function

GRIP1: glutamate receptor-interacting protein 1

GSK3β: glycogen synthase kinase 3β

HAP1: huntingtin-associated protein 1

HDAC6: histone deacetylase 6

HSP: heat-shock protein

i^3: integrated, inducible, isogenic

IAK: isoleucine-alanine-lysine

IM: induction medium

iPSC: induced pluripotent stem cell

ISL1: ISL LIM homeobox 1

KD: knock-down

KFERQ: lysine-phenylalanine-glutamate-arginine-glutamine

Khc: kinesin heavy chain

KIF: kinesin family member

KLC: kinesin light chain

KO: knock-out

LAMP2A: lysosome-associated membrane protein type 2A

LHX3: LIM homeobox 3
LIR: MAP1LC3-interacting region
LLPS: liquid-liquid phase separation
LMN: lower motor neuron
LOF: loss of function
LRP8/APOER2: LDL receptor related protein 8
MAP: microtubule-associated protein
MAP1LC3: microtubule-associated protein 1A/1B light chain 3
MAPK: mitogen-activated protein kinase
MAPK8IP3/JIP3: mitogen-activated protein kinase interacting protein 3
MFC: microfluidic chamber
MG132: Z-Leu-Leu-Leu
MM: motor neuron medium
MND: motor neuron disease
MNX1/HB9: motor neuron and pancreas homeobox 1
MTOC: microtubule-organising centre
NDEL1: nudE neurodevelopment protein 1 like 1
NEAA: non-essential amino acids
NEIMY: neonatal intractable myoclonus
NF: neurofilament
NF-H, NF-M, NF-L: neurofilament heavy, medium, and light subunits
NGN2: neurogenin 2
NH_4Cl: ammonium chloride
NMDA: *N*-methyl-*D*-aspartate
NP-40: Nonidet P-40
NTRK2/TRKB: neurotrophic receptor tyrosine kinase 2
PB1: Phox and Bem1p-1 domain
PBS: phosphate-buffered saline
PBS-T: PBS-Tween 20
Pen/Strep: penicillin/streptomycin
PGK: phosphoglycerate kinase
PI3KC3: phosphatidylinositol 3-kinase catalytic subunit type 3
PQC: protein quality control
RAB: Ras oncogene family member
RANBP2: RAN binding protein 2
RB1CC1/ATG17: RB1 inducible coiled-coil 1
RIPA: radioimmunoprecipitation assay
RNP: ribonucleoprotein
RHOT/Miro: Ras homology family member T
RT: room temperature
sALS: sporadic ALS
SBMA: spinal and bulbar muscular atrophy
SDS: sodium dodecylsulphate
SFPQ: splicings factor proline/glutamine-rich
SG: stress granule
SNAP: synaptosome-associated protein
SNARE: SNAP receptor
SPG: spastic paraplegia
SQSTM1/p62: sequestosome 1/p62
ST13/HIP: ST13 HSP70-interacting protein
STIP1/HOP: stress-induced phosphoprotein 1
STUB1: STIP1 and U-box containing protein 1
TBS-T: Tris-buffered saline with Tween 20
TDP-43: TAR DNA-binding protein 43
TFEB: transcription factor EB
TIA1: TIA1 cytotoxic granule associated RNA binding protein
TMT: trimethyltin chloride
TPR: tetratricopeptide repeat
TRAK/Milton: trafficking kinesin protein
γTuRC: γ-tubulin ring complex
UBA: ubiquitin-associated domain
ULK1: unc-51–like kinase 1
UPS: ubiquitin-proteasome system
WT: wild type
ZNRF2: zinc and ring finger 2

Abstract

Kinesin family member 5A (KIF5A) is a neuron-specific kinesin involved in anterograde axonal transport. Heterozygous variants within the three KIF5A domains are linked to distinct neurodegenerative or neurodevelopmental disorders. Missense and nonsense mutations in KIF5A motor and stalk domains are associated with hereditary spastic paraplegia type 10 (SPG10) and axonal Charcot-Marie-Tooth disease (CMT), while frameshifts in its tail are linked to amyotrophic lateral sclerosis (ALS) and neonatal intractable myoclonus (NEIMY). To date, the molecular bases underpinning such clinical heterogeneity have been only partially elucidated, while the wide range of *KIF5A* mutations prompts the need to compare the molecular mechanisms of different variants. Therefore, in this thesis five key KIF5A mutants (the novel R17Q, R280C, R864*, N999Vfs*40, and C975Vfs*73) covering the whole spectrum of *KIF5A*-related pathologies were functionally characterised in comparison to wild type (WT) KIF5A in a homogeneous experimental setting.

Overexpression in NSC-34 motor neuron-like cells resulted in an abnormal peripheral distribution for the CMT-linked R864* and the ALS-associated N999Vfs*40 KIF5A. Such aberrant localisation is due to an impairment in kinesin autoinhibition resulting from the loss or the modification of KIF5A tail domain, respectively. Moreover, expression of either R864* or N999Vfs*40 KIF5A altered mitochondrial distribution, suggesting the disruption of KIF5A transport competence. The N999Vfs*40 KIF5A mutant also formed sequestosome 1/p62 (SQSTM1/p62)-positive detergent-insoluble inclusions sequestering WT KIF5A, indicating a gain of toxic function.

Cycloheximide chase assays in SH-SY5Y neuroblastoma cells demonstrated a shorter half-life for the SPG10-related R17Q and ALS-related N999Vfs*40 mutants compared to WT KIF5A and proteasomal blockage led to their accumulation into detergent-insoluble inclusions, demonstrating that these mutants are degraded by the ubiquitin-proteasome system and that their aggregation may depend on proteostasis impairment. Of note, R280C and N999Vfs*40 KIF5A both competed for degradation with proteasomal substrates. Interestingly, the aberrant biochemical behaviour of the ALS mutant N999Vfs*40 KIF5A was more severely recapitulated by the NEIMY mutant C975Vfs*73 KIF5A, which shares the last portion of its abnormal C-terminal tail yet causes a neurodevelopmental disorder, on the opposite end of *KIF5A*-linked phenotypic spectrum compared to ALS.

Finally, integrated, inducible, isogenic lower motor neurons (i^3LMNs) were transduced with lentiviral particles harbouring WT or mutant KIF5A to establish a model to evaluate the impact of *KIF5A* mutations on bidirectional axonal trafficking in a more physiologically relevant context than immortalised cells. Unfortunately, this strategy was ineffective most likely due to the autoregulation of mutant KIF5A protein levels in i^3LMNs.

Altogether, data collected in this thesis support the pathogenicity of newly identified KIF5A mutants, shed light on previously uncharacterised aberrant behaviours of recurrent variants, and demonstrate that both unique and shared mechanisms are implicated in the pathogenesis of *KIF5A*-related neurodegenerative and neurodevelopmental diseases.

Riassunto

Kinesin family member 5A (KIF5A) è una chinesina espressa esclusivamente a livello neuronale e coinvolta nel trasporto assonale anterogrado. Mutazioni a carico del gene *KIF5A* causano diverse malattie neurodegenerative o del neurosviluppo a seconda di quale dei tre domini della proteina corrispondente viene colpito. Nel dettaglio, mutazioni missenso o nonsenso nelle sequenze codificanti il dominio motorio e il dominio di dimerizzazione di KIF5A sono associate alla paraparesi spastica ereditaria di tipo 10 (SPG10) e alla forma assonale della malattia di Charcot-Marie-Tooth (CMT), mentre mutazioni *frameshift* nella sequenza corrispondente al dominio di coda di KIF5A causano sclerosi laterale amiotrofica (ALS) o mioclono neonatale intrattabile (NEIMY). Ad oggi, i meccanismi molecolari alla base dell'eterogeneità clinica associata alle mutazioni di *KIF5A* sono noti solo in parte e non è ancora chiaro per quali ragioni mutazioni a carico del medesimo gene diano origine a patologie diverse fra loro. Per far luce su questi aspetti, in questa tesi sono state analizzate le caratteristiche biochimiche di cinque forme mutate di KIF5A (R17Q, di recente identificazione; R280C; R864*; N999Vfs*40; C975Vfs*73) che sono state poste a confronto tra loro e con la proteina *wild type* (WT) nel medesimo modello sperimentale, al fine di identificare potenziali meccanismi patogenetici associati alle mutazioni di *KIF5A* coprendo tutto lo spettro di condizioni ad esse legate. L'espressione delle forme mutate di KIF5A in cellule simil-motoneuronali NSC-34 ha rivelato l'alterata distribuzione intracellulare di KIF5A R864*, associata a CMT, e KIF5A N999Vfs*40, legata ad ALS. Infatti, esse localizzano prevalentemente nei prolungamenti cellulari a causa della perdita del meccanismo di autoinibizione caratteristico delle chinesine della famiglia di KIF5A. Nel caso di KIF5A R864* l'autoinibizione viene persa per la completa delezione del dominio di coda, mentre per quanto riguarda KIF5A N999Vfs*40 ciò dipende dalla modifica della sequenza di tale dominio prodotta dalla mutazione *frameshift*. Inoltre, l'espressione di KIF5A R864* o KIF5A N999Vfs*40 provoca un'alterazione della distribuzione mitocondriale che suggerisce la perdita della capacità di trasporto da parte di queste due forme mutate di KIF5A. Infine, KIF5A N999Vfs*40 forma inclusioni insolubili positive per il recettore autofagico *sequestosome 1/p62* (SQSTM1/p62) e in grado di sequestrare parzialmente KIF5A WT, suggerendo l'acquisto di una funzione neurotossica come conseguenza della mutazione.

In cellule di neuroblastoma umano SH-SY5Y, KIF5A R17Q, associata a SPG10, e KIF5A N999Vfs*40 sono risultate caratterizzate da un'emivita più breve rispetto alla proteina WT ed il blocco del proteasoma ne ha causato l'accumulo in inclusioni insolubili. Questi dati indicano che le forme mutate KIF5A R17Q e N999Vfs*40 sono degradate principalmente attraverso il sistema ubiquitina-proteasoma e che, in caso di difetti a carico di quest'ultimo, i due mutanti potrebbero andare incontro ad aggregazione, provocando tossicità. Inoltre, KIF5A R280C, l'altra forma mutata in studio

associata a SPG10, e KIF5A N999Vfs*40 hanno mostrato competizione con substrati specifici del proteasoma per la degradazione. Successivamente, è stata posta particolare attenzione sul confronto tra la forma mutata causativa di ALS KIF5A N999Vfs*40 e KIF5A C975Vfs*73, associata a NEIMY, dal momento che esse condividono la porzione C-terminale della loro coda mutata, ma causano malattie agli estremi opposti nello spettro di patologie legate a *KIF5A*. Le analisi svolte hanno evidenziato che KIF5A C975Vfs*73 mostra un comportamento aberrante analogo a quello di KIF5A N999Vfs*40 ma caratterizzato da un maggior grado di severità, coerentemente con la sua associazione con una patologia del neurosviluppo.

Da ultimo, per ottenere un modello più rilevante rispetto alle cellule immortalizzate per lo studio dell'impatto delle mutazioni di *KIF5A* sul trasporto assonale, cellule staminali pluripotenti indotte geneticamente modificate per essere differenziare rapidamente a motoneuroni inferiori (i^3LMNs) sono state trasdotte con vettori lentivirali codificanti KIF5A WT o mutata. Questa strategia si è però rivelata inefficace, probabilmente a causa di un meccanismo di autoregolazione dei livelli proteici di KIF5A nelle cellule i^3LMNs.

Nel loro complesso, i dati raccolti in questa tesi supportano la patogenicità di nuove varianti di *KIF5A*, identificano nuove caratteristiche aberranti di varianti note e dimostrano l'esistenza di meccanismi patogenetici sia condivisi che univoci alla base delle patologie neurodegenerative e del neurosviluppo legate a *KIF5A*.

SECTION 1 – KIF5A-linked pathways to neurodegeneration

Background

Neuronal transport

In eukaryotic cells, molecules and supramolecular complexes constantly move across the cytoplasm to ensure proper cell homeostasis and organisation. While small molecules can reach their intracellular destination through simple diffusion, larger cellular components such as protein complexes, vesicles, and organelles must be assisted in their movements by motor proteins, which move cargoes along cytoskeletal tracks. The intracellular transport mechanisms relying on molecular motors are finely regulated both spatially and temporally and are highly conserved across evolution[1].

Neurons display a highly polarised cellular anatomy. Short protrusions that originate from the cell body, named dendrites, and a single extension that emerge from the growth cone, named axon, form the complex neuronal arborisation, whose morphology needs to be preserved to ensure neuronal functionality. In this respect, axons are particularly delicate since they can extend up to one metre in length in the human body. Based on these features, intracellular transport plays an essential role in axonal functions by ensuring the proper distribution of cellular components across an extremely polarised system. Bidirectional trafficking of proteins, ribonucleoprotein (RNP) granules, vesicles, and organelles between the cell body and the axon tip occurs along microtubule tracks. Newly synthesised components that need to be moved in the anterograde direction, towards the growth cone or axonal synapses, are transported by kinesins, while cargoes travelling along the retrograde route depend on cytoplasmic dynein for trafficking. Both anterograde and retrograde transport processes are fuelled by ATP hydrolysis and might require adaptor proteins to interact with cargoes[2,3].

Neuronal cytoskeleton

The cytoskeleton is a structurally and functionally interconnected network of tubules and filaments. These components define the architecture and internal organisation of cells and provides them mechanical support. Since neurons are the longest cells in the human body, the neuronal cytoskeleton plays a key role in maintaining their shape and structure to ensure cell functionality. Cytoskeletal components also take part in numerous processes that are essential for cell activity and survival, including intracellular transport, cell division, adhesion, and movements.

The cytoskeleton comprises three classes of protein filaments that dynamically interact with one another, microtubules, microfilaments, and intermediate filaments[1] (Figure 1). Microtubules represent the largest cytoskeletal component and are hollow cylinders with a 25-nm external diameter. Each microtubule is made of 13 protofilaments composed of α- and β-tubulin heterodimers. α- and β-tubulin exist in various isoforms, each with a molecular weight of approximately 50 kDa. They are globular in structure and comprise an amino (N)-terminal domain for GTP binding and a carboxy (C)-terminal domain interacting with microtubule-associated proteins (MAPs), including molecular motors. The alternance between α- and β-tubulin in their structure makes microtubules polarised, with the plus-end exposing β-tubulin and the minus-end α-tubulin. While in axons and distal dendrites microtubules are uniformly oriented with the plus-end towards cell periphery, in proximal dendrites they display a mixed polarity[1,4]. Microtubules nucleate at the microtubule-organising centre (MTOC), a structure located in close proximity to the nucleus; the process starts from a γ-tubulin ring complex (γTuRC) that also protects their minus-ends[5]. Microtubules are extremely dynamic structures and their length is regulated by the addition and removal of tubulin heterodimers, two processes that occur at a faster rate at the plus and minus-ends, respectively, and that stochastically alternate through dynamic instability. Several factors regulate microtubule dynamics, including post-translational modifications and interaction with MAPs. Microtubule polymerisation and depolymerisation occur in a GTP-dependent fashion. GTP binds to tubulin heterodimers at the level of the β-tubulin subunit, that can act as GTPase and hydrolyse it. At microtubule plus-ends, GTP-bound tubulin heterodimers are added to protofilaments, forming a GTP cap that protects them from depolymerisation. The latter process only occurs when GTP is hydrolysed by β-tubulin, an event that is favoured at microtubule minus-ends[6]. In neurons, microtubules guide neurite extension and maintenance and act as main track for the trafficking of organelles and vesicles[1].

With their 7-nm diameter, microfilaments are the smallest cytoskeletal component. They are formed by 42-kDa actin monomers that polymerise in an ATP-dependent fashion to form linear structures that then organise into double-stranded helices of filamentous actin. Since monomers all display the same orientation within actin strands, microfilaments are characterised by intrinsic polarity, similarly to microtubules, and they only grow at their barbed end. Actin subunits can also be removed from microfilaments to ensure dynamicity to their network. Assembly, disassembly, and spatial organisation of microfilaments in cells is regulated by specific actin-binding proteins, once again comparably to microtubules[1]. In neurons, an actin network, with barbed ends pointing towards the plasma membrane, stabilises the morphology of synaptic terminals in dendrites and axons and modulates their structure in response to signals[7,8].

Intermediate filaments are the most stable cytoskeletal component and are mainly involved in providing mechanical resistance and rigidity to intracellular structures. They are 10-nm wide filaments composed of a family of proteins that share a common helical core but display structure and sequence variability at their extremities; on these bases, they are grouped into six tissue-specific classes (type I-VI intermediate filaments). Differently from microtubules and microfilaments, intermediate filaments do not display intrinsic polarity. Neurofilaments (NFs) are neuron-specific type-IV intermediate filaments and comprise heavy, medium, and light (NF-H, NF-M, NF-L) subunits. They participate in the stabilisation of axonal structures and support radial axonal growth[1].

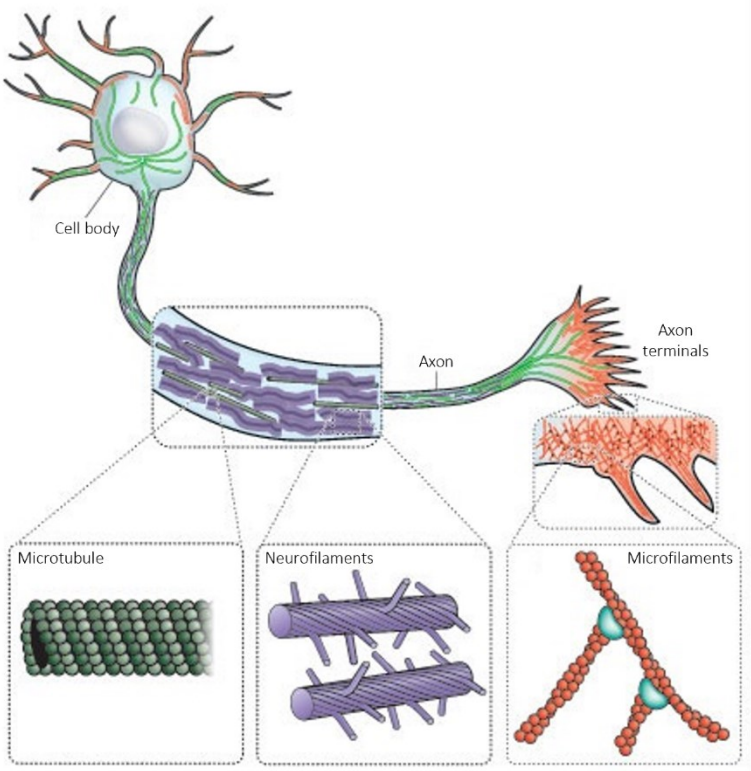

Figure 1 Schematic representation of the main components of the neuronal cytoskeleton. Adapted from Scitable (https://www.nature.com/scitable/topicpage/microtubules-and-filaments-14052932/)

Molecular motors in neurons

In neurons proteins, RNP granules, vesicles, and organelles are bidirectionally transported by molecular motors along cytoskeletal tracks to regulate neuronal physiology and functions. Similar to other cell types, the transport proteins involved in neuronal trafficking can be divided into three main classes, kinesins, dynein, and myosin. The first two groups of motor proteins move along microtubules, while myosin is an actin-based motor[8] (Table 1 and Figure 2).

The first ATP-dependent, microtubule-based molecular motor was isolated in 1985 from squid axoplasm and bovine brain and named kinesin[9,10]; in 1991 kinesin was shown to be a plus-end–

directed molecular motor[11]. Kinesins are now known to be a large superfamily of molecular motors: in the human genome, over 40 kinesins can be found and 38 of them are expressed in neurons. Kinesins belonging to distinct subfamilies differ in their holoenzyme structure, which ranges from monomers to tetramers, and in the ability to interact with adaptor proteins[12]. A standardised nomenclature organising kinesins into 15 subfamilies was proposed in 2004[13]. Most kinesins comprise a globular motor domain, a coiled-coil stalk, and a tail region[14]. The motor domain, often referred to as head, is required for ATP hydrolysis and microtubule binding. Based on the position of the head within the protein sequence, kinesins can be grouped into three categories: N-kinesins have their motor domain at the N-terminus, M-kinesins have it in the middle, and C-kinesins in the C-terminal region. All kinesins display microtubule plus-end-directed motility, except for some C-kinesins that travel in the opposite direction towards minus-ends. Differently from N- and C-kinesins, M-kinesins have their central motor domain flanked by two coiled-coil regions and two members of the kinesin 13 subfamily of M-kinesins, kinesin family members 2A and 2C (KIF2A/C), play their main role in ATP-dependent microtubule depolymerisation instead of trafficking[8]. While kinesin heads display high similarity between the different KIF subfamilies (30-60% sequence homology), the stalk and tail domains are variable. The stalk mediates kinesin conformational changes and dimerisation in the case of multimeric motors, whereas the tail region is involved in cargo or adaptor binding[15]. Besides intracellular transport, kinesins take part in a wide variety of cellular functions, including chromosome dynamics upon cell division and cytoskeletal regulation, and are often hijacked by viruses for trafficking[16]. In axons, kinesins can mediate either the fast transport (50-200 mm/day) of vesicles and organelles or the slow transport (0.1-3 mm/day) of cytoskeletal proteins such as tubulin and NFs[17]. In dendrites, kinesins are mainly responsible for the trafficking of RNP granules, vesicles, and proteins involved in synaptic transmission[8].

Dyneins are divided into two main groups, cytoplasmic dyneins and axonemal dyneins. Cytoplasmic dynein is the main microtubule-based retrograde motor and consists of a very large 1.5-MDa protein complex comprising two heavy chains (approximately 500 kDa), two intermediate chains (approximately 75 kDa), four intermediate light chains (approximately 35-60 kDa), and several light chains (approximately 10-15 kDa)[18,19]. Cytoplasmic dynein also interacts with another large protein complex named dynactin, which is essential to regulate dynein activity and cargo binding. The main dynactin components are dynactin subunits 1-6 (DCTN1-6), actin-related proteins 1 and 10 (ACTR1, ACTR10), and capping actin proteins α and β (CAPZA, CAPZB)[20]. Eukaryotes express several proteins of the dynein superfamily, but most of them belong to the axonemal subgroup and are involved in flagellar motility and intraflagellar trafficking[21,22]. Unlike the diverse kinesin and myosin families, there are only two ATP-dependent microtubule-binding heavy chains of dynein[23]. Dynein cytoplasmic 1 heavy chain 1 (DYNC1H1) is mainly involved in retrograde cytoplasmic transport,

including within axons and dendrites, while DYNC2H1 works within flagella[24]. DYNC1H1 can bind to cargoes either directly or through the recruitment of alternative forms of dynein intermediate, light intermediate, and light chains, as well as dynactin complex variants, providing a wide range of variability[8]. For example, dynein axonemal intermediate chain 1 (DNAI1), but not its cognate DNAI2, participates to the trafficking of neurotrophic receptor tyrosine kinase 2 (NTRK2 or TRKB), a key receptor for brain-derived neurotrophic factor (BDNF)[25], dynein light chains LC8-type 1 and 2 (DYNLL1, DYNLL2) bind gephyrin, a scaffold protein found in the postsynaptic terminal of inhibitory synapses[26]; and DCTN1 interacts with huntingtin-associated protein 1 (HAP1), an essential player in the bidirectional transport of BDNF vesicles that also interacts with kinesins[27]. Other cytoplasmic dynein-specific cargoes include mitochondria[28], lysosomes, and endosomes positive for Ras oncogene family members 5 and 7 (RAB5, RAB7), which are involved in the retrograde transport of neurotrophic factors[29,30].

Myosins are a large group of actin-based, ATP-dependent molecular motors divided into more than 20 subfamilies[31]. Most myosin motors work as dimers and comprise a motor head, a neck region, and a tail. In neurons, myosins participate in cell movement, membrane trafficking, and signal transduction[8]. Myosins Va, Vb, and VI play their main roles at the synapse. Myosin Va is involved in the trafficking of endoplasmic reticulum (ER) vesicles in axons[32], probably in association with conventional kinesins of the KIF5 subfamily[33], and of RNP granules in dendrites[34]. Myosin Vb, on the other hand, is involved in the recycling of α-amino-3-hydroxy-5-methylisoxazole-4-propionate (AMPA) glutamate receptors[35]. Both myosins Va and Vb, which are highly homologous, participate in the long-term potentiation of synaptic connections by undergoing Ca^{2+}-dependent activation[36] and promoting AMPA receptor exposure on the surface of dendritic spines[37,38]. Myosin VI is the only retrograde motor in the myosin superfamily and displays minus-end-directed movement[39]; it is involved in the stimulation-dependent internalisation of AMPA receptors[40] and the uptake of NTRK2-bound BDNF[41]. Myosin II, the main myosin in muscle contraction, is also involved in the glial-guided neuronal migration occurring during development in the central nervous system[42]. Additionally, at the presynaptic terminal, myosin II promotes neurotransmitter vesicle exocytosis[43], and it is also involved in regulating postsynaptic spine plasticity, particularly in response to synaptic stimulation[44]. Finally, while myosins I and VII take part in the morphogenesis of stereocilia in the inner ear[45], myosin X participates in vesicular transport processes occurring within filopodia, which are growth cone protrusions that form upon axon elongation during neuronal development[46].

Table 1 Main roles of kinesins, dyneins, and myosins in neurons.

Motor family	Neuronal compartment	Cargo
Kinesins	Axon	Fast transport of vesicles and organelles, slow transport of cytoskeletal proteins
	Dendrites	RNP granules, synaptic components
Dyneins	Axon and dendrites	Organelles, neurotrophic factors, synaptic components
Myosins	Axon and dendrites	ER vesicles, RNP granules, neurotrophic factors (retrograde transport), synaptic components (anterograde and retrograde transport)

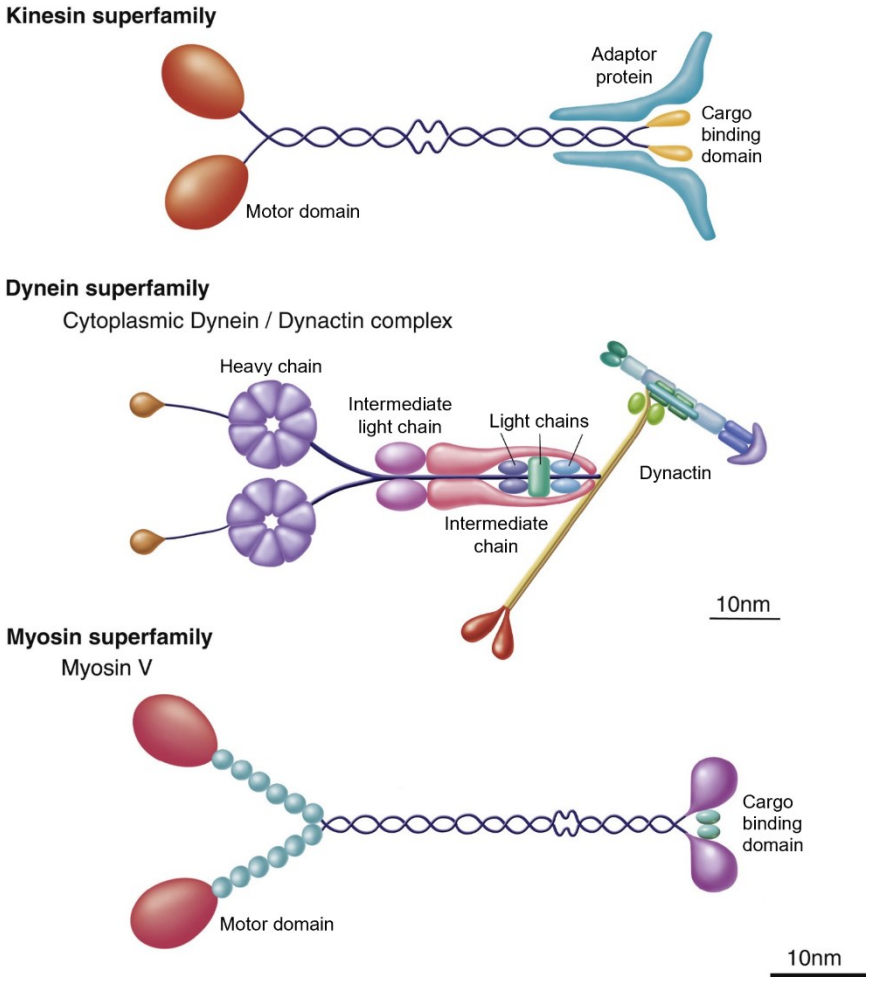

Figure 2 Schematic representation of kinesin (top), cytoplasmic dynein (middle), and myosin (bottom) motors. Adapted from: Hirokawa N, Niwa S, Tanaka Y. Molecular motors in neurons: transport mechanisms and roles in brain function, development, and disease. *Neuron* 68, 610-638 (2010).

Conventional kinesins or KIF5s

The first motor protein ever identified in 1985 was named conventional kinesin. Initially considered a single protein, it was later revealed to consist of three highly similar isoforms in mammals. Based

on the current nomenclature, conventional kinesin motors belong to the kinesin-1 or KIF5 subfamily[47,48]; among them KIF5B is ubiquitous, while KIF5A and KIF5C are exclusively expressed in neurons, with distinct specificities in terms of neuronal subtypes[49]. KIF5 functions in axonal transport are phylogenetically conserved from *Drosophila* to mammals[50].

KIF5 structure, stepping mechanism, and regulation

KIF5s are N-kinesins and their motor domain is structurally similar to the catalytic domain of myosin even in the absence of sequence homology[51]. KIF5 head contains a microtubule-binding site that displays higher affinity for axonal compared to dendritic microtubules. This differential affinity is essential during neurogenesis to allow the specification of a single axon from multiple neurites, because KIF5-dependent transport will mainly occur along a single protrusion. KIF5 recruitment to axons is supposed to depend on the different microtubule stabilities in the proximal axon and in dendrites; consistently, when microtubule dynamics are perturbed in developing neurons, neuronal polarity is disrupted[52,53]. KIF5 motors move on microtubules by taking 8-nm steps, corresponding to the distance between two neighbouring tubulin heterodimers[54]. The two heads in a KIF5 homodimer perform alternated ATP cycles at the level of their hydrolytic pockets, exchanging leading and trailing positions at each kinesin step in a hand-over-hand fashion[55,56]. Coordination between the two motor domains in ATP hydrolysis is achieved through specific gating strategies. KIF5 motors are characterised by high processivity and can take hundreds of sequential steps on microtubules before detachment[57]. In a KIF5 homodimer bound to microtubules, the front head associates with tubulin and exchanges ADP with ATP, while the rear head retains ADP weakly binding to microtubules until the first head associates to ATP; this allows the KIF5 motor to transition from a waiting state to an active one[58]. ATP binding to the front head immobilises a short sequence connecting the motor domain to the stalk, called neck-linker; this is followed by a conformational change that contextually moves the KIF5 rear head towards the microtubule plus-end, exchanging the relative positions of the two motor domains and therefore making KIF5 step forward[59,60]. When the now-front end finds the next binding site on the microtubule track, ADP is released and both kinesin heads tightly bind to tubulin. Subsequently, the now-rear head hydrolyses ATP, releasing the strain imposed by the contemporary binding of both KIF5 heads to the microtubule and allowing the now-front head to bind to ATP to initiate a new stepping cycle[58,60,61].

Apart from the neck-linker, the stalk domain of conventional kinesins comprises a series of coiled-coils through which KIF5s form homodimers[62]. About half of the homodimers found in cells form tetrameric holoenzymes by interacting with two kinesin light chain (KLC) molecules. Such

interaction occurs between the N-terminal region of KLCs and a KIF5 region spanning across the stalk and tail domains[63,64]. KIF5s can bind cargo either directly through a specific region of their tail domain downstream of the KLC binding site[65] or indirectly through KLCs, which exist in different isoforms (KLC1-4) produced by alternative splicing in their C-terminal tetratricopeptide repeat (TPR) domain, which is involved in cargo binding[66,67].

In the absence of cargo, KIF5s are found in the cytoplasm in an autoinhibited conformation, in which the tail domain folds onto the head to prevent ADP release. The interaction between head and tail is driven by the isoleucine-alanine-lysine (IAK) motif in the KIF5 C-terminal region. Autoinhibition is essential for proper KIF5 functioning since it prevents unnecessary ATP-wasting movements towards microtubule plus-ends of empty motors in absence of cargo. Consistently, deletion or mutation of the IAK motif generate constitutively active KIF5 motors. Upon interaction with cargoes or adaptor proteins, autoinhibition is released and the motor domain contacts cytoskeletal tracks to begin transport [68,69].

KIF5 movement along microtubules is also regulated by kinesin phosphorylation. Indeed, glycogen synthase kinase 3β (GSK3β) inhibits KIF5-mediate anterograde transport by phosphorylating KLC2, while KIF5 head phosphorylation by p38 mitogen-activated protein kinase (MAPK) or MAPK10 prevents microtubule binding[49].

Main KIF5 cargoes in neurons

Conventional kinesins take part in a wide variety of trafficking processes in neurons. The essential role of KIF5s in axonal transport is well demonstrated by the fact that mutations in the KIF5 homologue in *Drosophila*, named kinesin heavy chain (*Khc*), cause fatal motor neuron degeneration due to the accumulation of organelles and vesicles along axons, obstructing bidirectional trafficking[70,71]. Interestingly, a similar phenotype is observed upon loss of the *Klc* gene in flies[72].

Conventional kinesins are the main motors driving the slow anterograde trafficking of proteins in neurons. KIF5 protein cargoes include tubulin dimers, that are transported with the help of KLC or dihydropyrimidinase like 2 (DPYSL2 or CRMP2) adaptors[73]. This transport process is essential during mammalian development because it promotes axonal initiation and extension. In fact, KIF5s accumulate at growth cones and interact with disrupted in schizophrenia 1 scaffold protein (DISC1), an adaptor for the binding of the nudE neurodevelopment protein 1 like 1 (NDEL1) complex, contributing to axonal elongation[74]. Consistently with the centrality of conventional kinesins in this process, *kif5* knock-down (KD) in cultured hippocampal neurons drives a decrease in neurite length and blocks synapsin and growth associated protein 43 (GAP43) transport to neurite tips[75]. Besides tubulin, NFs, too, can be transported by conventional kinesins[76]. Slow axonal transport of

cytoplasmic proteins by KIF5s require KLCs and is regulated by the interaction between the TRP domain and the heat-shock protein A8 (HSPA8 or HSC70). HSPA8 binding to KLCs prevents them from interacting with membranes, therefore regulating the equilibrium between fast and slow anterograde axonal trafficking. Indeed, competitive inhibition of HSPA8-TRP domain binding in squid gian axons and overexpression of a dominant negative form of the TRP domain in mice were both shown to potentiate organelle transport while disrupting protein trafficking[8,77].

Concerning fast anterograde axonal transport, one of the main KIF5 roles is in the trafficking of vesicles required for synaptic transmission at the axon terminus. In particular, KIF5s drive along axons vesicles containing presynaptic membrane proteins required for synaptic vesicles to fuse with the plasma membrane and release neurotransmitters, including syntaxin and some components of the synaptosome-associated protein (SNAP) complex and its receptor (SNARE) like SNAP23, SNAP25, synaptotagmin and synaptobrevin[78,79]. SNAP25 displays direct binding to the KIF5 tail domain[80], while syntaxin interacts with conventional kinesins through syntabulin and bridges KIF5s to cargoes transported within presynaptic vesicles. The syntaxin-syntabulin-KIF5 complex has been shown to be a key player in the assembly of presynaptic terminals in hippocampal neurons during development[81,82].

Mitochondrial transport along axons is another fundamental process involving KIF5s. Syntabulin, RAN binding protein 2 (RANBP2), trafficking kinesin proteins 1 and 2 (TRAK1/2 or Milton), and Ras homology family member T1 and T2 (RHOT1/2 or Miro) all participate in linking mitochondria to KIF5 motors[83–86]. The centrality of conventional kinesin motors in mitochondrial trafficking is well illustrated by mutant and knock-out (KO) animal models. For example, *Kif5b* loss in mice determines perinuclear accumulation of mitochondria in cells which can be restored by exogenous expression of any human conventional kinesin motor[48,87]. A similar phenotype can be observed in *Kif5a* KO animal models[88,89]. It has been recently demonstrated that bidirectional mitochondrial transport in neurons is finely tuned by the motor adaptors TRAK1/2, which coordinates the formation of a complex linking mitochondria to both conventional kinesins and the dynein-dynactin complex[90]. In addition, mitochondrial trafficking in neurons critically depends on the integrity of microtubule-based bidirectional transport. In fact, individual depletion of conventional kinesin, dynein, or dynactin is sufficient to disrupt mitochondrial motility in both directions[91–93]. Interdependence between these essential molecular motors also manifests at the level of anterograde dynein trafficking to microtubule plus-ends, which is mediated by conventional kinesins and is required to allow proper initiation of dynein-mediated retrograde transport. Dynein intermediate chain was proven to directly bind to the stalk domain of conventional kinesins, including KIF5A, in hippocampal neurons for delivery towards microtubule plus-ends[94].

KIF5 motors are also involved in endolysosomal trafficking. Both early endosomes containing RAB4/5 and lysosomes are targeted by conventional kinesins[95–97]. Regarding lysosomes, these cargoes are transported by at least KIF5B, the KO of which prevents lysosome dispersion upon cytoplasm acidification[87], and KIF5A, the chemically-induced reduction of which causes lysosome accumulation in neurons[98]. Finally, additional cargoes that are transported along axons by conventional kinesins through interaction with KLCs include vesicles containing phosphorylated amyloid precursor protein (APP) or receptors for LDL receptor related protein 8 (LRP8 or APOER2)[99,100].

Conventional kinesins also play central roles in dendritic trafficking. For instance, they take part in the transport of glutamate receptor-interacting protein 1 (GRIP1), which acts as an adaptor for glutamate receptor 2 (GluR2), one of the subunits of AMPA receptors. Interestingly, binding to the GRIP1-GluR2 complex preferentially drives KIF5s from axons to dendrites and overexpression of a dominant negative KIF5 construct deprived of the motor domain in cultured neurons determined a drastic reduction in GluR2 clustering in dendrites, indicating the essential role played by KIF5 motors and GRIP1 in the process. Moreover, conventional kinesin-mediated GluR2 transport in dendrites was shown to be inhibited by overexpression of mitogen-activated protein kinase interacting protein 3 (MAPK8IP3 or JIP3), a scaffold protein competing with GRIP1 for GluR2 binding and requiring KLCs to interact with conventional kinesins[100,101]. KIF5s have also been reported to directly bind to HAP1 for the dendritic trafficking of γ-aminobutyric acid (GABA) type A receptors ($GABA_ARs$)[102]. Finally, KIF5s are implicated in the dendritic transport of RNP granules containing various mRNA species, like those encoding activity-regulated cytoskeleton-associated protein (ARC) and Ca^{2+}/calmodulin-dependent kinase 2α (CAMK2α), and at least 42 proteins, like fragile X messenger ribonucleoprotein 1 (FMR1 or FMRP)[103,104]. Transport of such RNP granules does not require KLCs[105].

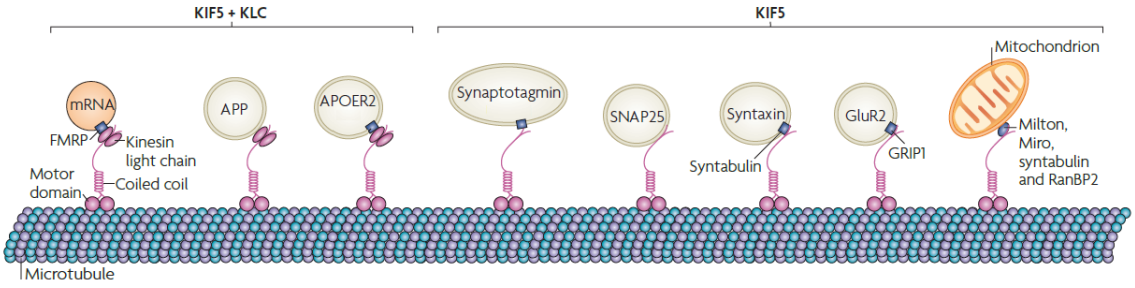

Figure 3 Schematic representation of the main KIF5 cargoes and adaptors involved in cargo binding. Adapted from: Hirokawa N, Noda Y, Tanaka Y, Nida S. Kinesin superfamily motor proteins and intracellular transport. *Nat. Rev. Mol. Cell Biol.* 10, 682-696 (2009).

KIF5A

KIF5A is a neuron-specific conventional kinesin. It is a 1032-amino acids protein encoded by the 29-exon *KIF5A* gene, located on chromosome 12q13.3[47]. KIF5A is the longest protein in the kinesin-1 subfamily, having 73 unique amino acids in its C-terminal tail[15]. A schematic representation of KIF5A gene and protein structures is reported in Figure 4.

KIF5A is involved in the anterograde transport of a wide variety of cargoes which are partially shared with the other conventional kinesins, but both constitutive and conditional *Kif5a* loss result in neonatally lethal in mice, even in the absence of trivial aberrations in brain histology. This suggests that KIF5A performs essential functions in neuronal transport[76,106]. As a support to this hypothesis, conditional *Kif5A* KO mice display NF accumulation in neuronal bodies and impaired bidirectional NF trafficking stemming from a strong decrease in anterograde transport frequency that can be only partially rescued by Kif5B and Kif5C overexpression[76,107]. Another key role seems to be played by KIF5A in mitochondrial trafficking, since *Kif5A* loss in murine motor neurons was reported to alter bidirectional mitochondrial transport, disrupting axonal morphology, and reducing neuron survival. Moreover, heterozygous truncating *kif5Aa* mutations in zebrafish resulted in the degeneration of peripheral sensory axons caused by a reduction in axonal mitochondria[88,89].

The uniqueness of some KIF5A roles is also suggested by the fact that knocking out the neuron-specific *KLC1* gene induces abnormal KIF5A accumulation in the distal Golgi, without impacting on KIF5B or KIF5C distribution[108]. An example cargo preferentially transported by KIF5A-KLC1 tetramers consists of the RNP granules containing splicing factor proline/glutamine-rich (SFPQ)[104,109]. In sensory and motor neurons, SFPQ binds to neurotrophin-regulated transcripts and drives them to axons for local translation by interacting with KIF5A-KLC1[110,111]. The specificity of SFPQ binding to these tetramers is related to the tail domain portion unique to KIF5A among the three conventional kinesins. Interestingly, overexpression of a disease-associated KIF5A variant (R280H) prevented the axonal localisation of SFPQ granules and induced axonal degeneration of murine dorsal root ganglion sensory neurons, although the R280H KIF5A mutant did not alter mitochondrial transport[109].

Another KIF5A-specific function is related to the trafficking of neurotransmitter receptors. As an example, Nakajima and colleagues found that mice depleted of *Kif5a* at the neuronal level suffer from severe epileptic seizures that they proved to depend on a reduction in the membrane levels of $GABA_A$Rs in the hippocampus caused by a decrease in their anterograde axonal trafficking. By knocking down *Kif5a* expression in hippocampal neurons, the authors observed a comparable phenotype that could be rescued only by overexpressing Kif5a, not Kif5b or Kif5c. KIF5A bridging to $GABA_A$Rs is mediated by $GABA_A$R-associated protein (GABARAP) or $GABA_A$R-associated protein-like

1 and 2 (GABARAPL1, GABARAPL2) adaptors, which interact with KIF5A via its unique 73-amino acid tail sequence. Of note, GABARAP-positive vesicles tend to accumulate within the proximal region of dendrites in conditional *Kif5a* KO hippocampal neurons, consistent with dendritic trafficking being KIF5A-dependent. Overall, *Kif5a* KO or KD in hippocampal neurons determines a reduction in the number, the size, and the anterograde velocity of vesicles containing $GABA_AR$ subunits[106]. Interestingly, besides inducing mitochondrial defects, *kif5Aa* truncation in zebrafish resulted in motor neuron hyperexcitability leading to muscle spasticity[89], suggesting that KIF5A involvement in the transport of components required for synaptic transmission is phylogenetically conserved. KIF5A was also found to be essential in the activity-dependent internalisation of AMPA receptors following *N*-methyl-*D*-aspartate (NMDA) receptor activation in the hippocampus, a process that is required to establish long-term synaptic depression[112,113]. Bridging between KIF5A and AMPARs is mediated by the vesicular adaptor protrudin, and KO or expression of dominant negative mutants of either component abolishes AMPA receptor removal from synaptic terminals upon NMDA signalling. This role in AMPA receptor trafficking is partially shared between KIF5A and KIF5C[113].

Finally, a specific role for KIF5A has been recently described in lysosomal transport. In fact, a reduction in KIF5A protein levels paralleled by the accumulation of microtubule-associated protein 1A/1B light chain 3 (MAP1LC3)- and sequestosome 1/p62 (SQSTM1/p62)-positive lysosomes displaying altered pH was observed in N2a cells treated with the neurotoxic compound trimethyltin chloride (TMT). Aberrant lysosomal distribution was reported to be a cause of a decrease in their KIF5A-mediated anterograde axonal transport, which requires the presence of GABARAP or GABARAPL1/2 adaptors. Of note, lysosomal degradative capacity and distribution were restored by *Kif5a* overexpression in TMT-treated N2a cells and murine hippocampus[98].

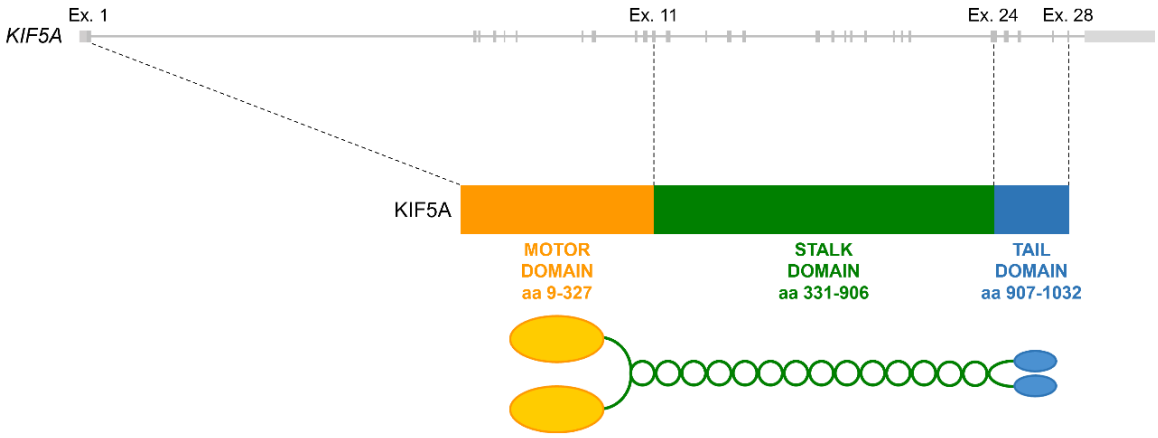

Figure 4 Schematic representation of KIF5A gene, protein, and dimer.

KIF5A-related motor neuron diseases

Motor neuron diseases (MNDs) are a heterogeneous group of genetic or sporadic neurodegenerative disorders characterised by the progressive loss of motor neurons. Clinically, MNDs are classified depending on the involvement of cortical/upper or spinal/lower motor neurons (LMNs), or both. The typical signs of upper MND include spasticity and clonus, while lower MNDs present with muscle atrophy, weakness, and reduced reflexes. When both types of motor neurons are affected, weakness and flaccid paralysis prevail over the initial spasticity symptoms with the progression of neurodegeneration[114]. Upper MNDs include primary lateral sclerosis and hereditary spastic paraplegias (SPGs), lower MNDs comprise spinal muscular atrophy, spinal and bulbar muscular atrophy (SBMA), and distal hereditary motor neuropathies, and mixed MNDs are amyotrophic lateral sclerosis (ALS) and progressive bulbar palsy[115,116] (Figure 5). Motor neuron loss in MNDs can be caused by the toxic events occurring within affected cells or depend at least partially on non-cell autonomous mechanisms taking place in glial or skeletal muscle cells[117,118].

MNDs can be appear in familial or sporadic forms. In the cases caused by mutations, it is possible to distinguish between MNDs associated with a loss of function (LOF) of the mutated gene product or a gain of function (GOF) through which the encoded protein exerts a novel and neurotoxic activity. In several cases, though, LOF and GOF co-exist[119]. Mutations in genes encoding proteins are involved in axonal trafficking are implicated in several MNDs, consistently with the prominent role played by such machinery in motor neuron function[8,16]. Transport-related processes that are also targeted by MND-linked mutations include mitochondrial dynamics, endosomal sorting, and autophagy[120]. In general, axonal transport alterations are found in MNDs regardless of the underlying mutation as well as in sporadic cases, also because trafficking along the axon tends to decline with ageing[121,122]. This duplicity makes it difficult to understand whether axonal trafficking impairments are a primary cause or a secondary consequence of motor neuron degeneration[123].

Mutations targeting the *KIF5A* gene are linked to three different MNDs: SPG10, Charcot-Marie-Tooth disease (CMT), and ALS.

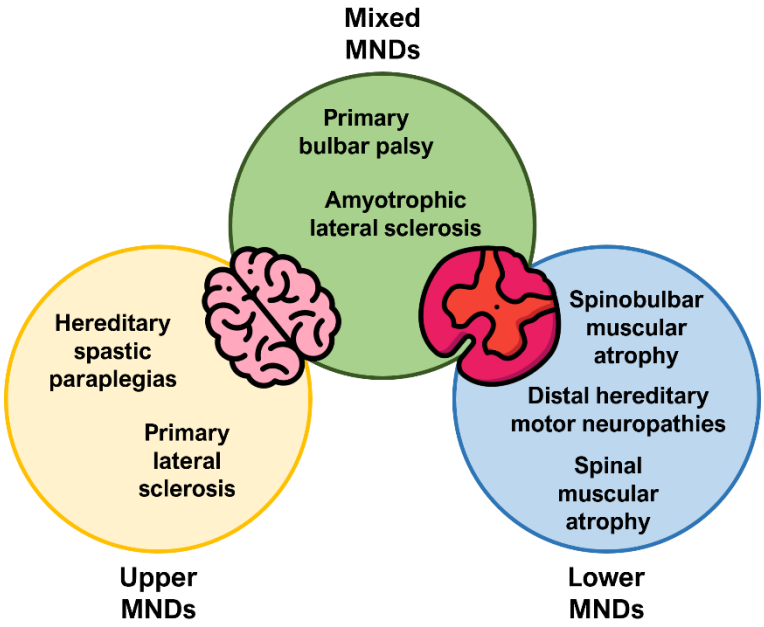

Figure 5 Upper MNDs affect motor neurons in the motor cortex and brainstem, lower MNDs target motor neurons in the spinal cord, while in mixed MNDs both types of motor neurons degenerate.

Spastic paraplegias

SPGs are a genetically and phenotypically heterogeneous group of adult-onset neurodegenerative diseases targeting spinal cord neurons classified as primary axonopathies. SPGs can be distinguished into a pure form and a complex or complicated form. Pure SPGs are mainly characterised by slowly progressive lower limb spasticity manifesting as a gait disturbance, often accompanied by asymptomatic upper limb hyperreflexia, brisk jaw jerk and sensory loss. Complex SPGs present with ataxia, cognitive impairment, epilepsy, peripheral neuropathy, and extrapyramidal signs in addition to leg spasticity. SPGs display an autosomal recessive, autosomal dominant, X-linked recessive, or mitochondrial pattern of inheritance and more than 80 loci have been associated with this group of diseases. Autosomal dominant SPG forms are less frequent than autosomal recessive ones and most complicated SPGs are inherited in the latter fashion. Moreover, only five SPG genetic subtypes are linked to the X chromosome, while mitochondrial inheritance is almost always sporadic. Overall, SPG prevalence is estimated to be about 1.8/100,000 cases. Currently, no cure is available for these neurodegenerative disorders[124].

At the cellular level, axonal degeneration in the spinal cord and distal muscle wasting are displayed by postmortem samples of SPG patients. Degeneration is usually more severe in the thoracic tracts but can also target cervical ones and even extend to peripheral nerves. Moreover, myelin abnormalities often accompany axonal loss. Concerning the molecular bases of the disease, genes targeted by SPG-related mutations hint at mitochondrial dysfunction, impairments in axonal

transport and membrane trafficking, myelination defects, and alterations in lipid metabolism as candidate mechanisms in SPG pathogenesis[125,126].

Charcot-Marie-Tooth disease

CMT is a genetically and clinically heterogeneous group of hereditary peripheral neuropathies targeting both the sensory and the motor systems and respresents the most common inherited neurological disease of the peripheral nervous system. The onset of most CMT forms occurs during the second decade of life [127]. Similarly to SPG, in CMT peripheral neurons degenerate through a dying-back mechanism which can depend either on demyelinisation or on axonal deterioration. Accordingly, CMT forms can be divided into four classes. Demyelinating forms are referred to as CMT1 when they have a dominant inheritance and CMT4 when they are recessive. Axonal forms are known as CMT2 regardless of their inheritance, while X-linked forms, which are usually characterised by childhood onset and a severe phenotype, are named CMT3. For each CMT type, several subtypes exist depending on the specific genetic cause. CMT subtypes can be clinically distinguished by electrophysiological studies and nerve biopsy and their frequency differs within distinct populations[128].

CMT symptoms usually start manifesting during adolescence in lower limbs and consist of foot drop and sensory loss in the lower legs and in feet. Progressive sensory and motor degeneration later spreads to the upper extremities, becoming evident as hand muscle weakness. Clinical severity is highly variable among CMT patients even when they share the same causing mutation, suggesting that environmental and susceptibility factors may contribute to pathogenesis[129,130].

In the last 30 years, more than 100 genes have been associated with CMT. In agreement with the clinical classification, causative genes of CMT1 and CMT4 are specifically expressed in Schwann cells and their mutation induces impairments in myelinogenesis or myelin deterioration, while genes mutated in CMT2 are mostly expressed by the neurons whose axons degenerate, but are also often found much more broadly across the body. Concerning the molecular mechanisms underpinning CMT pathogenesis, candidate processes include axonal transport impairments, alterations in mitochondrial dynamics and in the interactions between organelles, and disturbances in local axonal protein synthesis[131].

Amyotrophic lateral sclerosis

ALS is a rare, typically adult-onset MND in which both lower and upper motor neurons degenerate, leading to progressive muscular atrophy and causing death within 3-5 years after symptom onset. Besides motor neurons, glial cells and skeletal muscle can be affected by ALS[132,133]. Additionally,

ALS-related neurodegeneration may also target the frontotemporal cortex, leading to the development of a mixed form of MND and frontotemporal dementia (FTD) named ALS/FTD[134].

To date, ALS aetiology is still not completely characterised, and a combination of genetic and environmental factors is considered to underpin the disease. Around 90% ALS cases are sporadic (sALS), while approximately 10% are associated with familial inheritance (fALS). In terms of symptomatology, the two disease forms fully overlap, but fALS tends to display a faster and more severe progression compared to sALS. fALS cases are caused by LOF, GOF, and even mixed LOF-GOF mutations targeting more than 40 genes. Despite in the last 30 years great effort has been put into the identification of the genetic factors at the basis of ALS, around 30% of fALS have not yet been associated with a specific gene mutation. Noteworthily, sALS is characterised by alterations in the biochemical behaviour of the same proteins whose coding genes are found mutated in fALS, suggesting that the pathogenetic mechanisms underlying the two disease forms are probably partially shared[135].

Based on the function of ALS-associated genes, the main pathological mechanisms implicated in motor neuron loss include aberrant RNA processing, protein misfolding and aggregation, oxidative stress, mitochondrial dysfunction, ER stress, axonal transport impairments, excitotoxicity, and neuroinflammation[136,137]. A distinctive hallmark of most fALS forms is the presence of TAR DNA-binding protein 43 (TDP-43) inclusions in affected motor neurons. TDP-43 is a DNA/RNA-binding protein whose localisation is preferentially nuclear in healthy cells. In ALS motor neurons, TDP-43 translocates to the cytoplasm, where it aggregates, representing once again an example of combined loss of nuclear function and aberrant GOF linked to protein accumulation. Interestingly, TDP-43 inclusions are also found in the majority of patients suffering from FTD and ALS/FTD[138].

KIF5A mutations in diseases affecting motor neurons

Since the identification of the first *KIF5A* mutations in 2002[139], several other variants have been found and linked to distinct MNDs. Interestingly, *KIF5A* mutations associated with different diseases tend to cluster in different domains of the corresponding protein (Table 2). In detail, SPG10 and *KIF5A*-related axonal CMT are caused by point mutations targeting the head and stalk domains of the kinesin[139,140], while *KIF5A*-linked ALS is associated with frameshift mutations in the tail domain[141,142]. Interestingly, conditional KIF5A loss in animal models has been mainly associated with epilepsy, but not with motor symptoms[106], suggesting that both LOF and GOF mechanisms probably coexist in the pathogenesis of KIF5A-linked neurodegenerative diseases.

Concerning SPG10, it accounts for approximately 3% pure SPG cases and 10% complex SPG cases, making *KIF5A* mutations the most prevalent cause of the complicated form of the disease[143]. Most

mutations causing SPG10 cluster in proximity or within motor domain switches 1 and 2, that are part of KIF5A γ-phosphate-sensing region together with the phosphate-binding loop. These switches undergo conformational changes during ATP hydrolysis that are predicted to be essential for KIF5A function[144]. Consistently, Ebbing and colleagues demonstrated that K253N, N256S, and R280C KIF5A mutants display reduced affinity for microtubules compared to the wild type (WT) protein and can only move a few steps along these cytoskeletal tracks. These findings suggest that anterograde axonal transport of KIF5A cargoes might be delayed or impaired in neurons harbouring SPG10-linked *KIF5A* mutations[145,146]. In support of this hypothesis, Wang and colleagues reported that N256S KIF5A expression in mouse cortical neurons leads to a decrease in both anterograde and retrograde NF transport frequency, albeit without causing a significant NF depletion in distal axons[147]. Moreover, a *Drosophila* model harbouring the equivalent of the N256S KIF5A substitution (N262S Khc) evidenced axonal swellings, aberrant synaptic structure, and increased mortality compared to control flies, further confirming the impairment of axonal transport in the presence of SPG10 mutations[148]. SPG10 mutations also cluster in the region of the KIF5A motor domain involved in ATP hydrolysis. Even in this cases, mutant KIF5A displays decreased affinity for microtubules in the ATP-bound state, accompanied by a prominent reduction in the basal ATPase rate and/or by a limited microtubule gliding velocity[149]. Even the dimerisation of KIF5A motor heads or the transmission of the conformational changes following ATP hydrolysis to the neck and coiled-coil domains can be impacted by SPG10-related mutations, altering KIF5A ability to interact with or to step along microtubules and therefore leading to alterations in the velocity and/or intensity of axonal trafficking[146]. KIF5A mutations associated with axonal CMT are quite rare, even if the partial overlap between SPG10 forms with sensory involvement and CMT symptoms can make it difficult to properly discriminate between the two diseases. In general, no functional analysis of KIF5A mutants specifically linked to CMT has yet been performed.

ALS-related KIF5A mutations were identified for the first time in 2018 through whole-genome sequencing. Most of them are frameshifts occurring in KIF5A tail and leading to its elongation up to a novel stop codon 14 amino acids downstream to the WT one. Such shift in reading frame can be accompanied or not by the skipping of exon 27[141,142]. The aberrant tail that forms as a consequence of ALS-linked variants impairs KIF5A autoinhibition due to altered charge distribution around the IAK motif spanning residues 917-923, which represents the key region in KIF5A head blockage in the absence of cargo. Autoinhibition loss causes a GOF, generating a constitutively active motor that accumulates at microtubule plus-ends into SQSTM1-positive inclusions. Additionally, WT KIF5A is sequestered within these inclusions by mutant KIF5A through a dominant negative mechanism[150,151]. Interestingly, Baron *et al.* reported that overexpression of mutant *KIF5A* determined an increase in the fraction and velocity of anterogradely moving mitochondria in

cultured murine motor neurons[150], while Pant and colleagues did not observe co-distribution between KIF5A inclusions and mitochondria[151], so that the impact of ALS mutations of KIF5A-mediated axonal transport still needs to be fully elucidated.

Table 2 List of *KIF5A* mutations associated with neurodegenerative diseases (SPG10, CMT, ALS). The yellow background is for mutations in KIF5A motor domain, the green background for mutations in KIF5A stalk domain, and the blue background for mutations in KIF5A tail domain.

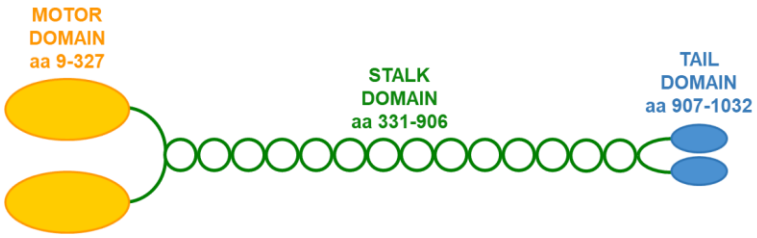

Gene	Protein	Phenotype	Reference	Note
c.50G>A	p.R17Q	SPG10	Santangelo 2023[152]	
c.130-943_c.1717-533del	p.G44_L572del	CMT	Pyromali 2021[153]	
c.188A>G	p.Y63C	SPG10	Goizet 2009[143]	
c.217G>A	p.D73N	SPG10	Schüle 2008[154]	abnormal splicing prediction
c.259C>G	p.Q87E	SPG10 with cerebellar ataxia	Qiu 2018[155]	
c.332G>C	p.R111P	CMT	Bacquet 2018[156]	
c.340C>T	p.R114*	ALS	Grassano 2022[157]	
c.395A>G	p.K132R	SPG10, CMT	Bacquet 2018[156] Méreaux 2022[158]	
c.396G>A	p.K132K	SPG10	van de Warrenburg 2016[159]	abnormal splicing prediction
c.416A>G	p.Y139C	SPG10	Méreaux 2022[158]	
c.484C>T	p.R162W	SPG10	Carosi 2015[160] Kaji 2016[161] Elert-Dobkowska 2019[162]	
c.485G>C	p.R162P	SPG10	Oliveira 2021[163]	

c.572G>A	p.R191H	SPG10	Morais 2017[164] Méreaux 2022[158]	
c.580G>C	p.A194P	SPG10	Collongues 2013[165]	
c.587C>A	p.T196N	CMT	Cortese 2020[166]	
c.593T>C	p.M198T	SPG10	Goizet 2009[143]	
c.604A>G	p.S202G	SPG10	Méreaux 2022[158]	
c.605G>A	p.S202N	SPG10	Crimella 2012[140] Méreaux 2022[158]	
c.608C>G	p.S203C	SPG10	Musumeci 2011[167]	
c.610C>T	p.R204W	SPG10 (+/- cerebellar ataxia), CMT	Tessa 2008[168] Liu 2014[169] Morais 2017[164] Nam 2018[170] Cuchanski 2018[171] He 2020[172] Méreaux 2022[158]	
c.611G>A	p.R204Q	SPG10	Goizet 2009[143] Crimella 2012[140] Neveling 2013[173] Liu 2014[169] Orsucci 2014[174] Jerath 2015[175] Lee 2020[176] Méreaux 2022[158]	
c.687T>A	p.Y229*	SPG10	Smedley 2021[177]	
c.691G>T	p.V231L	SPG10	Crimella 2012[140]	
c.694G>A	p.D232N	CMT	Liu 2014[169] Dellatte 2023[178]	
c.704G>A	p.G235E	CMT	Crimella 2012[140]	
c.710A>T	p.E237V	West syndrome and severe global developmental delay	Fukuoka 2021[179]	
c.728G>A	p.G243E	SPG10	Méreaux 2022[158]	

c.745C>G	p.L249V	SPG10	Lynch 2016[180]	
c.746T>C	p.L249P	SPG10	Perić 2022[181]	
c.751G>A	p.E251K	SPG10	Goizet 2009[143] Neveling 2013[173] Iqbal 2017[182] Méreaux 2022[158]	
c.759G>T	p.K253N	SPG10	Schüle 2008[154]	
c.763A>G	p.I255V	SPG10	Méreaux 2022[158]	
c.765C>G	p.I255M	SPG10	Citrigno 2018[183] Méreaux 2022[158]	
c.767A>G	p.N256S	SPG10	Reid 2002[139] Andréasson 2019[184] Méreaux 2022[158]	
c.768_770delCAA	p.N256del	SPG10	Schüle 2008[154]	
c.771G>C	p.K257N	SPG10	Goizet 2009[143]	
c.773C>T	p.S258L	SPG10	López 2015[185]	
c.776T>A	p.L259Q	SPG10 + congenital deafness	Muglia 2014[186]	
c.785T>C	p.L262P	SPG10, CMT	Dohrn 2017[187]	
c.802G>A	p.A268T	Adult-onset distal spinal muscular atrophy	de Fuenmayor-Fernández de la Hoz 2019[188]	
c.827A>G	p.Y276C	SPG10	Blair 2006[189]	
c.833C>T	p.P278L	SPG10	López 2015[185] Morais 2017[164] Méreaux 2022[158]	
c.838C>T	p.R280C°	SPG10, CMT	Fichera 2004[190] Goizet 2009[143] Liu 2014[169] Hsu 2019[191] Méreaux 2022[158]	
c.839G>A	p.R280H	SPG10, CMT	Goizet 2009[143] Liu 2014[169] Morais 2017[164] Nam 2018[170] Méreaux 2022[158] Panwala 2022[192]	
c.839G>T	p.R280L	SPG10	Goizet 2009[143]	

c.854C>T	p.T285I	SPG10, CMT	Bacquet 2018[156] Méreaux 2022[158]	
c.868G>C	p.D290H	SPG10	Morais 2017[164]	
c.889C>T	p.R297W	SPG10	Méreaux 2022[158]	
c.967C>T	p.R323W	SPG10	Rinaldi 2015[193] Andréasson 2019[184] Méreaux 2022[158]	
c.1022A>G	p.Q341R	SPG10	Giordani 2021[194]	
c.1082C>T	p.A361V	SPG10, primary progressive multiple sclerosis	Lo Giudice 2006[195] Jia 2018[196]2024-03-19 12:23:00 PM	
c.1086G>C	p.K362N	SPG10	Guinto 2017[197]	
c.1463T>G	p.L488R	ALS	Grassano 2022[157]	
c.1673T>C	p.L558P	CMT	Nam 2018[170]	
c.2263G>A	p.E755K	SPG10, ALS	Crimella 2012[140] Grassano 2022[157]	
c.2290C>T	p.Q764*	CMT	Hsu 2019[191]	
c.2539-605_*36 + 211del	p.L847_S1032delins33	CMT	Pyromali 2021[153]	
c.2590C>T	p.R864*	SPG10	Lynch 2016[180]	
c.2720A>T	p.K907M	Leber optic neuropathy	Pandya 2022[198]	
c.2757delC	p.K920Nfs*128	ALS	Grassano 2022[157]	
c.2987delA	p.D996fs	ALS	Nicolas 2018[141]	
c.2990delA	p.N997fs	ALS	Nicolas 2018[141]	
c.2993-14G>T	p.N999Vfs*40, ΔExon27	ALS/FTD	Saez-Atienzar 2020[199]	
c.2993-3C>A	p.N999Vfs*40, ΔExon27	ALS	Nakamura 2021[200]	
c.2993-3C>T	p.N999Vfs*40, ΔExon27	ALS	Nicolas 2018[141] Gu 2018[201]	
c.2993-1G>A	p.N999Vfs*40, ΔExon27	ALS	Brenner 2018[142] Nicolas 2018[141] Zhang 2019[202]	predicted to create a new splicing site: p.G998Efs*50
c.2996delA	p.N999fs	ALS	Nicolas 2018[141]	

c.2999delC	p.T1001Qfs	ALS	He 2020[172]	
c.3005A>G	p.(D1002G)	ALS	Tunca 2020[203]	predicted to affect splicing: p.D1002Gfs*41
c.3019A>G	p.R1007G	ALS	Brenner 2018[142] Nicolas 2018[141]	predicted to affect splicing
c.3020G>A	p.R1007K	ALS (+ signs of SPG10 and CMT)	Nicolas 2018[141] Dulski 2023[204]	predicted to affect splicing
c.3020+1G>A	p.N999Vfs*40, ΔExon27	ALS	Brenner 2018[142] Nicolas 2018[141] Naruse 2021[205]	
c.3020+2T>A	p.N999Vfs*40, ΔExon27	ALS	Nicolas 2018[141] Gu 2018[201]	
c.3020+2T>C	p.N999Vfs*40, ΔExon27	ALS	Brenner 2018[142]	
c.3020+3A>G	p.N999Vfs*40, ΔExon27	ALS (mixed with SPG10 and cerebellar ataxia)	Nicolas 2018[141] Faruq 2019[206] Naruse 2021[205]	
c.3020+3A>T	p.N999Vfs*40, ΔExon27	ALS (mixed with SPG10 and cerebellar ataxia)	Faruq 2019[206]	

°: mutation characterised as p.R280S by Ebbing *et al*.[145] and Dutta *et al*.[146] to avoid *in vitro* oxidation

Protein quality control

Protein quality control (PQC) refers to the group of molecular mechanisms that maintain protein homeostasis, or proteostasis, in eukaryotic cells. Specifically, the PQC system ensures proper protein folding and maturation at synthesis, eliminates misfolded proteins, and counteracts the accumulation of potentially toxic protein species in cells. The accumulation of misfolded proteins can lead to the formation of insoluble aggregates that can disturb metabolism and reduce cell viability, which is why cells have developed several defence mechanisms to fight proteotoxicity. The main players in PQC are specialised proteins named chaperones that co-operate with one another to preserve proteostasis. Eukaryotic cells host more than 180 chaperones and co-chaperones, and different subcellular compartments respond to alterations in proteostasis with distinct sets of chaperones and thus PQC mechanisms[207]. PQC activation also triggers the establishment of a transcriptional stress program aimed at enhancing chaperone synthesis, therefore representing a positive feedback loop[208].

Under normal conditions, the PQC system maintains protein homeostasis by helping nascent polypeptides unable to fold finding the proper conformation[209]. Chaperones can identify incorrectly folded proteins because the latters expose hydrophobic patches normally found at their core. If the folding attempt fails, chaperones drive misfolded proteins to proteolysis, that is achieved through either the ubiquitin-proteasome system (UPS) or the autophagy pathway[210]. However, when cellular stress occurs, for example with ageing or in the presence of aggregation-prone proteins, the ability of chaperones to keep protein misfolding under control may be overwhelmed and proteostasis may get impaired. This might eventually result in the uncontrolled accumulation of misfolded proteins leading to the development of disorders that are collectively known as proteinopathies. Among them, several neurodegenerative diseases and MNDs can be found, including Huntington's disease, Alzheimer's disease (AD), Parkinson's disease, transmissible spongiform encephalopathies, SMBA, and ALS[211].

Ubiquitin-proteasome system

The UPS is a cytosolic and nuclear degradative pathway highly conserved in eukaryotic cells. Through the UPS, misfolded proteins are targeted for clearance via polyubiquitination and are then moved to the 26S proteasome to be reduced to single amino acids[212] (Figure 6).

Polyubiquitination requires the ATP-dependent conjugation of several residues of ubiquitin, a 76-residue protein, to degradation targets. The process involves the concerted activity of a ubiquitin-activating enzyme E1, a ubiquitin-conjugating enzyme E2, and a ubiquitin-protein ligase E3. Initially, an E1 enzyme consumes one ATP molecule to adenylate ubiquitin on its C-terminal glycine and

forms a thioester bond between activated ubiquitin and a cysteine residue in its own catalytic site[213]. Subsequently, ubiquitin is moved from the E1 enzyme to the active site of an E2 enzyme by a transthioesterification reaction, and eventually the target protein is recruited by an E3 enzyme, which transfers ubiquitin from the E2 enzyme to the substrate by forming an isopeptide bond between the activated C-terminal glycine of ubiquitin and the ε-amino group of a lysine residue of the substrate. The process is then cyclically repeated, with the new ubiquitin moiety being conjugated to any of the seven lysines of the previously attached molecule, in particular the ones in positions 48 or 63[214].

The obtained polyubiquitin chain acts as targeting signal for the 26S proteasome, a barrel-shaped multi-subunit complex of approximately 2.5 MDa. The 26S proteasome is composed of two 19S particles responsible for the identification and unfolding of polyubiquitinated substrates and by a 20S component driving ATP-dependent proteolysis. Polyubiquitinated proteins are initially reduced to short peptides of 8-12 amino acids and then to single amino acids by aminopeptidases. Single amino acids are then recycled for protein synthesis[215].

Substrate delivery to the UPS can be promoted by protein complexes that specifically drive clients to degradation. An example is the complex formed by the chaperone HSP70, that identifies the targets to be eliminated, the ubiquitin-protein ligase STIP1 and U-box containing protein 1 (STUB1), that polyubiquitinates the substrates, and the Bcl-2 associated athanogene co-chaperone 1 (BAG1), that handles them to the 26S proteasome[216].

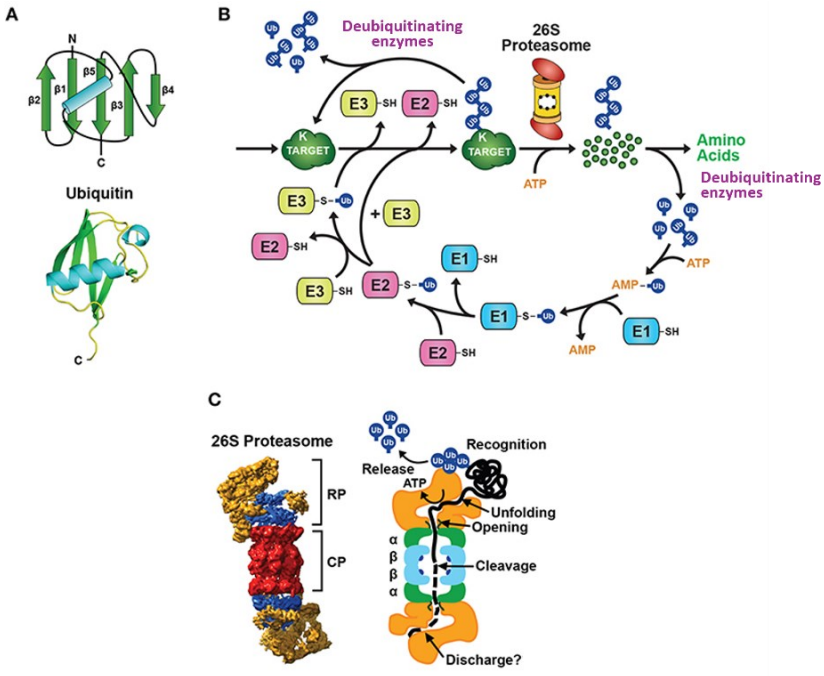

Figure 6 Schematic representation of **(A)** ubiquitin, **(B)** the ubiquitin-proteasome system pathway, and **(C)** the 26S proteasome structure. Adapted from: Marshall RS & Vierstra RD. Dynamic regulation of the 26S proteasome: from synthesis to degradation. *Front. Mol. Biosci.* 6, 40 (2019).

Autophagy

Autophagy is a phylogenetically conserved cellular mechanism that involves the degradation by lysosomal hydrolases of old, unnecessary, or dysfunctional cytosolic components to recycle substrates for metabolism and repair processes[217]. Both endogenous and exogenous material can be degraded via autophagy, that is connected to the endocytic pathway at multiple levels[218]. In normal conditions, autophagy works at low levels to contribute to homeostasis maintenance by avoiding the accumulation of potentially dangerous species that may be produced by normal cellular functions (e.g., misfolded proteins or damaged mitochondria)[219–221]. Moreover, autophagy responds to perturbations of the intracellular or extracellular environment by adapting the substrate degradation rate to them[222].

The autophagy pathway is usually divided into three separated branches (Figure 7). The first one is macroautophagy and consists in the removal of damaged organelles and cytosolic proteins through a double-membraned vesicle named autophagosome, which later fuses with a lysosome[217]. Macroautophagy starts with the nucleation of the membrane of the phagophore, the autophagosome precursor, from a donor compartment. The process is driven by a complex formed by autophagy-related 13 and 101 (ATG13, ATG101), unc-51–like kinase 1 (ULK1), and RB1 inducible coiled-coil 1 (RB1CC1 or ATG17). The activation of this complex at the phagophore membrane triggers the assembling of the phosphatidylinositol 3-kinase catalytic subunit type 3 (PI3KC3) complex, that promotes phosphatidylinositol phosphorylation, required to guide the curvature of the phagophore membrane[223]. Membrane nucleation is then followed by phagophore elongation, which is regulated by the ATG12-ATG5-ATG16L complex: this process consists in the wrapping of the phagophore membrane around the cytoplasmic portion to be engulfed[223,224]. At this stage, a key role is played also by MAP1LC3, which is processed by ATG3, ATG4, and ATG7 through proteolytic cleavage and addition of a phosphatidylethanolamine moiety and is subsequently inserted into the phagophore membrane to guide its curvature[225]. The phagophore then closes to form a double-membraned autophagosome, which eventually fuses with a lysosome for the degradation of the engulfed material[226]. Macroautophagy can occur either in bulk or selectively; autophagy processes displaying substrate specificity range from organelle degradation pathways (e.g., mitophagy for mitochondria, reticulophagy for the ER) to elimination routes that are selective for aggregates or even bacterial cells (respectively named aggrephagy and xenophagy)[227]. A branch of selective macroautophagy playing a relevant role in motor neurons and muscles is represented by the chaperone-assisted selective autophagy (CASA) pathway, consisting of the disposal of polyubiquitinated proteins through autophagy[228]. This pathway is mediated by the CASA complex, which is formed by the chaperones HSP70 and HSPB8, the co-chaperone BAG3, and STUB1[229]. CASA

substrates are bound by a HSPB8 dimer, which is bridged to HSP70 by BAG3. Transient interaction between HSP70 and STUB1 determines client polyubiquitination and induces the engagement of the autophagy receptor SQSTM1/p62, while BAG3 binding to dynein allows the CASA complex to be retrogradely transported to the MTOC. Engulfment of target proteins into a nascent autophagosome is eventually mediated by the interaction between SQSTM1/p62 and MAP1LC3[230]. Activity of the CASA complex has been shown to promote the elimination of protein aggregates associated with MNDs, including the mutant androgen receptor in SBMA and mutant SOD1, TDP-43 C-terminal fragments (TDP-25 and TDP-35), or dipeptide repeats deriving from the hexanucleotide repeat expansion in the chromosome 9 open reading frame 72 (C9ORF72), causing ALS[231]. Since also BAG1 can interact with HSP70-bound polyubiquitinated proteins to drive them to the UPS, competition occurs between the two co-chaperones BAG1 and BAG3. The equilibrium between the UPS and the CASA pathway in client targeting is mainly defined by the relative abundance of BAG1 and BAG3, that determines with which co-chaperone HSP70 will interact. When one of the two degradative pathways is impaired, polyubiquitinated proteins can be rapidly rerouted to the other one through the adjustment of the BAG1/BAG3 ratio[232].

Chaperone-mediated autophagy (CMA) involves the highly specific and direct uptake of cytosolic proteins containing a lysine-phenylalanine-glutamate-arginine-glutamine (KFERQ) motif into lysosomes[233,234]. Protein targeting to CMA is based on the recognition of the KFERQ sequence by a complex comprising the constitutively expressed chaperone HSPA8 and its co-chaperones STUB1, stress-induced phosphoprotein (STIP1 or HOP), ST13 HSP70-interacting protein (ST13 or HIP), and HSP40[235,236]. Substrates are driven by this chaperone complex to the lysosomal surface, where they interact with the lysosome-associated membrane protein type 2A (LAMP2A)[237,238]. When engaged, LAMP2A assembles into oligomers that translocate unfolded clients into the lysosome with the help of HSPA8[239,240]. Once translocation is completed, LAMP2A oligomers are dismantled by HSPA8, and both receptors and substrates are degraded by lysosomal proteases[241].

Finally, microautophagy consists of the direct uptake of cytoplasmic material into small vesicles at the surface of lysosomes or late endosomes[242]. Internalisation can occur either in bulk or selectively and involves proteins that contain KFERQ-like motifs. These substrates are targeted to late endosomes by HSPA8 in cooperation with endosomal sorting complex required for transport (ESCRT) proteins. Through this route, client uptake leads to the formation of multivesicular bodies[243,244].

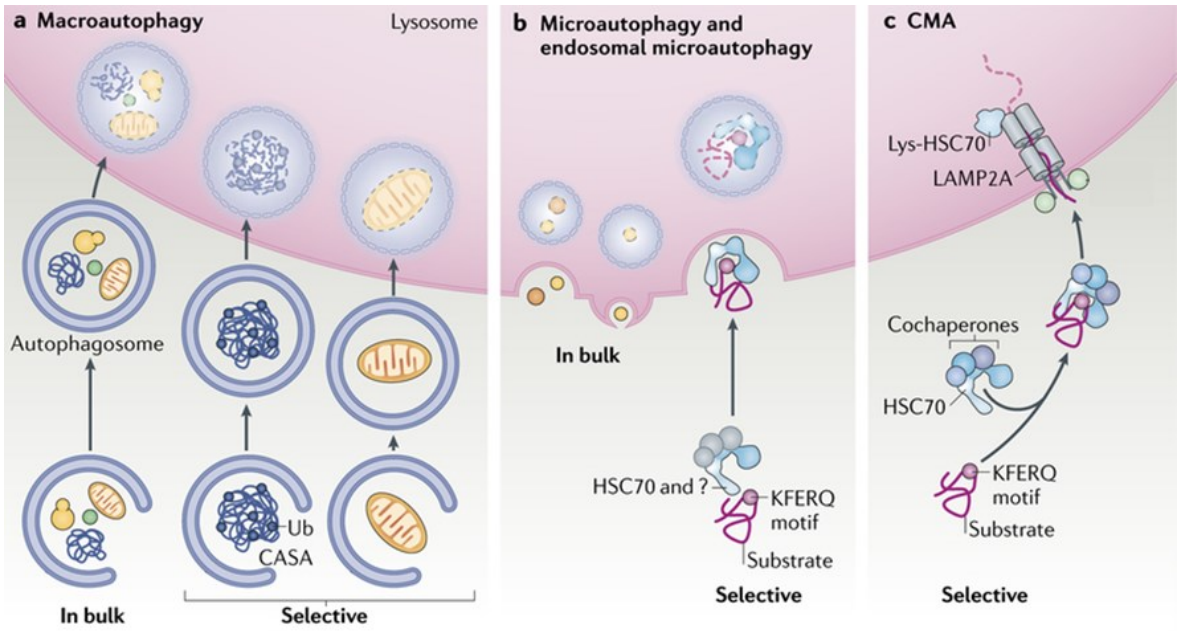

Figure 7 Schematic representation of the three main autophagy pathways. Adapted from: Kaushik S & Cuervo AM. The coming of age of chaperone-mediated autophagy. *Nat. Rev. Mol. Cell Biol*. 19, 365-381 (2018).

Role of SQSTM1/p62 in the interplay between the UPS and autophagy

SQSTM1/p62 is a multifunctional protein best characterised in its essential role as autophagy receptor. It comprises an N-terminal Phox and Bem1p-1 (PB1) ubiquitin-like domain guiding SQSTM1/p62 oligomerisation, a C-terminal ubiquitin-associated (UBA) domain involved in substrate binding, and a central MAP1LC3-interacting region (LIR) to associate with MAP1LC3 for cargo delivery to autophagosomes[230,245,246]. Additionally, the PB1 and UBA domains together participate in the interaction with other autophagy receptors like optineurin, an event that is required to coordinate autophagosome formation[247].

SQSTM1/p62 is a key player in autophagy and its levels in cells are finely regulated by a wide variety of stimuli. A potent inductor of SQSTM1/p62 upregulation is UPS dysfunction. Indeed, pharmacological blockage of the 26S proteasome leads to an increase in *SQSTM1* transcription to potentiate client degradation through autophagy[248,249]. *SQSTM1* upregulation is mediated by a wide number of transcription factors, including zinc and ring finger 2 (ZNRF2), which controls the expression of numerous genes involved in the antioxidant response, and transcription factor EB (TFEB), one of the master regulators of autophagy[250,251].

Besides its role in autophagy, SQSTM1/p62 is also known to participate in UPS-mediated protein degradation by delivering substrates directly to the 26S proteasome. The interaction between these two PQC components is mediated by SQSTM1/p62 PB1 domain, that binds to the proteasome at the level of its ATPase subunit[252]. The interaction between SQSTM1/p62 and the 26S proteasome is also essential for cells to degrade aged proteasome components through selective autophagy[253].

The interplay between SQSTM1/p62 and the UPS is thought to have a role in the impairments in proteasome-mediated degradation that can be observed when autophagy is inhibited[254,255], together with the accumulation of ubiquitinated substrates. In fact, upon prolonged autophagy blockage, SQSTM1/p62 is not only sequestered by accumulating clients, but it also recruits proteasome components and UPS regulators to these aggregates preventing them from performing their activities[252]. All the described features make SQSTM1/p62 a central regulator in the crosstalk between UPS and autophagy.

Aims

The neuron-specific conventional kinesin KIF5A is an ATP-fuelled motor protein involved in the anterograde axonal transport of a wide variety of cargoes, including proteins, RNP granules, and organelles[76,88,89,98,104]. KIF5A is organised into three protein domains. The N-terminal motor head of KIF5A binds to microtubules and hydrolyses ATP. The central coiled-coil stalk mediates KIF5A homodimerisation, interaction with KLCs, and conformational changes. The KIF5A C-terminal globular tail is required for the interaction with cargoes and adaptors, for microtubule sliding/bundling, and for autoinhibition[256], that is achieved through the direct interaction between the head and the IAK motif[68,69].

In the past 20 years, several mutations that target the *KIF5A* gene and give rise to MNDs have been identified. Heterozygous missense variants in the KIF5A head and stalk are linked to SPG10 and CMT[139,140], while frameshift mutations targeting the KIF5A tail are associated with ALS[141,142]. To date, the pathogenetic mechanisms whereby *KIF5A* mutations lead to neurodegeneration have been only partially characterised. Generally, variants in the KIF5A motor domain have been reported to impair microtubule binding and/or ATP hydrolysis, resulting in a reduction in KIF5A motility[145,148]. On the other hand, mutations causing KIF5A tail elongation (associated or not with exon 27 skipping) have been shown to abolish autoinhibition and to cause protein aggregation[150,151,257]. Despite this, the exact molecular bases by which mutations in different KIF5A domains give rise to distinct MNDs are yet to be resolved.

Based on these premises, four *KIF5A* mutations spanning the three domains of the corresponding protein and causing distinct MNDs were functionally characterised, with the aim of identifying unique and shared molecular mechanisms driving KIF5A-related disorders. The mutations (Figure 8) were selected among the ones identified through the genetic screening of a large cohort of Italian patients suffering from MNDs performed by Dr. Franco Taroni group (Fondazione IRCCS Istituto Neurologico “Carlo Besta”, Milan, Italy) and are:

- the SPG10-linked c.50A>G/p.R17Q[152] and c.838C>T/p.R280C[190] substitutions in the KIF5A head
- the CMT-associated c.2590C>T/p.R864* truncating mutation[180] in the KIF5A stalk
- the ALS-related c.3020+1G>A/p.N999Vfs*40 frameshift mutation[141,142] in the KIF5A tail.

The biochemical behaviour of the four KIF5A mutants was studied upon transient transfection of NSC-34 or SH-SY5Y cells in comparison to WT KIF5A.

Initially, mutant KIF5A distribution, solubility, protein levels, and turnover were evaluated. Then, the ability of mutant KIF5A to form dimers with the WT protein and to interact with mitochondria, well-established KIF5A cargoes, was studied, before assessing the interplay between PQC and mutant KIF5A.

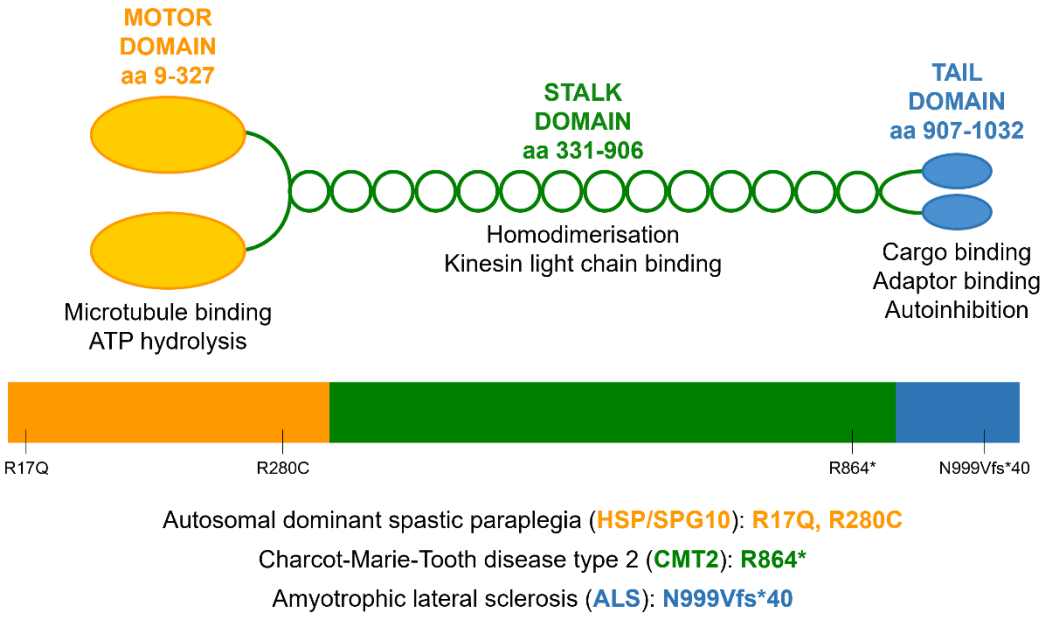

Figure 8 Schematic representation of KIF5A structure, including KIF5A domains, their main functions, and the four mutations under analysis in this thesis.

Materials and methods

Chemicals and antibodies

Cycloheximide (CHX, C6255), Z-Leu-Leu-Leu (MG132, C2211), and ammonium chloride (NH_4Cl, 254134) were purchased from Sigma-Aldrich. 10 μg/ml CHX was used to treat cells for 1, 2, 4 or 6 h to block protein synthesis and evaluate KIF5A stability. 10 μM MG132 was used to treat cells for 16 h to block the 26S proteasome. 20 mM NH_4Cl was used to treat cells for 16 h to inhibit autophagy. All antibodies used for the experiments described in this Section are listed in Table 3:

Table 3 List of the antibodies used for the experiments described in Section 1 (WB: western blot; IF: immunofluorescence).

Antibody	Dilution	Application	Source, catalogue number
Mouse monoclonal anti-KIF5A	1:1000	WB	Santa Cruz Biotechnology, sc-374666
Mouse monoclonal anti-FLAG	1:1000 1:500	WB IF	Sigma-Aldrich, F1804
Mouse monoclonal anti-GFP	1:1000	WB	Immunological Sciences, MAB-94345
Rabbit polyclonal anti-p62/SQSTM1	1:2000	WB	Sigma-Aldrich, P0067
Rabbit polyclonal anti-LC3	1: 2000	WB	Sigma-Aldrich, L8918
Mouse monoclonal anti-α-tubulin	1:2000	WB	Sigma-Aldrich, T6199
Mouse monoclonal anti-glyceraldehyde-3-phosphate dehydrogenase (GAPDH)	1:3000	WB	Immunological Sciences, MAB-10578
Rabbit monoclonal anti-β3-tubulin	1:400	IF	Cell Signaling Technologies, 5568
Alexa Fluor™ 594-conjugated goat anti-mouse IgG	1:1000	IF	Thermo Fisher Scientific, A11020
Alexa Fluor™ 594-conjugated anti-rabbit IgG	1:1000	IF	Thermo Fisher Scientific, A11072
Goat polyclonal anti-mouse IgG	1:10000	WB	Jackson ImmunoResearch, 115-035-003
Goat polyclonal anti-rabbit IgG	1:10000	WB	Jackson ImmunoResearch, 115-035-003

Plasmids and oligonucleotides

pKIF5A plasmids for the transient overexpression of WT or mutant *KIF5A* were generated by GenScript cloning the cDNA sequences of interest into the empty vector (EV) pcDNA3.1 (Invitrogen, V790-20). pFLAG-KIF5A, pGFP-KIF5A, and WT pmRFP-KIF5A plasmids were obtained starting from

pKIF5A constructs through restriction cloning. *FLAG* cDNA sequence was inserted between the AflII and NheI restriction sites immediately upstream to *KIF5A* cDNA sequence using an oligonucleotide produced by Eurofins Genomics. *GFP* and *mRFP* cDNA sequences were taken from already available donor plasmids. Both sequences were first added at their 3' with an oligonucleotide synthesised by Eurofins Genomics encoding a flexible glycine-serine linker () taking advantage of the NheI and BglII restriction sites. The *GFP/mRFP-linker* sequences were then cloned immediately upstream to *KIF5A* cDNA as described for the *FLAG* tag.

pcDNA3.1 was used as transfection mock. pEGFP-N1 (Clontech, U55762) was used to evaluate transfection efficiency in absence of fluorescent proteins/compounds or as control in immunofluorescence analyses. pYFP-α-tubulin (Evrogen, FP135) was used to label microtubules. pDsRed2-Mito (Takara, 632421) was used to label mitochondria. Ub-R-YFP was a gift from Prof. Nico Dantuma (Karolinska Institute, Stockholm, Sweden)[258]. pFLAG-VCP was kindly provided by Prof. J.P. Taylor (St. Jude Children's Research Hospital, Memphis, TN, USA).

Primers for qPCR were synthesized by Eurofins Genomics with the following sequences:

hKIF5A 5' – GGAGAACATGGAAACGGAGCA – 3' (forward), 5' – TATTCTTTGCCTCGTCCAGCAC – 3' (reverse)

hGAPDH 5' – GAAGGTGAAGGTCGGAGTC – 3' (forward), 5' – TTGATGGCAACAATATCCACTT – 3' (reverse).

Cell lines and transfection

The human neuroblastoma SH-SY5Y cell line was obtained from the American Type Culture Collection and short tandem repeat profiling was performed by Eurofins Genomics for cell line authentication. SH-SY5Y cells were cultured at 37°C in 5% CO_2 in Dulbecco's modified Eagle medium (DMEM) High Glucose (EuroClone, ECB7501L) supplemented with 10% heat-inactivated foetal bovine serum (FBS; Sigma-Aldrich, F7524), 1 mM *L*-glutamine (Sigma-Aldrich, ECB3004D), and antibiotics (penicillin, SERVA, 31749.04; streptomycin, SERVA, 35500.01). The murine motor neuron-like NSC-34 cell line was provided by Dr. Neil R. Cashman (University of British Columbia, Vancouver, BC, Canada)[259]. NSC-34 cells were cultured at 37°C in 5% CO_2 in DMEM High Glucose supplemented with 5% heat-inactivated FBS, 1 mM *L*-glutamine, and antibiotics. Both SH-SY5Y and NSC-34 cells were used between passages 5 and 25 to perform the experiments and were routinely tested for mycoplasma contamination. The SH-SY5Y neuroblastoma cell line was chosen to investigate mutant KIF5A biochemical behaviour because of its human origin. The murine NSC-34 cell line was used to analyse mutant KIF5A distribution and motility in a *bona fide* motoneuronal model not requiring differentiation.

SH-SY5Y and NSC-34 cells were transfected with Lipofectamine™ 3000 Transfection Reagent (Invitrogen, L3000015) diluted in Opti-MEM™ (Gibco, 31985070) 24 h after seeding, according to the manufacturer's instructions. The next day, cells were directly processed (SH-SY5Y cells, co-immunoprecipitation and CHX chase analysis), or the medium was changed to limit Lipofectamine™ 3000 toxicity.

Fluorescence microscopy and immunofluorescence

NSC-34 cells were seeded in 24-well plates onto 13-mm coverslips at 35,000 cells/well and transfected as previously described. 48 h after transfection, cells were fixed onto coverslips in a 1:1 solution of 4% paraformaldehyde and 4% sucrose in 0.2 M phosphate buffer (0.06 M KH_2PO_4, 0.31 M Na_2HPO_4; pH 7.4) for 25 min at 37 °C. For fluorescence microscopy analyses, nuclei were stained with 0.02% 4',6-diamidino-2-phenylindole (DAPI; Sigma-Aldrich, D9542) in phosphate-buffered saline (PBS) and coverslips were mounted with Mowiol® 4-88 Reagent (Merck, 475904). For immunofluorescence analyses, cells were incubated in PBS added with 0.1% Triton X-100, 1% bovine serum albumin (BSA; Sigma-Aldrich, A7030), and 10% heat-inactivated FBS for 45 min at room temperature (RT) for permeabilisation and blocking of nonspecific sites. Subsequently, cells were incubated with the required antibodies (Table 3) diluted in PBS containing 0.1% BSA. Primary antibodies were incubated overnight at 4°C, while secondary antibodies were incubated for 1 h at RT. Finally, nuclei were stained with DAPI and coverslips were mounted as described above. Images were acquired with a LSM 900 confocal microscope (ZEISS) using a 63× oil-immersion lens and were processed using ImageJ/Fiji (version 2.9.0).

RNA extraction from cells, reverse transcription, and quantitative PCR

SH-SY5Y cells were seeded in 12-well plates at 150,000 cells/well and transfected as previously described. 48 h after transfection, total RNA was extracted from cells using TRI Reagent® (Sigma-Aldrich, T9424) and 1-bromo-3-chloropropane (Sigma-Aldrich, B9673), following the manufacturer's instructions. RNA quantification was performed using a NanoDrop 2000 (Thermo Scientific), after which 1 µg/sample RNA was treated with DNase I (Sigma-Aldrich, AMPD1) and reverse transcribed to cDNA with the High-Capacity cDNA Reverse Transcription Kit (Applied Biosystems, 4368814). Subsequently, qPCR was performed using the iTaq SYBR Green Supermix (Bio-Rad, 1725124) in a total volume of 10 µl with 500 nmol primers (detailed above). A CFX96 Real Time System (Bio-Rad) was used according to the following cycling conditions: 94°C for 10 min, 94 °C for 15 s (40 cycles), 60 °C for 1 min. Data were expressed as C_t values and analysed with the CFX Manager™ Software (Bio-Rad; version 3.1).

Western blot

SH-SY5Y cells were seeded in 12-well plates at 150,000 cells/well and transfected as previously described. At the time of harvesting, cells were collected in their medium and centrifuged at 100 × *g* for 5 min at 4°C to remove the supernatant. Total proteins were then extracted and protein concentration was determined through bicinchoninic acid assay with QPRO BCA Kit Standard (Cyanagen, PRTD1), following the manufacturer's instructions. Subsequently, 15-20 µg total proteins were incubated for denaturation in sample buffer [0.6% Tris, 2% sodium dodecyl sulphate (SDS), 10% glycerol, 5% β-mercaptoethanol, pH 6.8] at 100°C for 5 min and loaded on 10%-15% SDS-polyacrylamide gels. Separated proteins were then transferred to 0.45-µm nitrocellulose membranes (Cytiva, GE10600002) using a Trans-Blot® Turbo™ Transfer System (Bio-Rad). For the immunochemical detection of proteins, membranes were initially incubated in 5% non-fat dried milk (Bio Basic, NB0669) diluted in Tris-buffered saline with Tween 20 (TBS-T; 20 mM Tris-HCl pH 7.5, 0.5 M NaCl, 0.05% Tween 20; pH 7.6) for 1 h at RT to block non-specific sites and then probed using the required antibodies at the conditions reported in Table 3. Primary antibodies were diluted in blocking solution and incubated overnight at 4°C, while secondary antibodies were diluted in TBS-T and incubated for 1 h at RT. Immunoreactivity was detected using Westar chemiluminescent reagents (Cyanagen). Images were acquired using a ChemiDoc™ XRS+ System (Bio-Rad) and optical density was analysed with the Image Lab™ Software (Bio-Rad; version 6.0.1).

To analyse KIF5A solubility, SH-SY5Y cells were harvested 48 h after transfection as described above, resuspended in Nonidet P-40 (NP-40) lysis buffer (150 mM NaCl, 20 mM Tris base, 0.05% NP-40, 1.5 mM $MgCl_2$, 3% glycerol; pH 7.4) added with 1 mM dithiothreitol (DTT; Roche, 3483-12-3) and Protease Inhibitor Cocktail (Sigma-Aldrich, P8340), and passed 10 times through a syringe needle (27G x 1/2") for lysis. Then, 20 µg total proteins were diluted in 15 µl NP-40 lysis buffer and were centrifuged at 16,100 × *g* for 15 min at 4°C. NP-40–soluble supernatants were collected, while NP-40–insoluble pellets were resuspended in the same volume of NP-40 lysis buffer (without protease inhibitor and DTT) and sonicated. Both NP-40–soluble and NP-40-insoluble fractions were then analysed.

To compare WT and mutant KIF5A turnover, 24 h after transfection SH-SY5Y cells were incubated with fresh medium added with CHX and collected at the previously indicated time points, except for control samples which were immediately harvested. After the last collection, cells were resuspended in PBS added with protease inhibitor and lysed through slight sonication to extract proteins.

In all other cases, SH-SY5Y cells were harvested 48 h after transfection and processed to extract proteins in PBS as described.

Co-immunoprecipitation

SH-SY5Y cells were seeded in 6-well plates at 300,000 cells/well and transfected as previously described. The next day, cells were harvested in their medium pooling 3 wells per experimental condition and centrifuged at 100 × *g* for 5 min at 4°C. Pellets were resuspended in radioimmunoprecipitation assay (RIPA) buffer (150 mM NaCl, 0.5% Na-deoxycholate, 100 µM Na-orthovanadate, 50 mM NaF, 50 mM M Tris-HCl pH 7.7, 10 mM EDTA pH 8, 0.08% SDS, 0.8% Triton X-100) added with cOmplete Protease Inhibitor Cocktail (Sigma-Aldrich, 4693116001), incubated on ice for 20 min, and centrifuged at 16,000 × *g* for 15 min at 4°C for clearing. 100 µl/sample SureBeads™ Protein G Magnetic Beads (Bio-Rad, 1614023) were conjugated to 2 µg/sample mouse monoclonal anti-FLAG antibody (Sigma-Aldrich, F1804) diluted in PBS with 0.1% Tween 20 (PBS-T) for 10 min at RT and washed in PBS-T. Antibody–conjugated beads were then incubated with 250 µg/sample RIPA-soluble protein extracts for 1 h at 4°C. After washing in PBS-T, immunoprecipitated proteins were eluted from the beads with Laemmli Sample Buffer (Bio-Rad, 1610737) added with 5% β-mercaptoethanol by incubating samples for 10 min at 70°C. Immunoprecipitation, input, and output samples were then loaded on 7.5% gels and analysed through western blot.

Proteasome activity assay

SH-SY5Y cells were seeded in 6-well plates at 300,000 cells/well and transfected as previously described. 48 h after transfection, cells were harvested in their medium, centrifuged at 600 × *g* for 5 min, and washed three times in PBS. Pellets were then homogenised in PBS with 0.5% NP-40 and centrifuged at 1300 × *g* for 15 min. Supernatants were subsequently collected, and protein concentration was quantified as described. Reaction mixtures were prepared diluting 50 µg total proteins in 50 mM HEPES-KOH pH 8.0 added with 5 mM EGTA and 5 mM ATP (Sigma-Aldrich, A1852) to a final volume of 500 µl. 50 nM 7-amino-4-methyl coumarin (AMC)-conjugated substrates were added to the reaction mixtures to quantify the chymotryptic-like (*N*-Suc-LLVY-AMC, Sigma-Aldrich, S6510) and the caspase-like (Z-LLE-AMC, Sigma-Aldrich, C0483) activities of the 26S proteasome. Finally, samples were incubated for 45 min at 37°C and fluorescence was measured at 340 nm excitation and 460 nm emission wavelengths using an Enspire® Multimode Plate Reader (Perkin Elmer).

Statistics

One- or two-way ANOVA tests followed by Dunnett's post-test or Fisher's LSD post-test were applied, according to figure captions. $P < 0.05$ was considered significant. All analyses were performed using the GraphPad PRISM software (version 8.0.2).

Results

C-terminal KIF5A mutants show an aberrant distribution in cells

To characterise the intracellular distribution of the selected KIF5A variants, NSC-34 cells were transiently transfected with pGFP-KIF5A constructs and analysed through immunofluorescence. β3-tubulin distribution was probed to label microtubules. As expected, WT KIF5A appeared diffused across the whole NSC-34 cytoplasm, both around the cell body and within neurites (Figure 9A). A similar distribution was observed for the SPG10-linked R17Q and R280C KIF5A mutants, even if the latter also accumulated into small perinuclear puncta in few cells (Figure 9A-B). On the other hand, both the CMT-related R864* and the ALS-associated N999Vfs*40 KIF5A mutants preferentially localised within neurites, and while the former appeared diffused within cell protrusions the latter accumulated into inclusions at neurite tips (Figure 9A). The intracellular distribution observed for the R864* and N999Vfs*40 KIF5A mutants could be a consequence of an impaired autoinhibitory function, that should result in a constitutively active kinesin moving to axon tips even in absence of cargo[68,69]. Altered autoinhibition could depend on the loss of KIF5A C-terminal tail for R864* KIF5A and on tail modification for N999Vfs*40 KIF5A, as already reported[150,151].

To exclude that the distribution observed for WT and mutant KIF5A could be affected by the GFP tag, the analysis was repeated transfecting NSC-34 cells with the pFLAG-KIF5A constructs. In this case, microtubules were labelled by transiently overexpressing YFP-tagged α-tubulin and KIF5A localisation was probed with an anti-FLAG antibody. The intracellular distribution displayed by FLAG-tagged WT and mutant KIF5A fully replicated the patterns observed for the GFP-tagged proteins (Figure 9C), indicating that mutant KIF5A localisation is not influenced by the protein tag. In both analyses, overexpression of WT or mutant KIF5A did not have any evident impact on the NSC-34 microtubule network.

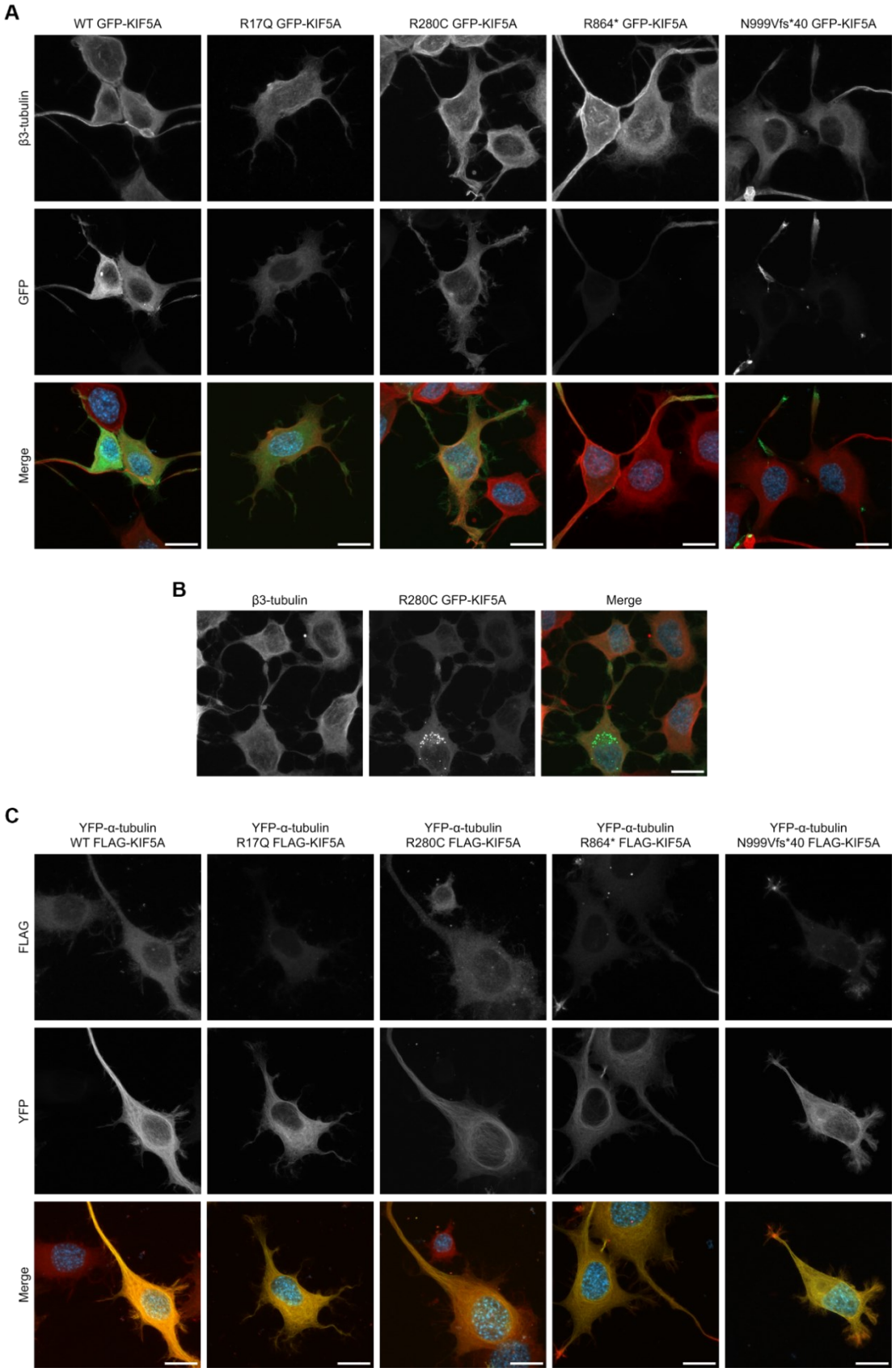

Figure 9 Mutant KIF5A localisation. (A, B) Confocal microscopy analysis (63× magnification) of NSC-34 cells transiently transfected with pGFP-KIF5A constructs (wild type-WT). Endogenous β3-tubulin was stained in red. Nuclei were stained with DAPI. Scale bars 20 µm. **(C)** Confocal microscopy analysis (63× magnification) of NSC-34 cells transiently co-transfected with pFLAG-KIF5A constructs and pTagYFP-α-tubulin. Nuclei were stained with DAPI. Scale bars 20 µm.

Mutant KIF5A displays altered protein levels and solubility

To further characterise the biochemical features of the four KIF5A mutants under investigation, SH-SY5Y cells were transiently transfected with pKIF5A constructs and processed for total RNA or protein extraction 48 h after transfection. qRT-PCR analysis evidenced comparable WT and mutant *KIF5A* overexpression levels in SH-SY5Y cells when compared with cells transfected with the EV pcDNA3.1 (Figure 10A). Similarly, protein levels were equivalent between WT and R280C KIF5A; however, the R17Q and N999Vfs*40 KIF5A mutants displayed significantly lower protein levels, while R864* KIF5A displayed a trend towards higher protein levels compared to WT KIF5A (Figure 10B). In parallel, total proteins extracted from SH-SY5Y cells transiently transfected with pKIF5A constructs were separated based on their NP-40 solubility. Consistently with the inclusions in neuronal processes observed via immunofluorescence (Figure 9), N999Vfs*40 KIF5A equally partitioned between the soluble and insoluble protein fractions, differently from WT KIF5A and the other KIF5A mutants, which were largely detergent-soluble (Figure 10C). This suggests a potential gain of toxic function for N999Vfs*40 KIF5A.

Taking together the qRT-PCR and western blot results, the differences in protein levels observed between WT and mutant KIF5A appeared to depend on distinct protein stability or turnover rather than on transcription-related mechanisms. To confirm this hypothesis, mutant KIF5A turnover was assessed by transiently transfecting SH-SY5Y cells with constructs encoding untagged WT, R17Q, R864*, or N999Vfs*40 KIF5A for 24 h and then performing CHX chase, which restricts translation via ribosome inhibition. As expected, while WT KIF5A displayed a half-life of approximately 6 h, the protein levels of the R17Q and N999Vfs*40 KIF5A mutants were reduced by approximately 90% and 75% in the same time interval, respectively. On the other hand, no differences were observed between R864* and WT KIF5A degradation profiles (Figure 10D). Therefore, a significant reduction in protein levels caused by protein instability and potentially restricting the pool of KIF5A motors available for anterograde transport was observed for R17Q and N999Vfs*40 KIF5A, but not for the other mutants under investigation.

To look for potential molecular mechanisms underpinning the fast turnover displayed by R17Q KIF5A, the three-dimensional structure of its motor domain was reconstructed with Swiss-MODEL to test whether the associated change in amino acid could alter KIF5A conformation. Although this was not the case, Swiss-MODEL analysis predicted a weakening in the ability to bind to ATP for the R17Q KIF5A mutant compared to WT KIF5A, possibly because of the change in steric hindrance produced by the arginine-to-glutamine substitution in close proximity to the nucleotide-binding pocket of KIF5A motor domain (Figure 10E).

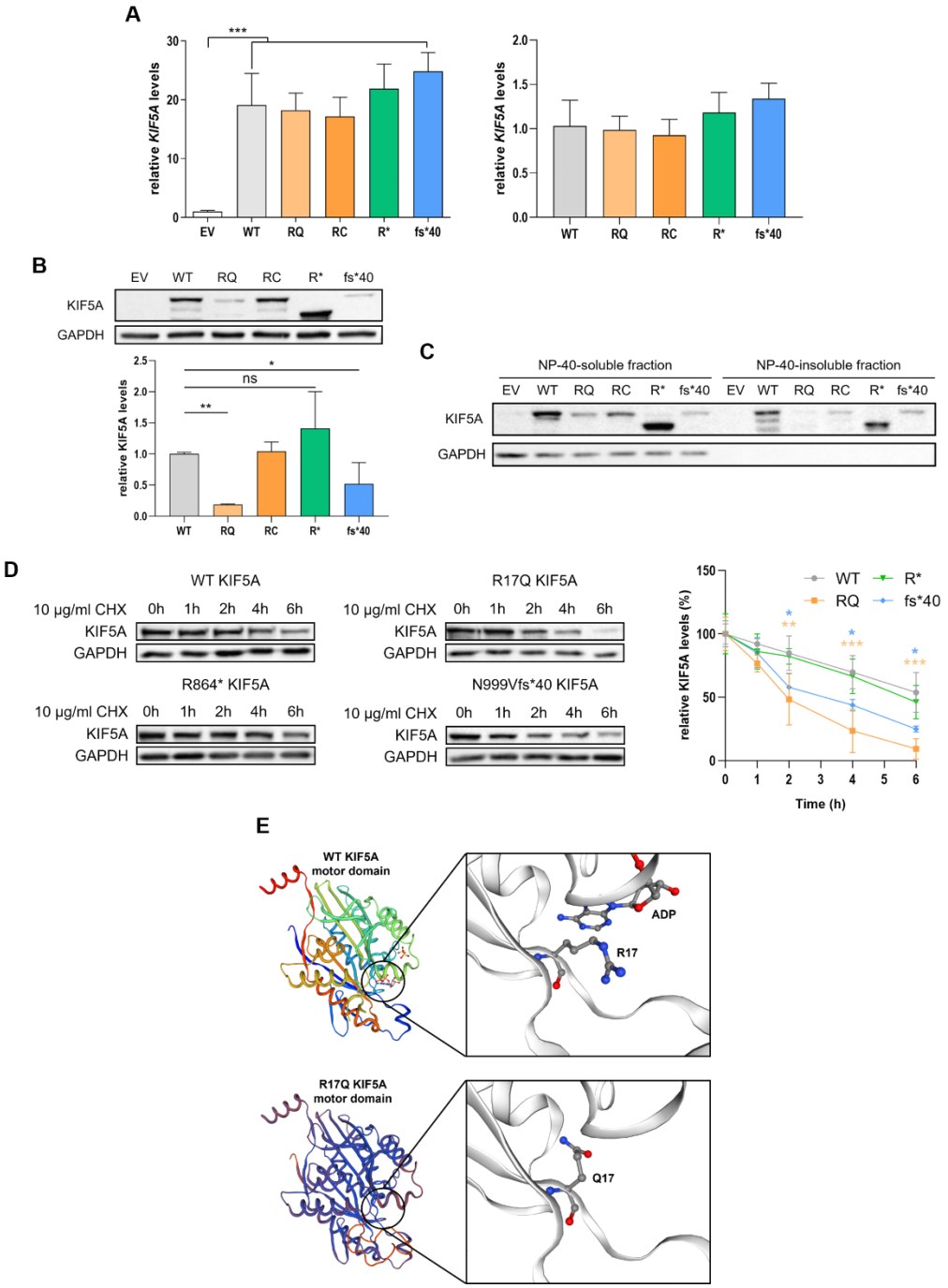

Figure 10 Mutant KIF5A levels and solubility. (A) RT-qPCR analysis of *KIF5A* mRNA levels in SH-SY5Y cells transiently transfected with pKIF5A constructs (wild type-WT, R17Q-RQ, R280C-RC, R864*-R*, N999Vfs*40-fs*40). *GAPDH* mRNA levels were used for normalisation. Bar graphs represent mean *KIF5A* mRNA levels relatively to samples transfected with the empty vector (EV; left graph) or overexpressing WT *KIF5A* (right graph) ± SD. n = 3; ***: P < 0.001. **(B)** Western blot analysis of KIF5A protein levels in SH-SY5Y cells transiently transfected with pKIF5A constructs. GAPDH protein levels were used for normalisation. Bar graph represents mean optical densities relative to samples overexpressing WT KIF5A ± SD. One-way ANOVA with Fisher's LSD post-test was performed. n = 4; ns = not significant; * = P < 0.05; ** = P < 0.01. **(C)** Western blot analysis of KIF5A fractionation between the NP-40–soluble and the NP-40–insoluble protein fraction in SH-SY5Y cells transiently transfected with pKIF5A constructs. **(D)** Western blot analysis of KIF5A protein levels in SH-SY5Y cells transiently transfected with WT, R17Q, R864*, or N999Vfs*40 pKIF5A constructs and treated with 10µg/ml cycloheximide (CHX) for 1, 2, 4 or 6 h. GAPDH protein levels were used for normalisation. Graph represents mean optical densities expressed as percentages of either WT or mutant KIF5A baseline (i.e., 0h) levels ± SD. Two-way ANOVA with Dunnett's post-test was performed comparing WT and mutant KIF5A protein levels at each time point. n = 3; * = P <0.05; ** = P < 0.01; *** = P < 0.001. **(E)** R17Q KIF5A motor domain structure modelled by SWISS-MODEL using WT KIF5A head as template (SMTL ID: 1mkj.1). Modelling predicts the alteration of the ATP-binding site in KIF5A motor domain as a consequence of the R17Q substitution.

Mutant KIF5A dimerises with the WT protein and C-terminal mutants lack interaction with mitochondria

In neurons, KIF5A participates in anterograde axonal transport as homodimer[62]. To test whether the KIF5A mutants under analysis can dimerise with the WT protein, NSC-34 cells were co-transfected with the same amount of WT pmRFP-KIF5A and pGFP-KIF5A constructs and analysed through immunofluorescence to assess WT and mutant KIF5A reciprocal distribution. As shown in Figure 11A, WT KIF5A co-distributed with all the mutants in study. Of note, N999Vfs*40 KIF5A partially sequestered the WT protein to cell periphery within its aggregates, a finding in line with previous reports on ALS-KIF5A variants[150,151]. The interaction between WT and mutant KIF5A was confirmed by co-immunoprecipitating WT GFP-KIF5A with mutant FLAG-KIF5A from SH-SY5Y RIPA extracts (Figure 11B). These observations hint at a possible dominant negative effect of partial WT KIF5A sequestration exerted by the N999Vfs*40 KIF5A mutant.

Since KIF5A transports mitochondria in neurons[88,89], the reciprocal distribution of mutant KIF5A and mitochondria was tested by co-transfecting NSC-34 cells with the mitochondrial reporter pDsRed2-Mito and pGFP-KIF5A constructs. Confocal microscopy analysis showed a similar co-distribution with mitochondria for the R17Q and R280C KIF5A mutants compared to the WT protein, while only partial co-distribution of the R864* and N999Vfs*40 KIF5A mutants and mitochondria was observed (Figure 11C). This suggests that the R864* and N999Vfs*40 KIF5A mutants are defective in interacting with one of the best characterised KIF5A cargoes, potentially contributing to pathogenesis. Indeed, mitochondrial dysfunction is tightly linked to several MNDs, including *KIF5A*-related phenotypes [260]. Notably, a similar alteration in mitochondrial distribution was recently reported in an ALS-KIF5A *Drosophila* model[261].

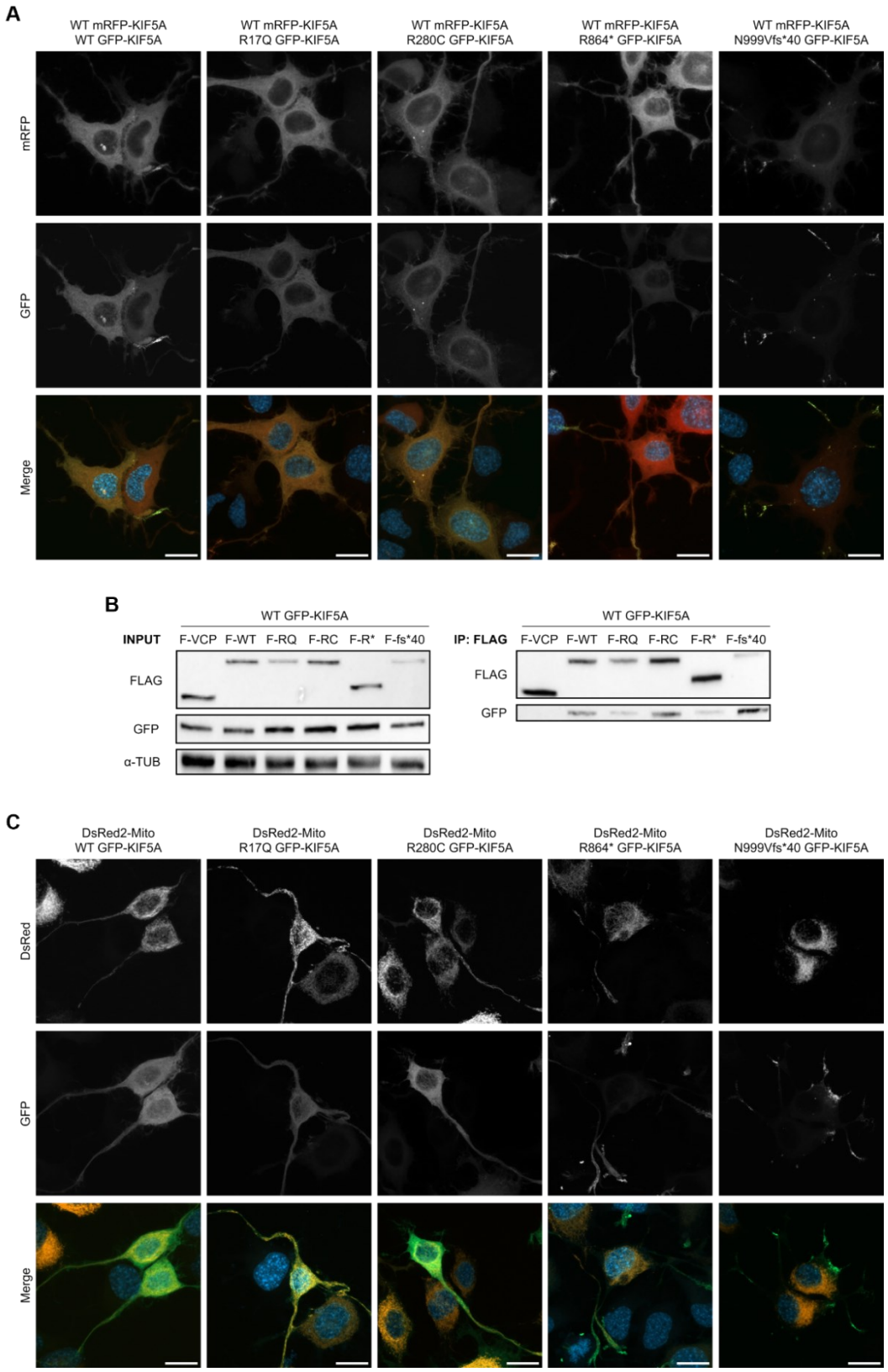

Figure 11 Reciprocal distribution of mutant KIF5A and the WT protein or mitochondria. (A) Confocal microscopy analysis (63× magnification) of NSC-34 cells transiently co-transfected with equal amounts of wild type (WT) pmRFP-KIF5A and pGFP-KIF5A constructs. Nuclei were stained with DAPI. Scale bars 20 µm. **(B)** Co-immunoprecipitation between mutant and WT KIF5A extracted from SH-SY5Y cells transiently co-transfected with equal amounts of WT pGFP-KIF5A and pFLAG-KIF5A constructs (FLAG-F, wild type-WT, R17Q-RQ, R280C-RC, R864*-R*, N999Vfs*40-fs*40). FLAG-VCP (F-VCP) was used as control for anti-FLAG immunoprecipitation. **(C)** Confocal microscopy analysis (63× magnification) of NSC-34 transiently co-transfected with pDsRed2-Mito and pGFP-KIF5A constructs. Nuclei were stained with DAPI. Scale bars 20 µm.

Mutant KIF5A does not alter the basal autophagy flux but ALS-KIF5A shows an aberrant interaction with SQSTM1/p62

Conventional kinesins like KIF5A are known to take part in lysosomal transport[98,262,263]. This role makes the KIF5s potential players in autophagy, which is one of the main protein degradation pathways in cells particularly for protein aggregates[231]. Since two of the KIF5A mutants under analysis display faster protein turnover and/or an aggregation-prone behaviour (Figure 10), the possible interplay between autophagy and mutant KIF5A was investigated.

Initially, the basal protein levels of the autophagy markers SQSTM1/p62 and MAP1LC3 were quantified in SH-SY5Y cells transiently transfected with pKIF5A constructs. Both SQSTM1/p62 and MAP1LC3 protein levels were unaltered by KIF5A overexpression in all tested conditions (Figure 12A). Immunofluorescence analysis performed on NSC-34 cells transiently transfected with pGFP-KIF5A constructs did not evidence any alteration in endogenous MAP1LC3 intracellular localisation, while N999Vfs*40 GFP-KIF5A aggregates were found to be positive for SQSTM1/p62, even if the overall distribution of the autophagy receptor did not change in transfected cells (Figure 12B). The direct interaction between N999Vfs*40 KIF5A and endogenous SQSTM1/p62 was confirmed by co-immunoprecipitation performed on SH-SY5Y cells transiently transfected with pFLAG-KIF5A constructs (Figure 12C).

The abnormal interaction between N999Vfs*40 KIF5A and SQSTM1/p62 is consistent with previous reports[150,151] and indicates that this short-lived and aggregation-prone mutant could be targeted for degradation by the autophagy receptor SQSTM1/p62. Therefore, to test whether mutant KIF5A was recycled via autophagy, autophagosome-lysosome fusion was inhibited with NH_4Cl in SH-SY5Y cells transiently transfected with pKIF5A constructs and KIF5A protein levels were assessed through western blot. Both WT and mutant KIF5A did not accumulate upon treatment despite the increase in SQSTM1/p62 and MAP1LC3-II protein levels confirming autophagy inhibition. This suggests that autophagy does not represent the preferential degradation route for WT and mutant KIF5A (Figure 12D). Autophagy blockage did not induce any alterations in KIF5A distribution, too, as observed in NSC-34 cells transiently transfected with pGFP-KIF5A constructs and treated with NH_4Cl (Figure 12E).

Together, these results show that KIF5A overexpression does not alter basal autophagy and that this pathway does not represent the main degradation route for KIF5A in spite of the aberrant interaction observed between SQSTM1/p62 and the N999Vfs*40 KIF5A mutant.

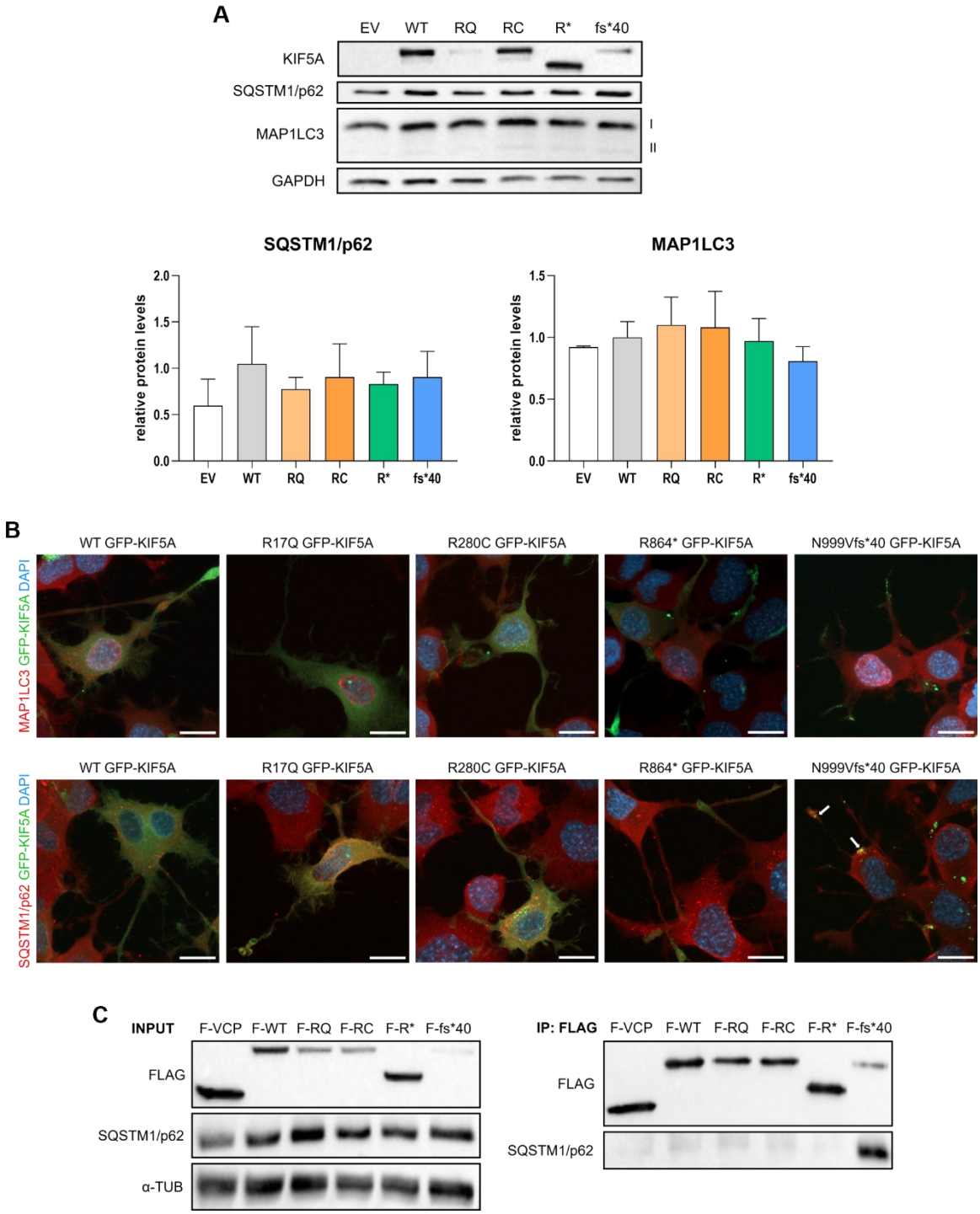
A
EV
WT
RQ
RC
R*
fs*40
KIF5A
SQSTM1/p62
MAP1LC3
I
II
GAPDH
SQSTM1/p62
MAP1LC3
relative protein levels
2.0
1.5
1.0
0.5
0.0
EV
WT
RQ
RC
R*
fs*40
B
WT GFP-KIF5A
R17Q GFP-KIF5A
R280C GFP-KIF5A
R864* GFP-KIF5A
N999Vfs*40 GFP-KIF5A
MAP1LC3 GFP-KIF5A DAPI
SQSTM1/p62 GFP-KIF5A DAPI
C
INPUT
F-VCP
F-WT
F-RQ
F-RC
F-R*
F-fs*40
FLAG
SQSTM1/p62
α-TUB
IP: FLAG
F-VCP
F-WT
F-RQ
F-RC
F-R*
F-fs*40
FLAG
SQSTM1/p62

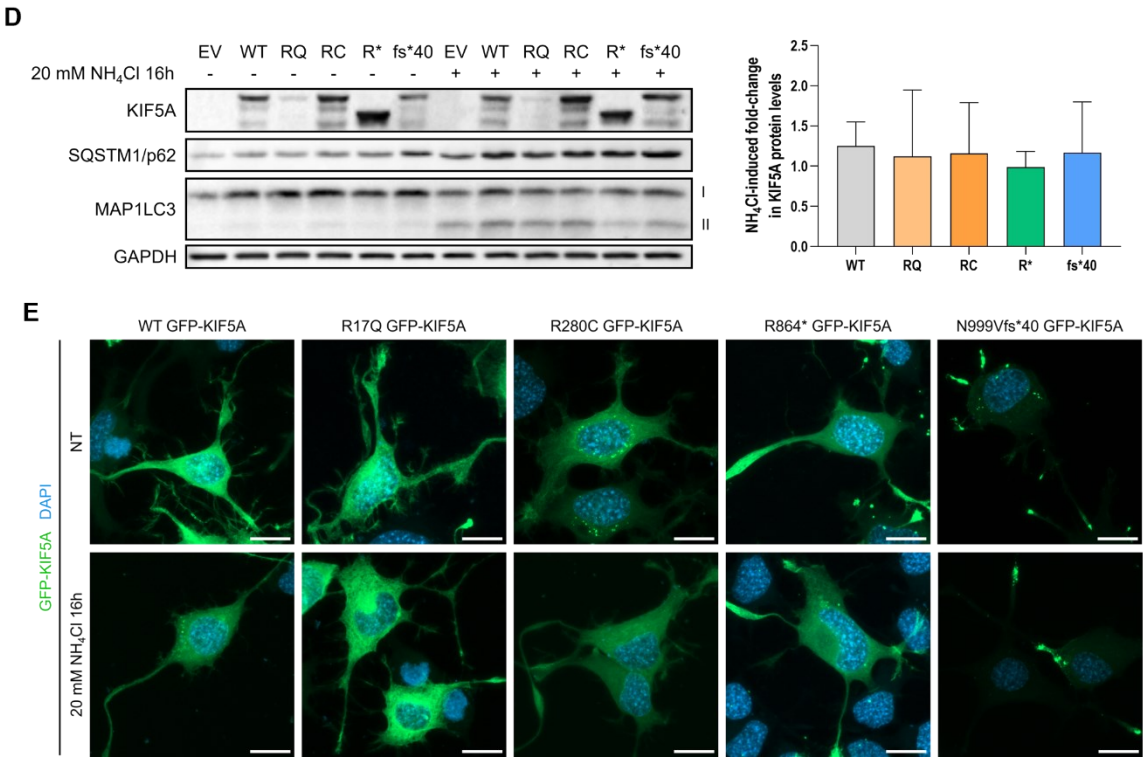

Figure 12 Interplay between mutant KIF5A and autophagy. (A) Western blot analysis of basal SQSTM1/p62 and MAP1LC3 protein levels in SH-SY5Y cells transiently transfected with pKIF5A constructs (empty vector-EV, wild type-WT, R17Q-RQ, R280C-RC, R864*-R*, N999Vfs*40-fs*40). GAPDH protein levels were used for normalisation. Bar graphs represent mean SQSTM1/p62 (left graph) and MAP1LC3 (right graph) optical densities relative to samples overexpressing WT KIF5A ± SD. One-way ANOVA with Fisher's LSD post-test was performed. n = 3. **(B)** Confocal microscopy analysis (63× magnification) of NSC-34 cells transiently transfected with pGFP-KIF5A constructs. Endogenous MAP1LC3 (top panel) or SQSTM1/p62 (bottom panel) were stained in red. Nuclei were stained with DAPI. Arrows highlight co-localisation between N999Vfs*40 KIF5A and SQSTM1/p62. Scale bars 20 µm. **(C)** Co-immunoprecipitation between N999Vfs*40 KIF5A and endogenous SQSTM1/p62 extracted from SH-SY5Y cells transiently transfected with pFLAG-KIF5A constructs (FLAG-F, wild type-WT, R17Q-RQ, R280C-RC, R864*-R*, N999Vfs*40-fs*40). FLAG-VCP (F-VCP) was used as control for anti-FLAG immunoprecipitation. (**D**) Western blot analysis of KIF5A protein levels in SH-SY5Y cells transiently transfected with pKIF5A constructs and treated with 20 mM ammonium chloride (NH_4Cl) for 16 h. GAPDH protein levels were used for normalisation. Bar graphs represent fold-change of WT or mutant KIF5A protein levels induced by the treatment. One-way ANOVA with Fisher's LSD post-test was performed. n = 3. **(E)** Confocal microscopy analysis (63× magnification) of NSC-34 cells transiently transfected with pGFP-KIF5A constructs and treated with 20 mM NH_4Cl for 16 h. Scale bars 20 µm.

Degradation of WT and mutant KIF5A is mainly mediated by the UPS

Since no significant involvement of autophagy in KIF5A degradation was observed, the role of the UPS in the enhanced turnover of R17Q and N999Vfs*40 KIF5A was subsequently evaluated. Importantly, SQSTM1/p62 can either act as autophagy receptor[230] or directly deliver ubiquitinated substrates to the 26S proteasome[252]. SQSTM1/p62 co-localisation with N999Vfs*40 KIF5A could therefore underpin its targeting to the UPS rather than autophagy.

Initially, SH-SY5Y cells were transiently transfected with pKIF5A constructs and treated with the 26S proteasome inhibitor MG132. Western blot analysis showed an increase in protein levels for both WT and mutant KIF5A upon treatment, suggesting that they are mainly degraded by the UPS. Notably, such accumulation (i.e., fold-change of GAPDH-normalised KIF5A protein levels induced by MG132) was statistically higher for the short-lived R17Q and N999Vfs*40 KIF5A mutants compared with the WT protein (Figure 13A). Moreover, the NP-40 fractionation of proteins extracted from treated cells evidenced that proteasome blockage induced preferential partitioning in the insoluble fraction for N999Vfs*40 KIF5A, which was already observed to be partially NP-40–insoluble (Figure 8), and even for the R17Q KIF5A mutant, that on the other hand was completely soluble in NP-40 in basal conditions (Figure 13B). Confocal microscopy analysis of NSC-34 cells transiently transfected with pGFP-KIF5A constructs and treated with MG132 confirmed the formation of large inclusions localising around the cell body upon proteasome inhibition by R17Q and N999Vfs*40 KIF5A, differently from WT KIF5A and the other mutants in study, that remained largely diffused in the cytoplasm (Figure 13C). These observations indicate that the R17Q and N999Vfs*40 KIF5A mutants may form harmful aggregates in neurons upon proteostasis impairment.

To further investigate the interplay between the UPS and mutant KIF5A, SH-SY5Y cells were transiently co-transfected with pKIF5A constructs and with the Ub-R-YFP reporter, encoding an N-end rule degradation substrate that is rapidly eliminated by the 26S proteasome in basal conditions, but accumulates in cells upon UPS impairment[258]. Western blot analysis showed that Ub-R-YFP significantly accumulated in SH-SY5Y cells overexpressing R280C or N999Vfs*40 KIF5A compared to cells overexpressing the WT protein (Figure 13D), hinting that both KIF5A mutants may have a direct impact on proteasome activity. Since Ub-R-YFP accumulation in cells may result either from UPS inhibition or through competition between proteasome substrates, the activity of the 26S proteasome was assayed in SH-SY5Y cells transiently transfected with pKIF5A constructs to test which was the case. The assay was performed by measuring the conversion rate of two AMC-conjugated substrates specifically targeted by the chymotrypsin-like and the caspase-like activity of the 26S proteasome, respectively, namely *N*-Suc-LLVY-AMC and Z-LLE-AMC. AMC-emitted

fluorescence was therefore considered directly proportional to UPS engagement. The analysis indicated that the UPS was not inhibited by KIF5A overexpression, as its chymotrypsin- and caspase-like activities were similar in all tested conditions (Figure 11E). These results suggest that the R280C and N999Vfs*40 KIF5A mutants compete with Ub-R-YFP for degradation.

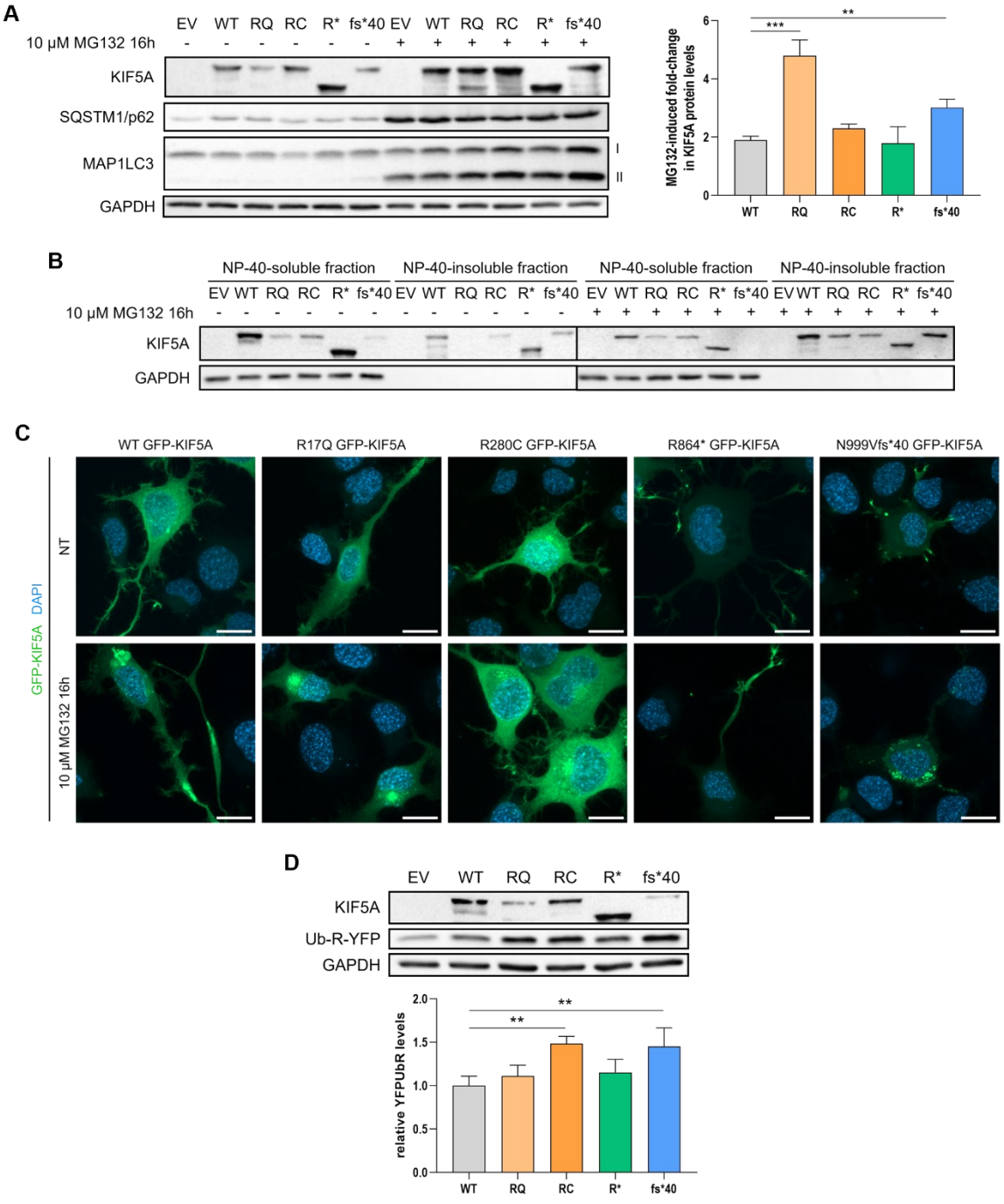

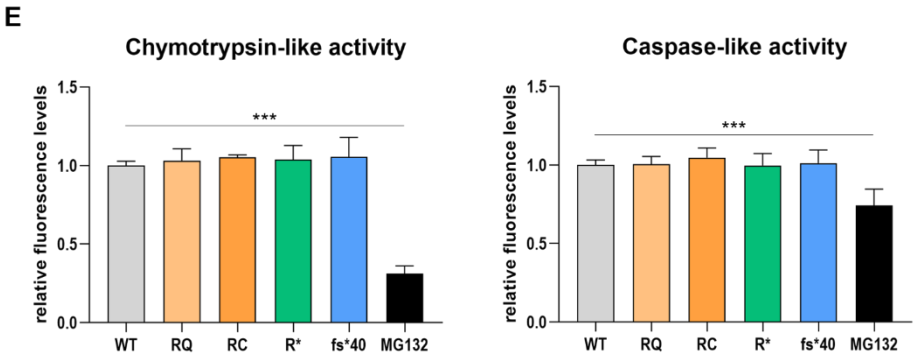

Figure 13 Interplay between mutant KIF5A and the ubiquitin-proteasome system. (A) Western blot analysis of KIF5A protein levels in SH-SY5Y cells transiently transfected with pKIF5A constructs (empty vector-EV, wild type-WT, R17Q-RQ, R280C-RC, R864*-R*, N999Vfs*40-fs*40) and treated with 10 µM Z-Leu-Leu-Leu (MG132) for 16 h. GAPDH protein levels were used for normalisation. Bar graphs represent fold-change of wild type (WT) or mutant KIF5A protein levels induced by the treatment. One-way ANOVA with Fisher's LSD post-test was performed. n = 3; ** = $P < 0.01$; *** = $P < 0.001$. **(B)** Western blot analysis of KIF5A fractionation between the NP-40–soluble and the NP-40–insoluble protein fraction in SH-SY5Y transiently transfected with pKIF5A constructs and treated with 10 µM MG132 for 16 h. **(C)** Confocal microscopy analysis (63× magnification) of NSC-34 cells transiently transfected with pGFP-KIF5A constructs and treated with 10 µM MG132 for 16 h. Nuclei were stained with DAPI. Scale bars 20 µm. **(D)** Western blot analysis of Ub-R-YFP protein levels in SH-SY5Y transiently co-transfected with Ub-R-YFP and pKIF5A constructs. GAPDH protein levels were used for normalisation. Bar graph represents mean Ub-R-YFP optical densities relatively to samples overexpressing WT KIF5A ± SD. One-way ANOVA with Fisher's LSD post-test was performed. n = 3; ** = $P < 0.01$. **(E)** Proteasome activity analysis in SH-SY5Y cells overexpressing pKIF5A constructs. Specific 7-amino-4-methyl coumarin (AMC)-conjugated peptides (N-Suc-LLVY-AMC and Z-LLE-AMC) were used to evaluate chymotrypsin-like (left graph) and caspase-like (right graph) proteasome activities. Untransfected samples treated with 1 µM MG132 for 16 h were used as control. Bar graphs represent mean fluorescence levels relatively to samples overexpressing WT KIF5A ± SD. One-way ANOVA with Fisher's LSD post-test was performed. n = 3; * = $P < 0.05$; *** = $P < 0.001$.

Discussion

The neuron specific kinesin KIF5A, a key player in axonal transport, comprises three domains: the KIF5A head acts as ATP-dependent and microtubule-based motor domain, its stalk mediates dimerisation and conformational changes, and its tail binds to cargoes and adaptors and is essential for autoinhibition[15]. *KIF5A* mutations give rise to distinct MNDs depending on which of the corresponding protein domains is targeted, but the processes underpinning such genotype/phenotype heterogeneity are not yet fully clear. The experiments described in this Section were aimed at functionally characterising four disease-associated KIF5A mutants (R17Q, R280C, R864*, N999Vfs*40 KIF5A) to elucidate the shared and unique molecular mechanisms underpinning KIF5A-related neurodegeneration (Figure 14).

The first biochemical behaviour shared by the KIF5A mutants under analysis in this thesis is the peripheral localisation of the C-terminal mutants R864* and N999Vfs*40 KIF5A. Such distribution is consistent with the inability of these KIF5A mutants to perform autoinhibition. The R864* KIF5A mutant lacks the IAK motif due to premature protein truncation, which possibly justifies its altered intracellular localisation. Concerning the loss of KIF5A autoinhibition observed for N999Vfs*40 KIF5A, it has been linked to the substitution of seven negatively charged amino acids with nine positively charged ones in the ALS-KIF5A C-terminal domain generated by frameshift mutations: this change in charge is predicted to tamper with the stability of the KIF5A autoinhibited state[150]. Besides the waste of cellular energy, the main functional consequence of autoinhibition loss is the rapid depletion from the pool of motors available for anterograde transport of mutant KIF5A, and this could cause imbalances in axonal trafficking.

An additional shared molecular feature between R864* and N999Vfs*40 KIF5A is that both may be unable to interact with KIF5A-specific cargoes, due to C-terminus truncation for the R864* KIF5A mutant and to the translational frameshift affecting the tail domain for N999Vfs*40 KIF5A. Since not all adaptor binding sites on the KIF5A stalk are fully deleted by the R864* truncation (e.g., KLC binding is mediated by amino acids 770-811 in the KIF5A central domain[63]), the interaction with specific cargoes should be preserved; accordingly, additional analyses are required to better define R864* KIF5A interactome and to evaluate the impact of this truncated mutant on axonal transport. Regarding N999Vfs*40 KIF5A, conflicting data on its ability to bind to cargoes, particularly to mitochondria, are present in the literature. Indeed, Baron *et al.*[150] reported an increase in the percentage of moving mitochondria and in their anterograde velocity in primary motor neurons upon ALS-KIF5A overexpression in comparison to cells overexpressing WT KIF5A; oppositely, Pant and colleagues[151] did not observe any co-distribution between mitochondria and ALS-KIF5A inclusions in primary cortical neurons. Although quantification of immunofluorescence analyses

evaluating mitochondrial distribution upon mutant KIF5A overexpression or immunoprecipitation experiments testing the interaction between mutant KIF5A and mitochondria were not performed, the pieces of evidence presented in this thesis are in line with the observations made by Pant *et al*. Absence of co-distribution between mitochondria and ALS-KIF5A is not necessarily a sign of the inability of individual mutant KIF5A motors to interact with these organelles, but it indicates that this interaction may be lost when ALS-KIF5A undergoes oligomerisation and aggregation. In such context, the combination of the distal accumulation of mitochondria or other KIF5A cargoes occurring via soluble KIF5A motors and the impaired recycling of oligomerised ALS-KIF5A to the perinuclear region may also result in an opposite effect of enhanced retrograde trafficking, causing additional imbalances in axonal transport. This loop might be further exacerbated by WT KIF5A sequestration into mutant KIF5A aggregates, which other kinesins would be unable to counteract when the cargoes are KIF5A-specific. A similar alteration in the equilibrium of axonal trafficking may occur in the presence of the R864* KIF5A mutant, which could promote the rapid removal of the WT protein from the cytoplasm through direct interaction within heterodimers. Additional analyses aimed at better characterising the impact of ALS-KIF5A on both anterograde and retrograde axonal transport are required to unravel this aspect.

Another interesting feature identified in this thesis is the rapid protein turnover displayed by both N999Vfs*40 KIF5A and the SPG10-linked R17Q KIF5A mutant. Among the two branches of the PQC system, the UPS was determined to be mainly responsible for WT and mutant KIF5A degradation; notably when the 26S proteasome was inhibited both R17Q and N999Vfs*40 KIF5A accumulated into insoluble aggregates. Since both R17Q and N999Vfs*40 KIF5A dimerise with the WT protein, the fast turnover may affect mutant KIF5A homodimers as well as WT-mutant KIF5A heterodimers, restricting the pool of motors available for anterograde trafficking to WT KIF5A homodimers. The *in-silico* prediction of an alteration in the R17Q KIF5A nucleotide-binding pocket may not only impair the ability of the mutant to fuel transport, but could also destabilise R17Q KIF5A, possibly promoting its rapid elimination from neurons. In the case of the R17Q KIF5A mutant, haploinsufficiency is in line with the already described link between KIF5A LOF and SPG10[145]. Concerning N999Vfs*40 KIF5A, its reduced half-life is consistent with the lower protein levels identified for mutant KIF5A compared to WT in induced pluripotent stem cell (iPSC)-derived ALS-KIF5A motor neuron lines and in ALS-KIF5A animal models[150,261,264,265]. Moreover, the fact that WT and mutant KIF5A are mainly degraded by the UPS might explain the apparent discrepancy between reduced protein stability and increased protein aggregation observed for N999Vfs*40 KIF5A. Indeed, the 26S proteasome has a low capacity for degradation, and it can be rapidly saturated upon substrate accumulation. Therefore, even if soluble ALS-KIF5A species may be efficiently removed by the UPS, the limited degradative capacity of the system is probably insufficient to

counteract mutant KIF5A accumulation into insoluble aggregates that might become progressively less accessible to the 26S proteasome due to the increase in their size. Deposition at the neuron periphery may then further promote ALS-KIF5A accumulation while impeding its recycling by dynein.

The other SPG10-associated KIF5A mutant analysed in this thesis, R280C KIF5A, displayed another similarity to N999Vfs*40 KIF5A. The R-to-C missense found in the microtubule-binding site of KIF5A motor domain has been linked to a strong reduction in the affinity for microtubules of the KIF5A head without altering its microtubule gliding velocity or showing a dominant negative effect on WT KIF5A. Nevertheless, the R280C KIF5A mutant competes with the WT protein for cargo binding, resulting in substrate sequestration to transport-incompetent motors[145]. This mechanism could also be associated with R17Q KIF5A, since its tail is intact while its ATP-binding site is disrupted. Notably, R280C KIF5A tended to accumulate into small perinuclear puncta, likely due to its defective interaction with microtubules, and competed for degradation with the UPS-specific substrate Ub-R-YFP. Both these biochemical behaviours are reminiscent of N999Vfs*40 KIF5A.

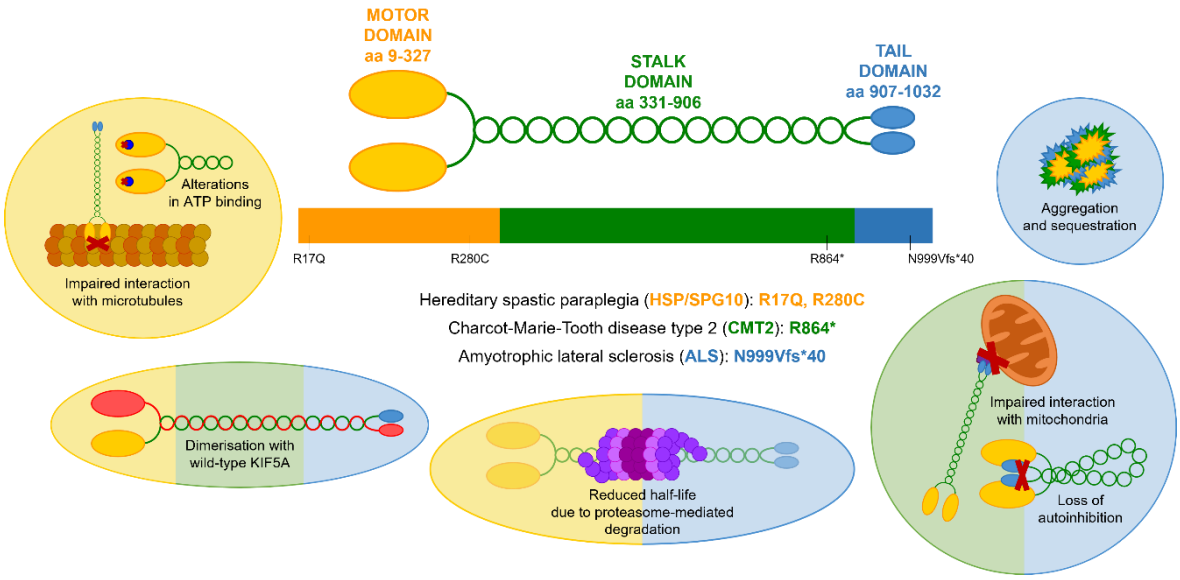

Figure 14 Schematic representation of the main biochemical behaviours identified for the KIF5A mutants under analysis in this thesis. Coloured backgrounds refer to the affected protein domain and the corresponding disease.

SECTION 2 – Comparison between ALS- and NEIMY-KIF5A mutants

Background

Most of the background literature relevant to the experiments described in this Section has already been reported in Section 1. Additional information is detailed in the following paragraphs.

Neonatal intractable myoclonus

Apart from causing neurodegeneration, mutations in *KIF5A* are associated with a neurodevelopmental phenotype named neonatal intractable myoclonus (NEIMY). NEIMY is a severe neurologic disease manifesting through drug-resistant myoclonic seizures soon after patients are born that often lead them to death during infancy. Besides myoclonus, NEIMY symptoms include myopathy, hypotonia, intermittent apnoea, pallor of the optic nerve and abnormal eye movements, dysphagia, and developmental arrest. Brain imaging of NEIMY patients may also show progressive leukoencephalopathy.

NEIMY was first described in 2016 and is driven by *de novo* frameshift mutations in *KIF5A* targeting the C-terminal tail domain of the corresponding protein[266,267]. Initially, Duis *et al*. reported two single-base deletions in *KIF5A* (c.2854delC and c.2934delG), leading to translational frameshifts (p.Q952Rfs*96 and p.S978Lfs*66, respectively) and protein elongation to a common novel stop codon 42 bases downstream of the WT one[266]. Subsequently, Rydzanicz *et al*. reported a c.2922delC/p.C975Vfs*73 (or c.2921delC/p.S974fs) mutation in a child suffering from myoclonic seizures and leukoencephalopathy[267]. In both cases, the authors speculate about mitochondrial disturbances as the main molecular mechanism underpinning NEIMY pathogenesis, that would be consistent with the essential role played by KIF5A in mitochondrial transport along axons[89]. In particular, Rydzanicz and colleagues refer to the finding of a S978fs mutation by DaRe *et al*.[268], which the authors identify as potential cause of a mitochondrial disease, and suggest that the C975Vfs*73 mutation might impair KIF5A ability to bind to adaptors required for mitochondrial trafficking, like TRAK2, whose interaction with KIF5A is indeed reduced upon truncation of the kinesin tail (from residue 962)[269]. On the other hand, Duis and colleagues speculate about the possible involvement of a dominant negative effect exerted by elongated KIF5A variants on the WT protein suggesting that it could disrupt KIF5A-mediated axonal transport[266], similarly to what has been more recently hypothesised for ALS-related KIF5A variants[150,270]. Moreover, the authors reflect on a potential dysfunction of $GABA_A$Rs, which are essential components of the inhibitory

neurotransmission machinery and whose axonal transport relies on the interaction between GABARAP and the 73-amino acid sequence unique to the KIF5A tail among conventional kinesins. According to Duis *et al*., dysfunctional $GABA_AR$ transport and positioning at synapses might account for the myoclonic seizures characterising NEIMY patients[266].

Stress granules

Stress granules (SGs) are cytoplasmic structures comprising RNA and proteins that form upon stress. Together with the constitutively present processing bodies, they represent a hub where cells store RNA species that contribute to the mounting of a proper stress response. Initially described in mammalian cells, SG orthologues can be found in several eukaryotic species. SGs form in response to both biotic and abiotic stressors capable of causing translational arrest in cells, including viral infections, mitochondrial stress, and many others. Upon exposure to such stressing agents, the translational machinery tends to stall, which provokes the release of mRNA and its binding proteins from polysomes. Such release promotes the recruitment of additional RNA molecules and RNA-binding proteins, inducing an increase in their local concentration that facilitates RNA-RNA, protein-protein, and RNA-protein interactions, favouring their physical separation from the cytoplasmic environment through a process named liquid-liquid phase separation (LLPS)[271]. Intrinsically disordered and low-complexity protein regions promote LLPS through the enhancement of protein-protein interactions and indeed several proteins found in SGs are enriched in such sequences. Interestingly, overexpression of some of these proteins is sufficient to promote SG nucleation even in the absence of a stress source. Proteins forming the core of SGs comprise G3BP stress granule assembly factor 1 (G3BP1), TIA1 cytotoxic granule associated RNA binding protein (TIA1), and FMR1. After nucleation occurs, several other proteins able to bind the SG core, including ATPases and protein modifiers, condensate with nascent SGs. In general, SG composition tends to vary with cell type, stressor, and disease[272–274]. An example of a non-nucleating protein in SGs is histone deacetylase 6 (HDAC6), a class IIb deacetylase whose best characterised roles are in promoting cell motility through microtubule and cortactin deacetylation and in the delivery of misfolded proteins to aggresomes. HDAC6 interacts with G3BP1 to recruit SGs to motor proteins and promote their movement along microtubule tracks. Despite not being part of the core proteins, the role of HDAC6 in SG formation is essential, as the process is impaired upon depletion or pharmacological inhibition of HDAC6 [275].

LLPS is a reversible process that makes SGs highly dynamic structures, continuously exchanging RNA and protein species with the cytoplasm (Figure 15). The ability to undergo continuous assembly and disassembly is a key factor in the rapid response to stress for cells and makes SGs an essential

translational reprogramming hub facilitating the isolation of non-essential mRNAs and the translation of priority transcripts when needed. For example, transcripts encoding HSP70 and HSP90 are systematically released from SGs during heat shock, while mRNAs for the housekeeping factors GAPDH and β-actin are sequestered. Importantly, around 10% of the cellular mRNA can be found within SGs upon stress, but the amount of a given transcript in SGs can vary from less than 1% to more than 95% depending on the general conditions of the cell and on the type of stressor[276,277].

SG dynamics are altered in several disease states, including viral infections, cancer, and neurodegeneration, thus tampering with the ability of cells to respond to stress. Different neurodegenerative diseases are associated with altered SG composition. Mutations in the genes encoding SG core proteins can be the cause of such aberrations, as in the case of *FMR1* mutations in fragile X syndrome. In other cases, like in AD, proteins involved in SG nucleation are sequestered by pathological inclusions. In the case of ALS, both scenarios are possible because ALS-linked mutations are found in SG-associated proteins like TIA1, and TDP-43 aggregates co-localise with SGs. In all cases, SGs tend to persist in affected neurons, making them unable to mount a proper stress response[278].

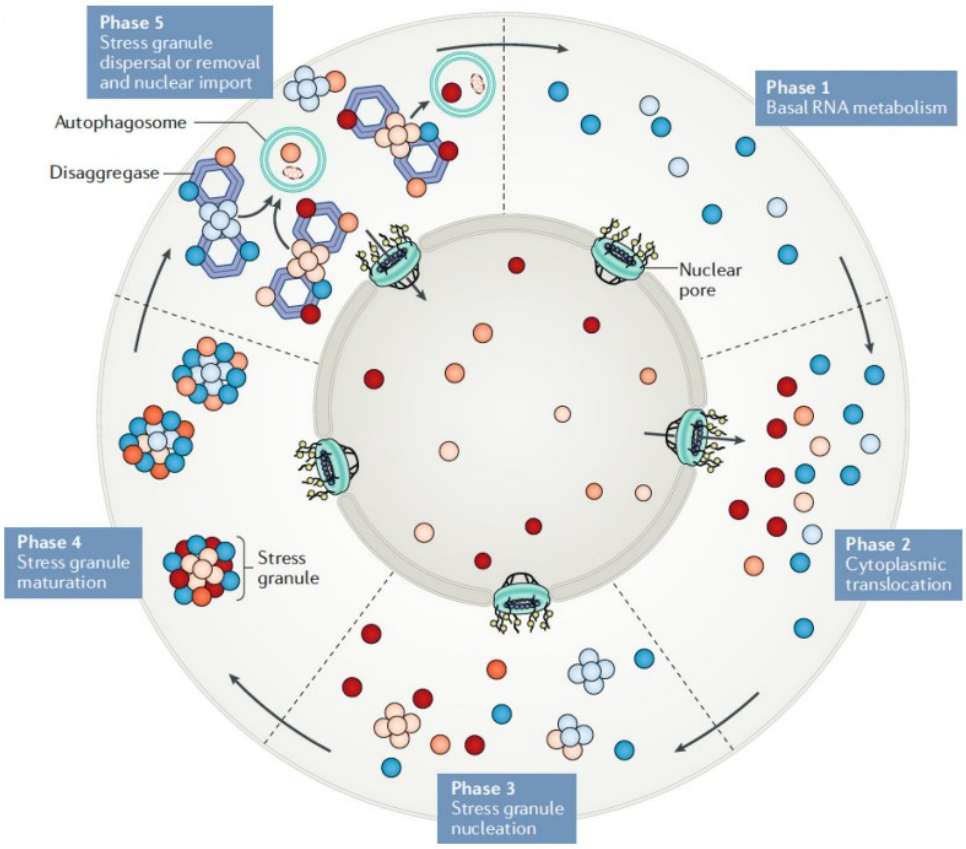

Figure 15 Main phases of the stress granule cycle. Adapted from: Wolozin B, Ivanov P. Stress granules and neurodegeneration. *Nat. Rev. Neurosci.* 20, 649–666 (2019).

Aims

Since 2016, several frameshift mutations targeting the KIF5A tail have been identified and associated with ALS or NEIMY. These frameshift mutations are expected to produce partially overlapping effects on KIF5A[151,266,267] since the novel frame and stop codons are shared between the two classes of KIF5A mutants (Figure 13). Nevertheless, NEIMY and ALS are strikingly different diseases: the former is a rare and complex neurodevelopmental syndrome manifesting with both epileptic and motor symptoms, while the latter is a pure MND with adult onset. Therefore, it would be interesting to identify common and distinct biochemical features between ALS and NEIMY KIF5A mutants sharing the same aberrant C-terminal sequence. To do so, representative ALS- and NEIMY-KIF5A mutants were functionally compared with one another keeping WT KIF5A behaviour as reference. The already characterised ALS-linked N999Vfs*40 KIF5A mutant was chosen to take into account the potential effects of the loss of exon 27, which is fully mutated in the three known NEIMY mutants (Q952Rfs*96, C975Vfs*73, S978Vfs*70 KIF5A). After an *in-silico* analysis of the aberrant C-terminal tails of ALS- and NEIMY-KIF5A, the C975Vfs*73 mutant was chosen as representative because its aberrant tail comprises all the low-solubility sequences shared by NEIMY-KIF5A mutants. Initially, the aggregation-prone behaviour hypothesised for NEIMY-KIF5A after the *in-silico* evaluation was confirmed by analysing its distribution and solubility. Then, the interplay between PQC and NEIMY-KIF5A and its ability to dimerise with the WT protein and to interact with mitochondria was studied. Finally, the composition, motility, and dynamicity of ALS- and NEIMY-KIF5A aggregates were investigated.

Figure 16 Schematic representation of WT, ALS-, and NEIMY-KIF5A C-terminal tails. The aberrant residues specific to the Q952Rfs*96 KIF5A mutant are in dark blue, those shared between all NEIMY-KIF5A mutants are in cerulean blue, while the 40-residue sequence common to ALS- and NEIMY-KIF5A is in light blue. The amino acid sequence encoded by exon 27 is highlighted.

Materials and methods

The experiments described in this Section were performed on NSC-34 or SH-SY5Y cells following the protocols reported in Section 1. Additional experiments and variations with respect to Section 1 are detailed in the following paragraphs.

Plasmids and antibodies

C975Vfs*73 pKIF5A, pFLAG-KIF5A, and pGFP-KIF5A constructs were generated as described in Section 1.

pGFP-G3BP1 (Addgene #135997) was a gift from Dr. Anthony K. L. Leung (Bloomberg School of Public Health, Johns Hopkins University, Baltimore, MD, USA)[279].

In the immunofluorescence experiments reported in this Section, the rabbit monoclonal anti-HDAC6 antibody (1:500; Abcam, ab117516), the mouse monoclonal anti-ubiquitinated proteins (FK2) antibody (1:500; Merck, 04-263), and the mouse monoclonal anti-BAG1 antibody (1:50; Santa Cruz Biotechnology, sc-376848) were used together with the antibodies listed in Table 3.

Protein solubility predictions

CamSol (http://www-vendruscolo.ch.cam.ac.uk/camsolmethod.html; last accessed on November 20th, 2022) was used to predict the solubility profile of WT, N999Vfs*40, and C975Vfs*73 KIF5A C-terminal tails. The analysis was performed using the CamSol Intrinsic method, according to which scores larger than 1 denote highly soluble regions, scores smaller than -1 indicate poorly soluble ones, while neutral regions are marked by scores between -1 and 1[280].

The following sequences were used as input:

YFANSCTSSGATSSGGPLASYQKANMDNGNATDINDNRSDLPCGYEAEDQAKLFPLHQETAAS for WT KIF5A (amino acids 970-1032)

YFANSCTSSGATSSGGPLASYQKANMDNGVTCRVAMRLRTRPSFSLSTKRQQPANLPHPRLHTCTFSF for N999Vfs*40 KIF5A (amino acids 970-1037)

YFANSVPAVDPHLLAAPWLPTRRPTWTMDMPQISMTIGVTCRVAMRLRTRPSFSLSTKRQQPANLPHPRLHTCTFSF for C975Vfs*73 KIF5A (amino acids 970-1046).

Live imaging and fluorescence recovery after photobleaching

NSC-34 cells were seeded in 35-mm glass bottom dishes (MatTek, P35G-0-10-C) at 50,000 cells/dish and transfected with 1.5 μg/dish N999Vfs*40 or C975Vfs*73 pGFP-KIF5A constructs with Lipofectamine™ 3000, as described in Section 1. 24 h or 48 h after transfection, cells were imaged in their medium added with 20 mM HEPES pH 7.4 at 37°C and 5% CO_2 with a LSM 900 confocal microscope (ZEISS) using a 63× oil-immersion lens. Areas of interest of approximately 512 × 100-250 pixels were selected and images were acquired every 1.5-2 s (4× or 8× averaging) for up to 300 s. For fluorescence recovery after photobleaching (FRAP) analysis, one pre-bleach image of N999Vfs*40 or C975Vfs*73 KIF5A aggregates was taken and photobleaching regions were drawn within them. Then, photobleaching was performed with a 5 mW 488 nm laser at 100% for up to 5 s prior to imaging. All images were processed using ImageJ/Fiji (version 2.9.0).

Results

Comparison of the intrinsic solubility profile of the aberrant tail of ALS- and NEIMY-KIF5A mutants

Initially, the intrinsic solubility profiles of WT, ALS-, and NEIMY-KIF5A tails were compared using CamSol. The analysis confirmed that the C-terminal 40-residue sequence shared by ALS- and NEIMY-KIF5A displays lower solubility with respect to the WT KIF5A tail, but also revealed the presence of a poorly soluble amino acid string in the NEIMY-KIF5A mutants that is absent in both WT and ALS-KIF5A. Of note, the low-solubility sequence corresponds to the amino acids encoded by *KIF5A* exon 27, that is either skipped or preserved in its WT form in ALS-KIF5A mutants (Figure 17). This hints that NEIMY-KIF5A may be even less soluble than ALS-KIF5A. CamSol Intrinsic analysis also showed that the 23 amino acids specific to the NEIMY-related Q952Rfs*96 KIF5A aberrant tail are not predicted to affect protein solubility, since most of them display an intrinsic solubility score comprised between -1 and 1 (Figure 17). Together with the observation that the S978Vfs*70 KIF5A tail is fully comprised within the tail of C975Vfs*73 KIF5A, this suggests that at least some aspects of the C975Vfs*73 KIF5A biochemical behaviour are probably shared by Q952Rfs*96 and S978Vfs*70 KIF5A, making of C975Vfs*73 KIF5A a valid representative of all known NEIMY-KIF5A mutants.

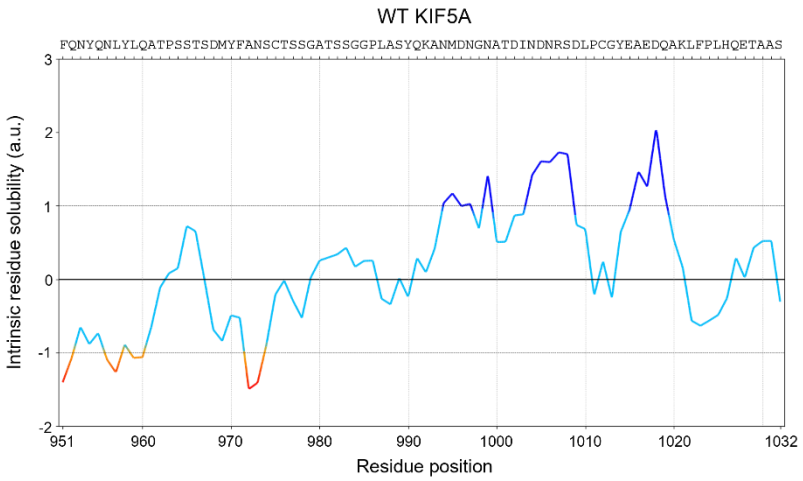

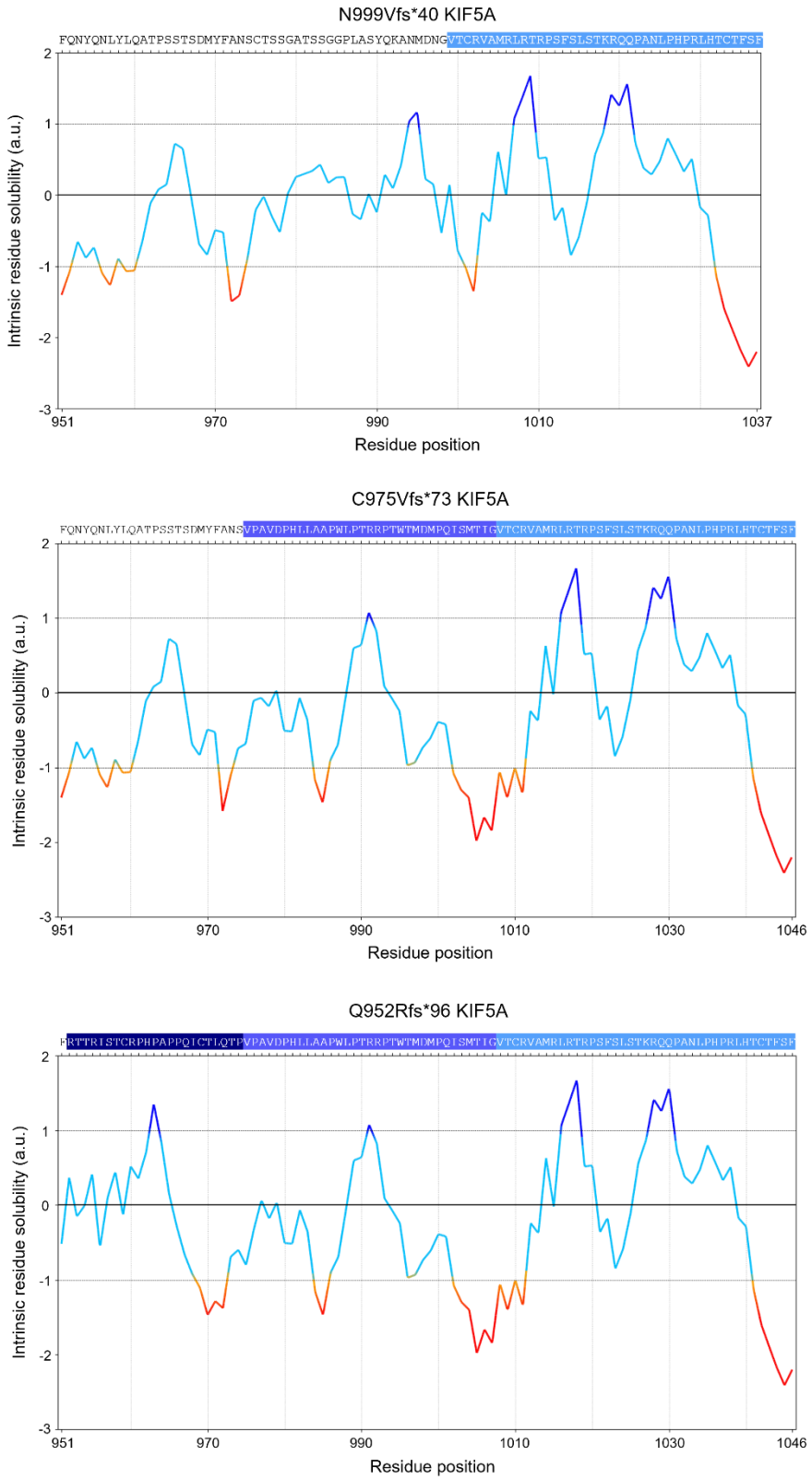

Figure 17 Intrinsic solubility profile of WT, ALS-, and NEIMY-KIF5A C-terminal tails based on the CamSol Intrinsic method.

The aberrant behaviours characterising ALS-KIF5A are recapitulated by NEIMY-KIF5A

Based on the results of the *in-silico* analysis of the N999Vfs*40 and C975Vfs*73 KIF5A aberrant tails, the biochemical behaviour of the two mutant proteins was compared, always referring to WT KIF5A molecular phenotype as control. Initially, the intracellular distribution of the two mutants was evaluated by transiently transfecting NSC-34 cells with pGFP-KIF5A constructs, probing for the β3-tubulin distribution to identify microtubules. Confocal microscopy analysis evidenced that C975Vfs*73 KIF5A accumulates both within neurites and in the cell body into inclusions that are larger than those formed by the N999Vfs*40 KIF5A mutant (Figure 18A), consistently with autoinhibition loss and with the additional low-solubility residue string found in the C975Vfs*73 KIF5A aberrant tail. Moreover, the microtubule network of NSC-34 cells was not altered by the overexpression of C975Vfs*73 KIF5A (Figure 18A).

Subsequently, proteins extracted from SH-SY5Y cells transiently transfected with pKIF5A constructs were fractioned in NP-40 lysis buffer to further confirm the *in-silico* prediction of low protein solubility for C975Vfs*73 KIF5A. As expected, NEIMY-KIF5A fully partitioned in the detergent-insoluble fraction similarly to ALS-KIF5A, while the WT protein was largely NP-40–soluble. Of note, the N999Vfs*40 KIF5A mutant sequestered a larger amount of the ubiquitin-binding autophagy receptor SQSTM1/p62 into the NP-40–insoluble fraction compared to C975fs*73 KIF5A (Figure 18B). The direct interaction between endogenous SQSTM1/p62 and NEIMY-KIF5A was confirmed by co-immunoprecipitation in SH-SY5Y cells transiently transfected with pFLAG-KIF5A constructs (Figure 18C). Nonetheless, confocal microscopy analysis of NSC-34 cells transfected with pGFP-KIF5A showed that SQSTM1/p62 was exclusively found at the rim of C975Vfs*73 KIF5A aggregates, while it was clearly observed within those of N999Vfs*40 KIF5A, in line with the NP-40 fractionation assay. On the other hand, no co-distribution between NEIMY-KIF5A and endogenous MAP1LC3 or alterations in MAP1LC3 localisation were evidenced upon C975Vfs*73 KIF5A overexpression, similarly to ALS-KIF5A (Figure 18D). Interestingly, larger N999Vfs*40 and C975fs*73 KIF5A aggregates often resulted in ubiquitination and positivity for the ubiquitin-binding protein BAG1 in NSC-34 cells transiently transfected with pGFP-KIF5A constructs (Figure 18E). Collectively, these observations suggest that the interaction between SQSTM1/p62 and ALS- and NEIMY-KIF5A aggregates might be ubiquitin-dependent and may drive them to UPS-mediated degradation, as shown for WT and mutant KIF5A in Section 1. Consistently, proteasomal blockage by MG132 caused strong C975Vfs*73 KIF5A accumulation into SH-SY5Y cells overexpressing pKIF5A constructs, while autophagy inhibition by NH_4Cl did not significantly alter NEIMY-KIF5A protein levels, similarly to WT and ALS-KIF5A (Figure 18F).

Co-immunoprecipitation in SH-SY5Y cells also confirmed the direct interaction between WT and C975Vfs*73 KIF5A (Figure 18C). The subsequent confocal microscopy analysis of NSC-34 cells co-transfected with the same amount of WT pmRFP-KIF5A and of pGFP- KIF5A constructs evidenced an even stronger sequestration of the WT protein by NEIMY-KIF5A compared to ALS-KIF5A (Figure 18G), suggesting a stronger dominant negative effect which is consistent with the high aggregation propensity of C975Vfs*73 KIF5A.

Lastly, the C975Vfs*73 KIF5A reciprocal distribution with mitochondria was studied by co-transfecting NSC-34 cells with pDsRed2-Mito and pGFP-KIF5A. Confocal microscopy analysis evidenced altered mitochondrial localisation and no co-distribution with NEIMY-KIF5A (Figure 18H), another feature shared with ALS-KIF5A and suggestive of a similar loss of transport function for the two KIF5A mutants likely depending on the amino acid alterations in their tails. Such LOF would be consistent with reports implicating mitochondrial dysfunction in both ALS and NEIMY[260,266,267].

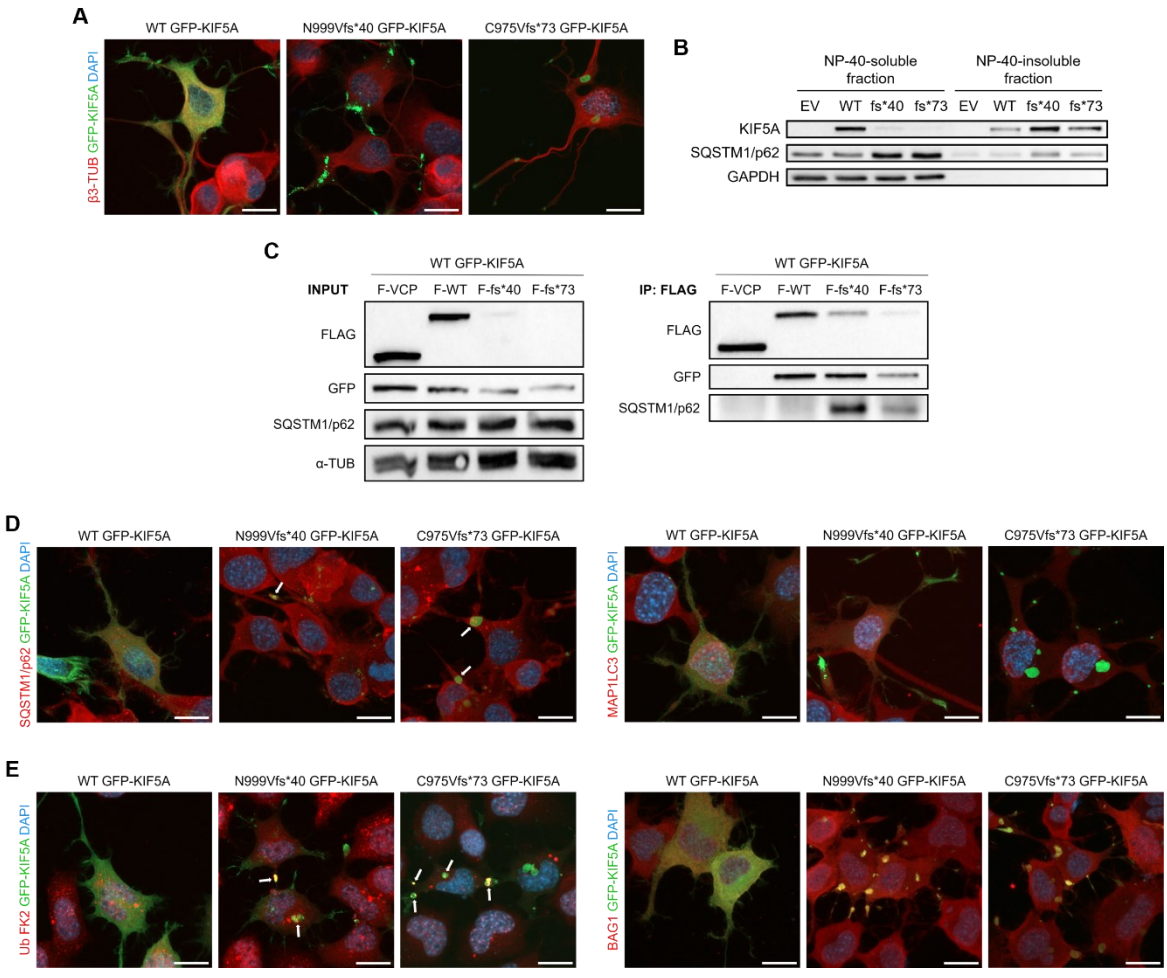

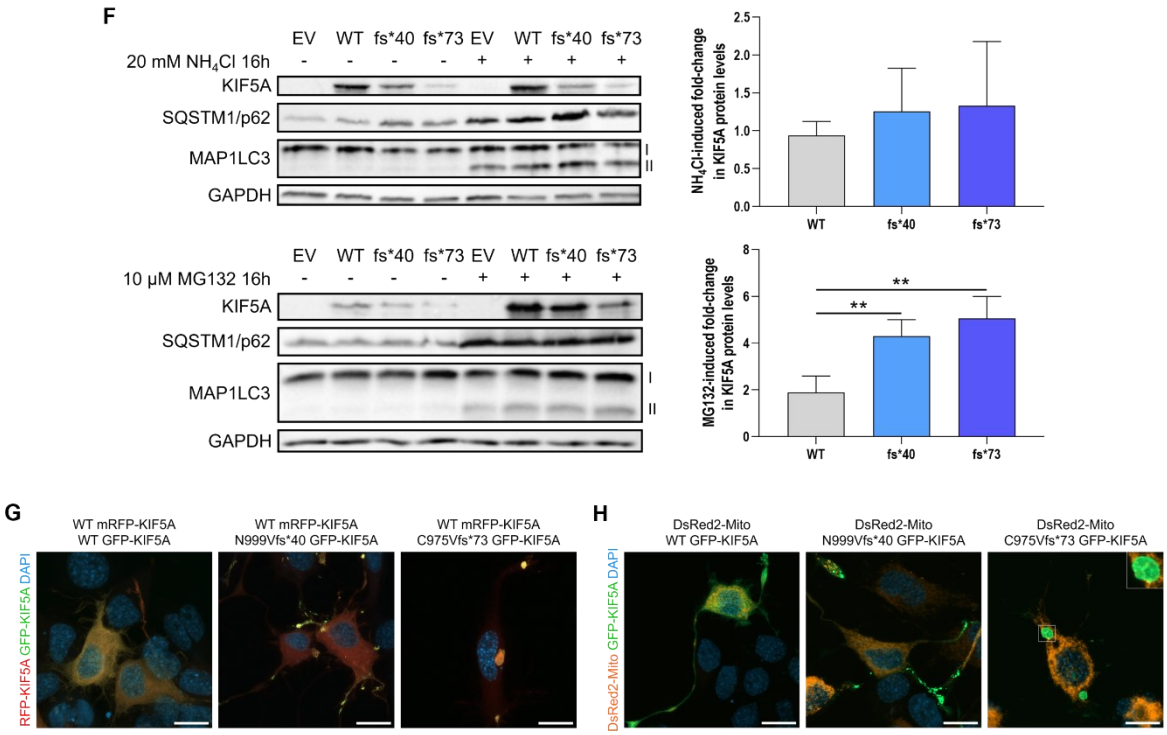

Figure 18 Similarities between ALS- and NEIMY-KIF5A. (A) Confocal microscopy analysis (63× magnification) of NSC-34 cells transiently transfected with pGFP-KIF5A constructs (wild type-WT). Endogenous β3-tubulin was stained in red. Nuclei were stained with DAPI. Scale bars 20 µm. **(B)** Western blot analysis of KIF5A and SQSTM1/p62 fractionation between the NP-40–soluble and the NP-40–insoluble protein fraction in SH-SY5Y cells transiently transfected with pKIF5A constructs (empty vector-EV, wild type-WT, N999Vfs*40-fs*40, C975Vfs*73-fs*73). **(C)** Co-immunoprecipitation between frameshift KIF5A mutants and WT KIF5A or endogenous SQSTM1/p62 extracted from SH-SY5Y cells transiently co-transfected with equal amounts of WT pGFP-KIF5A and pFLAG-KIF5A constructs (FLAG-F, wild type-WT, N999Vfs*40-fs*40, C975Vfs*73-fs*73). FLAG-VCP (F-VCP) was used as control for anti-FLAG immunoprecipitation. **(D)** Confocal microscopy analysis (63× magnification) of NSC-34 cells transiently transfected with pGFP-KIF5A constructs. Endogenous SQSTM1/p62 (left panel) or MAP1LC3 (right panel) were stained in red. Nuclei were stained with DAPI. Arrows highlight co-localisation between frameshift KIF5A mutants and SQSTM1/p62. Scale bars 20 µm. **(E)** Confocal microscopy analysis (63× magnification) of NSC-34 cells transiently transfected with pGFP-KIF5A constructs. Endogenous ubiquitinated proteins (Ub FK2; left panel) or BAG1 (right panel) were stained in red. Nuclei were stained with DAPI. Arrows highlight ubiquitinated frameshift KIF5A aggregates. Scale bars 20 µm. **(F)** Western blot analysis of KIF5A protein levels in SH-SY5Y cells transiently transfected with pKIF5A constructs and treated with 20 mM ammonium chloride (NH_4Cl) for 16 h (top panel) or 10 µM Z-Leu-Leu-Leu (MG132) for 16 h (bottom panel). GAPDH protein levels were used for normalisation. Bar graphs represent fold-change of WT or frameshift KIF5A protein levels induced by the treatment. One-way ANOVA with Fisher's LSD post-test was performed. n = 3; ** = $P < 0.01$. **(G)** Confocal microscopy analysis (63× magnification) of NSC-34 cells transiently co-transfected with equal amounts of WT or frameshift pGFP-KIF5A and WT pmRFP-KIF5A constructs. Nuclei were stained with DAPI. Scale bars 20 µm. **(H)** Confocal microscopy analysis (63× magnification) of NSC-34 cells transiently co-transfected with WT or frameshift pGFP-KIF5A constructs and pDsRed2-Mito. Nuclei were stained with DAPI. Scale bars 20 µm.

NEIMY-KIF5A aggregates are positive for stress granule markers and exhibit a solid-like behaviour

Further characterisation of frameshift KIF5A aggregates also revealed features that are unique to NEIMY-KIF5A. Specifically, confocal microscopy analysis of NSC-34 cells transiently overexpressing WT or mutant KIF5A evidenced that C975Vfs*73 KIF5A aggregates, but not those of N999Vfs*40 KIF5A, resulted positive for the SG markers HDAC6 and GFP-G3BP1 (Figure 19A-B). This suggests that the protein-RNA condensation phenomena typical of SG formation may promote the initial deposition of NEIMY-KIF5A aggregates, too.

Interestingly, live imaging analysis of NSC-34 cells transfected with pGFP-KIF5A constructs showed that both ALS- and NEIMY-KIF5A aggregates were motile and displayed aggregate-aggregate interactions after 24 h of overexpression, but at 48 h the largest C975Vfs*73 KIF5A aggregates had lost most of their motility, while N999Vfs*40 KIF5A aggregates continued to move and fuse with one another, growing in size (Figure 19C). Consistently, while both ALS- and NEIMY-KIF5A aggregates recovered fluorescence following photobleaching 24 h after transfection, only N999Vfs*40 KIF5A retained such dynamic behaviour at 48 h (Figure 19D). This is apparently in contrast with the dynamic properties of SGs, that continuously form and disassemble according to environmental cues, and suggests that the initially dynamic C975fs*73 KIF5A aggregates may mature over time into solid-like structures unable to revert to a soluble state and eventually exerting toxicity on neurons.

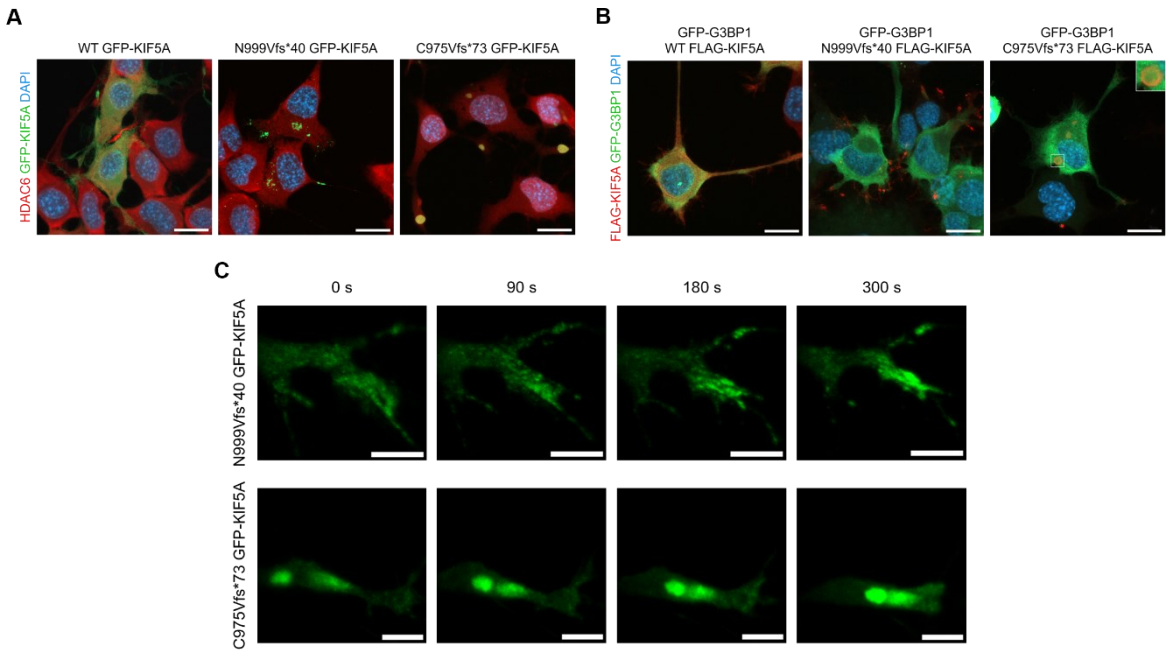

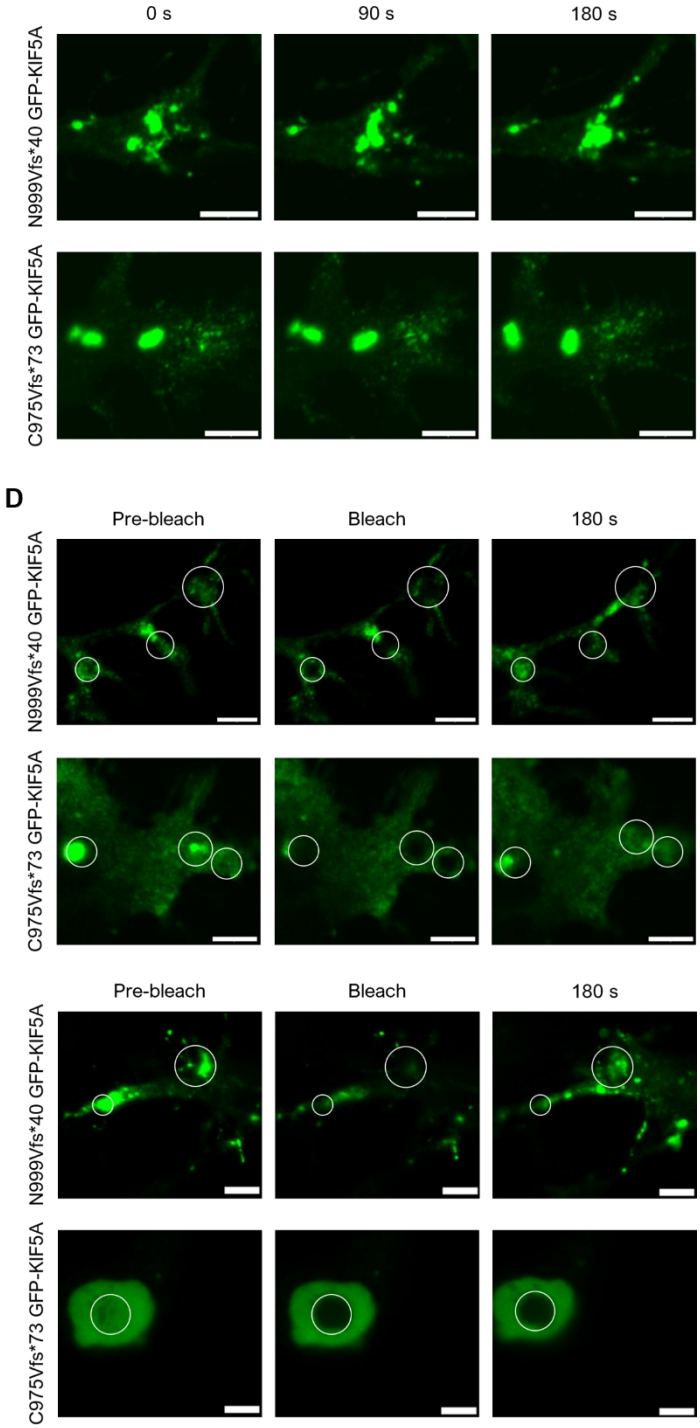

Figure 19 Differences between ALS- and NEIMY-KIF5A. (A) Confocal microscopy analysis (63× magnification) of NSC-34 cells transiently transfected with pGFP-KIF5A constructs (wild type-WT). Endogenous HDAC6 was stained in red. Nuclei were stained with DAPI. Scale bars 20 µm. **(B)** Confocal microscopy analysis (63× magnification) of NSC-34 cells transiently co-transfected with pGFP-G3BP1 and pFLAG-KIF5A constructs. Nuclei were stained with DAPI. Scale bars 20 µm. **(C)** Live imaging analysis on frameshift GFP-KIF5A inclusions in NSC-34 cells 24h (top panel) and 48h (bottom panel) after transient transfection with pGFP-KIF5A constructs. Scale bars 5µm. **(D)** FRAP analysis of frameshift KIF5A inclusions in NSC-34 cells 24h (top panel) and 48h (bottom panel) after transient transfection with pGFP-KIF5A constructs. Scale bars 5µm.

Discussion

Since 2016, several frameshift mutations targeting the KIF5A tail have been identified. *KIF5A* mutations causing ALS can lead to exon 27 splicing associated with translational frameshift if they target the 5' splice junction of the exon or to translational frameshift alone[264], but in both cases, they alter KIF5A C-terminal sequence and determine protein elongation up to a novel stop codon 14 nucleotide triplets downstream of the WT canonical stop codon[141,142]. Notably, all three known NEIMY-linked *KIF5A* mutations occur upstream of exon 27[266,267], whose sequence is therefore modified, but share with ALS-related variants the +1 shift in the reading frame, the new stop codon, and the abnormal 40-amino acid C-terminal sequence. Despite this similarity, ALS and NEIMY are very different diseases – the former being an adult-onset MND and the latter consisting in a complex and severe neurodevelopmental condition.

To identify distinct and shared molecular behaviours underpinning KIF5A-linked ALS and NEIMY, two representative mutants were characterised – the ALS-associated N999Vfs*40 and the NEIMY-related C975Vfs*73. The *in-silico* analysis of the aberrant C-terminal tails of ALS- and NEIMY-KIF5A evidenced that both display a short sequence of poorly soluble amino acids at their very end, but that NEIMY-KIF5A tail also includes a low-solubility string of residues encoded by the +1 frame of exon 27. Such additional poorly soluble sequence could account for the differences in ALS- and NEIMY-KIF5A phenotype.

The experiments described in this Section identify several similarities but also important distinctions in the biochemical behaviour of ALS- and NEIMY-KIF5A. In detail, C975Vfs*73 KIF5A recapitulates most of the aberrant behaviours characteristic of the N999Vfs*40 KIF5A mutant, including aggregation, distal distribution due to autoinhibition loss, negative dominance on WT KIF5A, and deficient interaction with mitochondria. The aggregates formed by the C975Vfs*73 KIF5A mutant are larger and often closer to the cell body than those of N999Vfs*40 KIF5A. Although quantification of immunofluorescence analyses to assess the significance of these features was not performed, these observations support the hypothesis of a higher oligomerisation propensity for NEIMY-KIF5A, leading to the formation of insoluble aggregates that deposit not only at microtubule plus-ends, but also along their tracks. Moreover, C975Vfs*39 KIF5A aggregates seem less accessible to SQSTM1/p62 than ALS-KIF5A ones, which suggests that the UPS, the PQC pathway regulating their degradation, may fail in clearing them from neurons. Finally, the positivity of NEIMY-KIF5A aggregates for SG markers indicates their higher sequestration capability compared to those of ALS-KIF5A. NEIMY-KIF5A aggregates probably form similarly to SGs and then mature into solid-like structures that can no longer undergo liquid-liquid phase partitioning like normal RNP

condensates.[271] Protein and/or mRNA sequestration could also occur into these structures, further exacerbating NEIMY-KIF5A toxicity.

The clinical symptoms affecting the NEIMY patients described in the literature are similar regardless of the underlying *KIF5A* mutation,[266,267] and they have been previously proposed to depend on impaired excitatory/inhibitory equilibrium and mitochondrial dysfunction[179,266,267]. Both defects are consistent with an impairment of KIF5A-mediated trafficking of $GABA_A$ receptor subunits[106] and mitochondria[88,89]. Interestingly, neuron-specific *Kif5a* depletion in newborn mice results in an epileptic phenotype[106] reminiscent of NEIMY patients, further supporting the hypothesis of a KIF5A LOF in this early-onset neurodevelopmental disease. Interestingly, synaptic vesicle accumulation and alteration in synaptic transmission have been observed in ALS-KIF5A *Drosophila* larvae[261], suggesting another LOF mechanism shared between ALS and NEIMY.

Altogether, data collected on the N999Vfs*40 and C975Vfs*73 KIF5A mutants show that a combination of a toxic GOF due to protein aggregation and WT KIF5A sequestration and a LOF in axonal transport may underlie both KIF5A-linked ALS and NEIMY (Figure 20), bridging the dichotomy between KIF5A-related neurodegenerative and neurodevelopmental diseases.

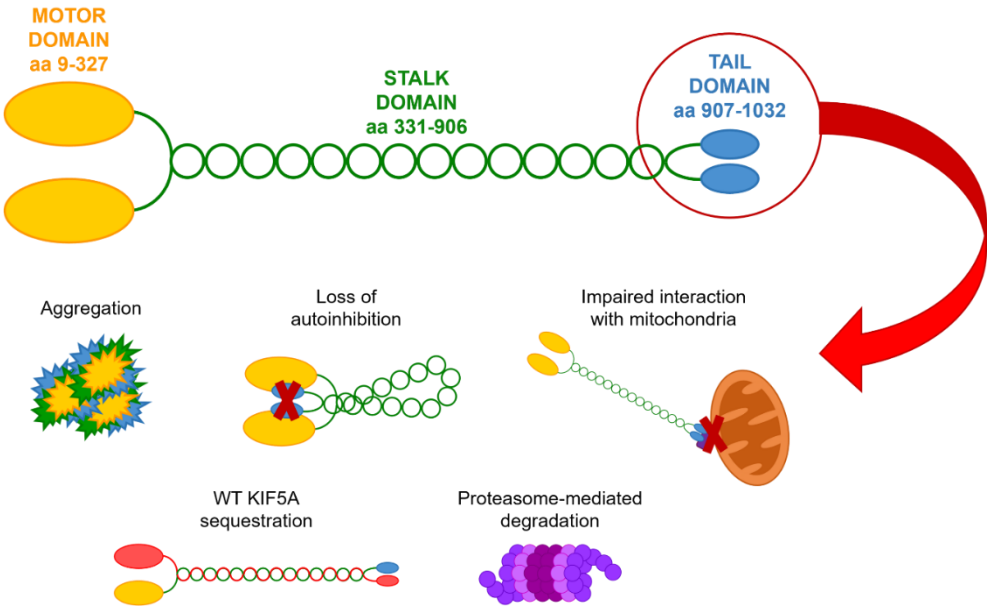

Figure 20 Schematic representation of the biochemical features shared by ALS- and NEIMY-KIF5A mutants targeting the tail domain of the protein.

SECTION 3 – Using i^{3}LMNs to study mutant KIF5A-linked alterations in axonal transport

Background

Induced pluripotent stem cells

Due to its unique complexity, the human nervous system is very difficult to accurately recapitulate with animal models, especially when studying neuronal disorders. In this respect iPSCs, that allow the transcription factor-mediated reprogramming of somatic cells and their subsequent differentiation into virtually all cell types[281], represent an essential tool in the study of neuronal biology. Since 2007, several methods to differentiate iPSCs into specific neuronal subpopulations relying on small molecules have been rapidly developed. These strategies take advantage of a combination of pharmacological inhibitors to drive iPSCs towards neuroectodermal commitment, generating neuronal progenitor cells that can then be further differentiated into the desired neuronal subtype with growth factors and additional small molecules[282,283]. However, the efficiency of these differentiation approaches is limited, both because distinct iPSC lines can differentially respond to the same small molecules and because individual cells in a population undergo maturation at different rates. These factors produce a mixed population of various neuronal subtypes, glial cells, and progenitors in which proliferative cells can outcompete terminally differentiated ones, often complicating downstream analyses. Additionally, small molecule-based iPSC differentiation methods are often expensive and time consuming (e.g., up to 70 days long)[284]. More recently, strategies based on the overexpression of transcription factors in iPSCs to promote their neuronal commitment have been developed to overcome the limitations of small-molecule methods. These approaches stem from the observation that the overexpression of neurogenin 2 (NGN2), the master regulator of neuron-specific transcriptional programmes, determines the single-step differentiation of iPSCs to fully competent glutamatergic cortical neurons within 2 weeks and with 90% efficiency[285,286]. The NGN2 overexpression approach has now been perfectioned through the generation of iPSC lines stably integrating its coding sequence in a safe-harbour locus under the control of a doxycycline-inducible promoter: these pluripotent cells can be differentiated into integrated, inducible, isogenic neurons (i^{3}Neurons) with almost 100% efficiency[287]. By adding the transcription factors ISL LIM homeobox 1 (ISL1) and LIM homeobox 3 (LHX3) to the doxycycline-inducible NGN2 cassette, iPSC lines called hNIL (from the initials of the three overexpressed transcription factors) can now be generated and efficiently differentiated into i^{3}LMNs via a two-

step protocol lasting only 10 days[284] (Figure 21). Therefore, iPSC differentiation through transcription factor overexpression represents a promising improvement compared to small molecule-based protocols and is currently increasingly applied in the study of the human nervous system.

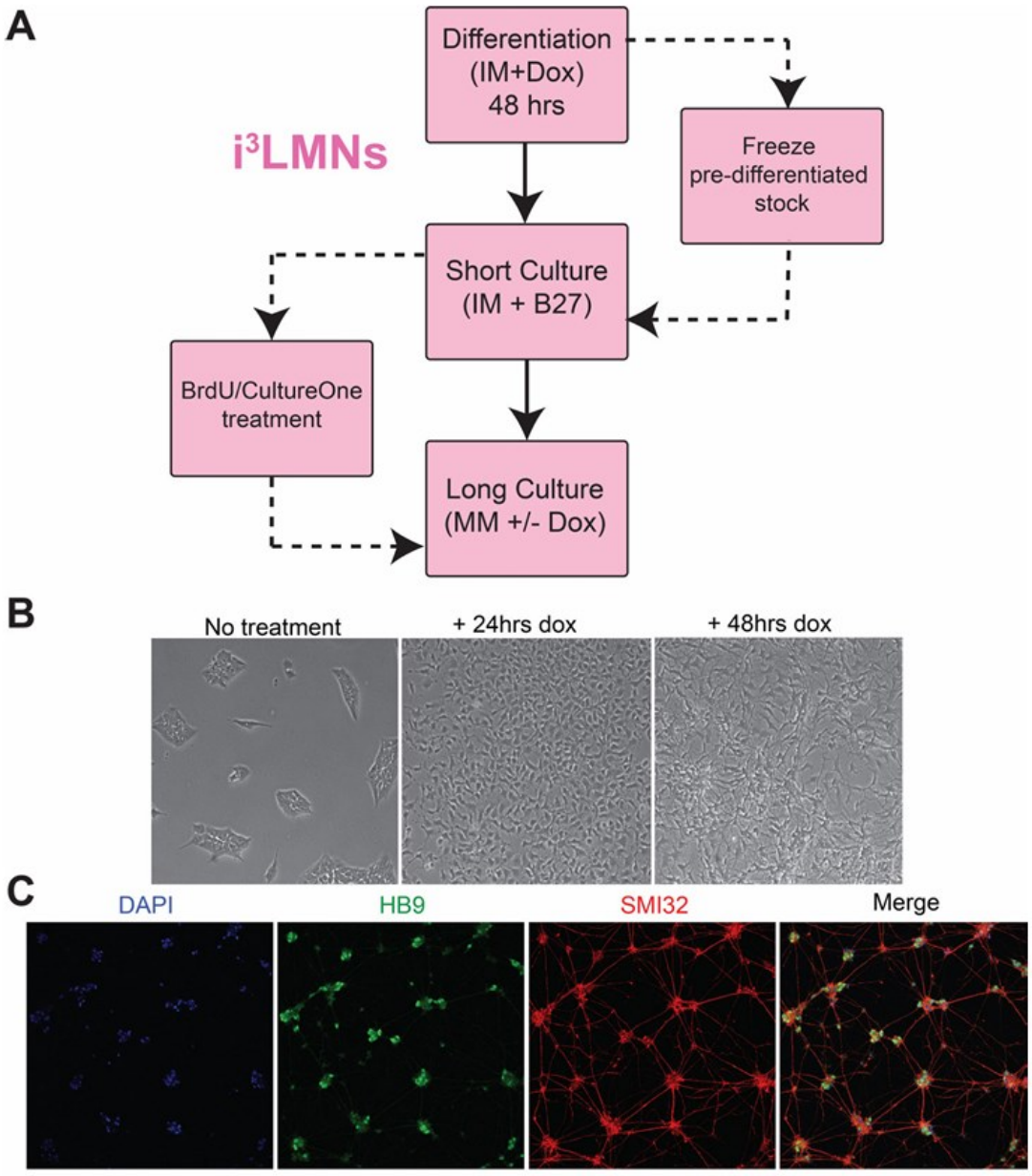

Figure 21 (**A**) Scheme of the workflow for culturing and differentiating i³LMNs from hNIL iPSCs. (**B**) Initial steps of hNIL iPSC differentiation into i³LMNs upon exposure to doxycycline (dox). (**C**) i³LMN staining for the motor neuron-specific markers motor neuron and pancreas homeobox 1 (MNX1 or HB9) and NF-H (SMI32). Adapted from: Fernandopulle M. S. *et al*. Transcription factor-mediated differentiation of human iPSCs into neurons. *Curr. Protoc. Cell Biol.* 79, e51 (2018); scale bar unavailable.

Aims

Evidence in the literature and experimental data presented in Sections 1 and 2 support the hypothesis that all five of the disease-associated KIF5A mutants under analysis in this thesis display altered microtubule-based motility. In fact, the R17Q and R280C substitutions target KIF5A residues lying within the ATP- and microtubule-binding regions of the motor domain, respectively; these mutations could thus alter KIF5A ability to fuel and drive anterograde axonal transport. Oppositely, the R864*, N999Vfs*40, and C975Vfs*73 KIF5A mutants lack the ability to undergo autoinhibition and are therefore expected to move at a faster rate compared to the WT protein. Such predicted disturbances in KIF5A motility might alter anterograde axonal trafficking in a parallel way. The hypothesised alterations in KIF5A-driven motility might have an impact on dynein-mediated transport, too, based on the strong interdependence between anterograde and retrograde motors. Therefore, the main aim of the experiments described in this Section was to establish a model to study the impact on bidirectional axonal transport of disease-associated KIF5A mutants in a more physiologically relevant context than immortalised cells like NSC-34 or SH-SY5Y. To this purpose, hNIL iPSCs were differentiated into i^3LMNs that were then transduced with lentiviral vectors to overexpress WT or mutant KIF5A. The experiments described in this section were performed in the laboratories of Prof. Giampietro Schiavo and Dr. James N. Sleigh (University College London, London, UK).

Materials and methods

Plasmids

pMD2.G/VSV-G (Addgene, 12259), pRSV-Rev (Addgene, 12253), and pMDLg/pRRE (Addgene, 12251) were a gift from Dr. Didier Trono (École Polytechnique Fédérale de Lausanne, Lausanne, CH). pCDH-PGK (Addgene, 72268) was a gift from Dr. Kazuhiro Oka (Baylor College of Medicine, Houston, TX, USA) and was used to generate transfer vectors for the overexpression of GFP-tagged WT or mutant KIF5A and mRFP-tagged WT KIF5A (pCDH-KIF5A) in hNIL iPSCs and i^3LMNs through restriction cloning. The pCDH-PGK construct was chosen to drive transgene expression under the control of the murine phosphoglycerate kinase (PGK) promoter, which is known to provide robust and prolonged overexpression in primary cultures[288] and not be silenced in either hNIL iPSCs or i^3LMNs[284].

Mito-mEmerald was kindly provided by Dr. Matt Keuss (University College London, London, UK) and was used to try to increase KIF5A overexpression in hNIL iPSCs or i^3LMNs taking advantage of the human elongation factor-1α (EF-1α) promoter. Indeed, this promoter was reported to provide long-term transgene overexpression during stem cell differentiation, and it is generally considered stronger than the PGK promoter[289,290]. Briefly, the cDNA sequence encoding the mitochondrial cytochrome *c* oxidase subunit VIII presequence fused to mEmerald was replaced with the one for GFP-tagged WT KIF5A to put it under the control of the EF-1α promoter, generating the EF1α-KIF5A construct.

Cell lines

HEK-293T cells were obtained from the American Type Culture Collection and used as packaging cells to produce lentiviral particles harbouring pCDH-KIF5A constructs. HEK-293T cells were cultured in DMEM High Glucose supplemented with 10% FBS (Gibco, 10270106), penicillin/streptomycin (Pen/Strep 100x; Gibco, 15140122), non-essential amino acids (NEAA 100x; Gibco, 11140050), 1 mM *L*-glutamine, and sodium pyruvate (Gibco, 11360070).

Lenti-X™ 293T cells were obtained from Takara Bio and used as packaging cells to produce lentiviral particles harbouring Mito-mEmerald or EF1α-KIF5A constructs. Lenti-X™ 293T cells were cultured in DMEM/F12 + GlutaMAX (Gibco, 31331093) supplemented with 10% FBS, Pen/Strep 100x, and NEAA 100x.

hNIL iPSCs were kindly provided by Dr. Christopher Grunseich (National Institute of Neurological Disorders and Stroke, Bethesda, MD, USA). Prior to differentiation, hNIL iPSCs were expanded in 10-cm dishes coated with Geltrex™ (Gibco, A1413202) in complete Essential 8™ Flex medium

(Gibco, A2858501) supplemented with Pen/Strep 100x. The medium was changed every other day and supplemented with ROCK inhibitor Y-27632 (Tocris, 1254) for 24 h upon hNIL iPSC splitting. All cell lines were incubated at 37°C in 5% CO_2 and kept in line for not more than 15 passages.

Lentiviral particle production

Lentiviral particles harbouring pCDH-KIF5A constructs were produced in HEK-293T cells transiently transfected through calcium phosphate precipitation. Briefly, cells were plated in 15-cm dishes in their medium the day before transfection. At least 2 h before transfection, the medium was changed to DMEM High Glucose Iscove (Euroclone, ECM0192L) added with the same supplements and the cells were transfected with pCDH-KIF5A, pMD2.G/VSV-G, pRSV-Rev, and pMDLg/pRRE in a 4:2:1:1 ratio diluted in a 1:1 solution of 2.5 M $CaCl_2$ + HEPES-buffered saline (HBS; 50 mM HEPES, 1.5 mM Na_2HPO_4 and 0.285M NaCl in H_2O, pH 7.12). The next day the medium was refreshed to interrupt transfection and the day after virus-containing supernatants were filtered through 0.45-um filters. Lentiviral particles were then collected through supernatant ultracentrifugation in a SW 32 Ti rotor (Beckmann, 369694) at 100 000 × *g* for 2 h at 4°C and resuspended in PBS.
Lentiviral particles harbouring Mito-mEmerald or EF1α-KIF5A constructs were produced in Lenti-X™ 293T cells transiently transfected with Lipofectamine 3000 (as described in Section 1) and the same plasmid ratios. Lentiviral particles were isolated using the Lenti-X Concentrator (Takara Bio, 631231), according to the manufacturer's instructions.

hNIL iPSC differentiation into i^{3}LMNs

hNIL iPSCs were differentiated into i^{3}LMNs following the protocol described by Fernandopulle *et al*.[284]. On the first day of differentiation (D1), 80-90% confluent hNIL iPSCs were washed in PBS, incubated with induction medium (IM), and grown for 48 h, monitoring differentiation. On D3, induced hNIL iPSCs were washed in PBS and dissociated with Accutase (Gibco, A1110501) to be either frozen or replated onto glass bottom dishes (MatTek, P35G-1.5-10-C) or homemade microfluidic chambers (MFCs)[291] coated with 10% poly-*D*-lysine (Gibco, A3890401) in sterile H2O and 0.8% BSA (Sigma, A3311) and 25 µg/ml laminin (Gibco, 23017015) in DMEM/F-12 in IM supplemented with laminin and CultureOne™. On the next day (D4), the medium was changed to motor neuron medium (MM), which was refreshed every other day until D7, when i^{3}LMNs are considered mature, and every 4 to 7 days until the end of the experiment. Medium compositions are reported in Table 4.

Table 4 Composition of the media used differentiate hNIL iPSCs to i^{3}LMNs.

Medium	Component	Source, catalogue number
Induction medium (IM)	DMEM/F-12 + GlutaMAX	Gibco, 31331093
	NEAA 100x	Gibco, 11140050
	N-2 Supplement 100x	Gibco, 17502048
	Pen/Strep 100x	Gibco, 15140122
	2 µg/ml doxycycline	Sigma-Aldrich, D9891
	0.2 µM Compound E	Calbiochem,565790
	10 µM ROCK inhibitor Y-27632	Tocris, 1254
	1 µg/ml laminin upon replating	Gibco, 23017015
	CultureOne™ Supplement 100x upon replating	Gibco, A3320201
Motor neuron medium (MM)	Neurobasal™ medium	Gibco, 21103049
	NEAA 100x	Gibco, 11140050
	GlutaMAX™ 100x	Gibco, 35050061
	N-2 Supplement 100x	Gibco, 17502048
	B-27™ Supplement 50x	Gibco, 17504044
	Pen/Strep 100x	Gibco, 15140122
	2 µg/ml doxycycline	Sigma-Aldrich, D9891
	1 µg/ml laminin	Gibco, 23017015
	CultureOne™ Supplement 100x	Gibco, A3320201

Imaging

During hNIL iPSC induction and i^{3}LMN differentiation, images were taken every day with a fluorescent microscope to monitor morphology and GFP/mRFP expression. Images of D8 i^{3}LMNs transduced with the pCDH-KIF5A vectors were taken with a LSM 780 (Zeiss) confocal microscope, while images of i^{3}LMNs transduced with the Mito-mEmerald or EF1α-KIF5A constructs were taken with a fluorescent microscope.

For immunofluorescence, D12-i^{3}LMNs plated in MFCs were fixed with 4% paraformaldehyde in PBS, permeabilised with 5% BSA and 0.1% saponin (Sigma-Aldrich, 47036) in PBS for 1 h at RT, and stained with antibodies and DAPI diluted in PBS containing 5% BSA and 0.05% saponin, with PBS washes applied between steps. Images were taken with the LSM 780 microscope. Antibodies used for staining are reported in Table 5.

All images were processed with ImageJ.

Table 5 List of the antibodies used for the stainings presented in Section 3

Antibody	Dilution	Source, catalogue number
Mouse monoclonal anti–β3-tubulin	1:1000	BioLegend, 801202
Chicken polyclonal anti-NF-H	1:1000	Chemicon, AB5539
Chicken polyclonal anti–β3-tubulin	1:500	Synaptic Systems, 302306
Goat polyclonal anti-choline acetyltransferase (ChAT)	1:50	Chemicon, AB144P
Alexa Fluor™ 555-conjugated donkey anti-mouse IgG	1:1000	Invitrogen, A-31570
Alexa Fluor™ 488-conjugated donkey anti-chicken IgY	1:1000	Invitrogen, A78948
Alex Fluor™ 555-conjugated donkey anti-chicken IgY	1:1000	Invitrogen, A78949
Alexa Fluor™ 488-conjugated donkey anti-goat 488 IgG	1:1000	Invitrogen, A32814

Results

Successful hNIL iPSC differentiation into i^{3}LMNs

Following the protocol described by Fernandopulle *et al.*[284], hNIL iPSCs were differentiated into i^{3}LMNs. Cell morphology analysis confirmed the commitment of hNIL iPSCs to a neuronal precursor fate during induction since cells started to shrink and grow neurite-like protrusions upon doxycycline exposure (Figure 22A). After induction, differentiating hNIL iPSCs were re-plated in the final growth support and further monitored during motor neuron specification, evidencing neurite maturation into axon-like extensions (Figure 22B). Immunofluorescence analysis performed on D12 cells in MFCs confirmed the expression and appropriate intracellular localisation of the motor neuron-specific markers β3-tubulin, NF-H, and ChAT, indicating that i^{3}LMNs were successfully obtained (Figure 22C).

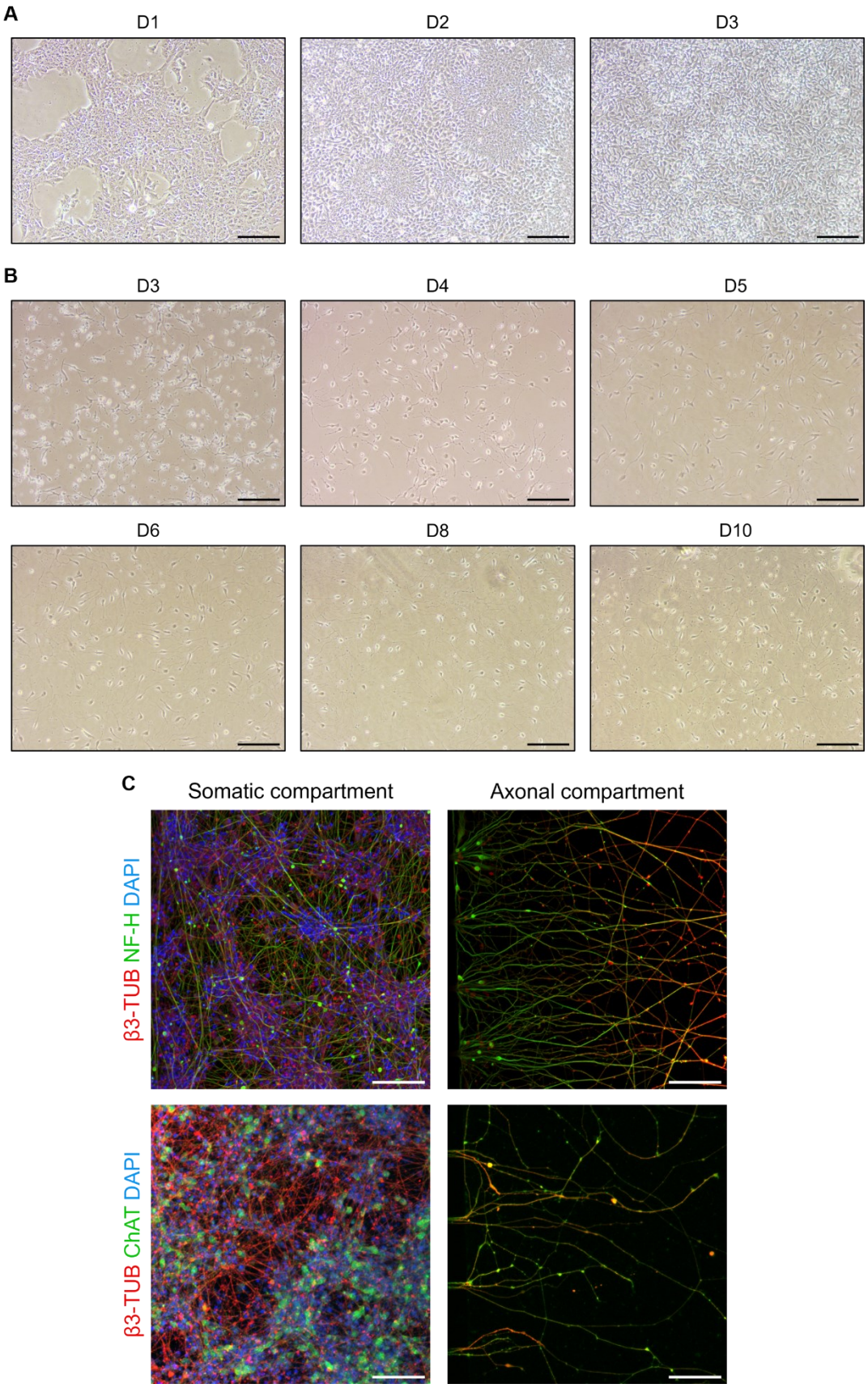

Figure 22 hNIL iPSC differentiation into i^{3}LMNs. (A) Microscopy analysis of hNIL iPSCs undergoing induction (day-D). Scale bars 100 µm **(B)** Microscopy analysis of i^{3}LMNs undergoing differentiation. Scale bars 100 µm **(C)** Confocal microscopy analysis of D12-i^{3}LMN cell bodies and axons in MFCs. β3-tubulin was stained in red, while NF-H or ChAT were stained in green. Nuclei were stained with DAPI. Scale bars 80 µm.

Very low KIF5A levels are observed upon i^{3}LMN transduction

To overexpress WT or mutant KIF5A in i^{3}LMNs, cells were transduced with increasing amounts of lentiviral particles harbouring pCDH-KIF5A constructs; however, only low levels of expression were obtained. Indeed, even if the distribution of WT and mutant KIF5A in i^{3}LMNs was consistent with previous observations in immortalised cells (Sections 1 and 2), GFP or mRFP fluorescence was only detectable by confocal microscopy and only in a few neurons surviving for 3 to 7 days after transduction, regardless of i^{3}LMN maturity at the day of infection (Figure 23A). Comparable results were obtained upon i^{3}LMN liposome-mediated transfection and primary cortical neuron transduction, too (data not shown).

To try to increase KIF5A overexpression in i^{3}LMNs, the EF1α-KIF5A transfer construct was cloned into Mito-mEmerald and lentiviral particles harbouring either vector were then produced in parallel to compare their transduction efficiency. As expected, i^{3}LMNs were efficiently transduced with the Mito-mEmerald construct and displayed abundant mEmerald-positive mitochondria. On the other hand, although the EF-1α-dependent construct improved WT GFP-KIF5A overexpression in i^{3}LMNs compared to pCDH-PGK ones, fluorescence was rapidly lost (Figure 23B). This suggests that the low KIF5A overexpression observed in i^{3}LMNs is independent of the transfer construct and promoter in use.

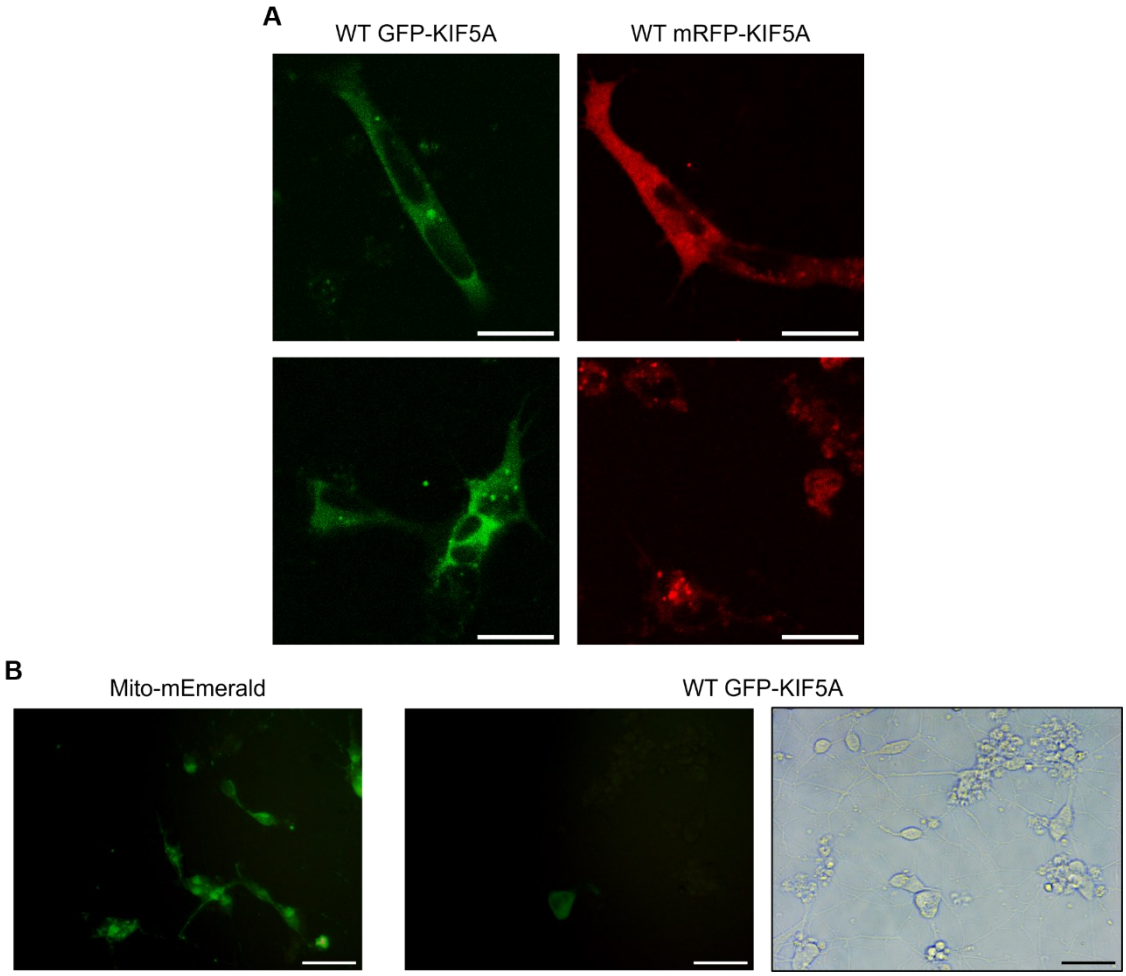

Figure 23 KIF5A overexpression in transduced i^{3}LMNs. (A) Confocal microscopy analysis of D8- i^{3}LMNs 3 days after transduction with wild type (WT) pCDH-KIF5A vectors. Scale bars 20 µm **(B)** Microscopy analysis of D10-i^{3}LMNs 5 days after transduction with Mito-mEmerald or WT EF1α-KIF5A vectors. Scale bars 100 µm.

KIF5A levels progressively decrease with differentiation into i^{3}LMNs in transduced hNIL iPSCs

In another attempt to enhance KIF5A overexpression, hNIL iPSCs were transduced prior to induction with lentiviral particles harbouring EF1α-KIF5A; once again, Mito-mEmerald was used as control. Infected hNIL iPSCs started overexpressing GFP-KIF5A 24 h after transduction, although efficiency appeared to be lower compared to cells receiving the Mito-mEmerald construct. Interestingly, GFP-positive hNIL iPSCs started emitting protrusions, too (Figure 24A), a behaviour that has already been observed upon KIF5A overexpression in different cell types[292]. During differentiation into i^{3}LMNs, though, transduced hNIL cells were progressively lost and an overall reduction in fluorescence intensity was observed in the remaining GFP-positive cells (Figure 24B), differently from mEmerald-positive i^{3}LMNs.

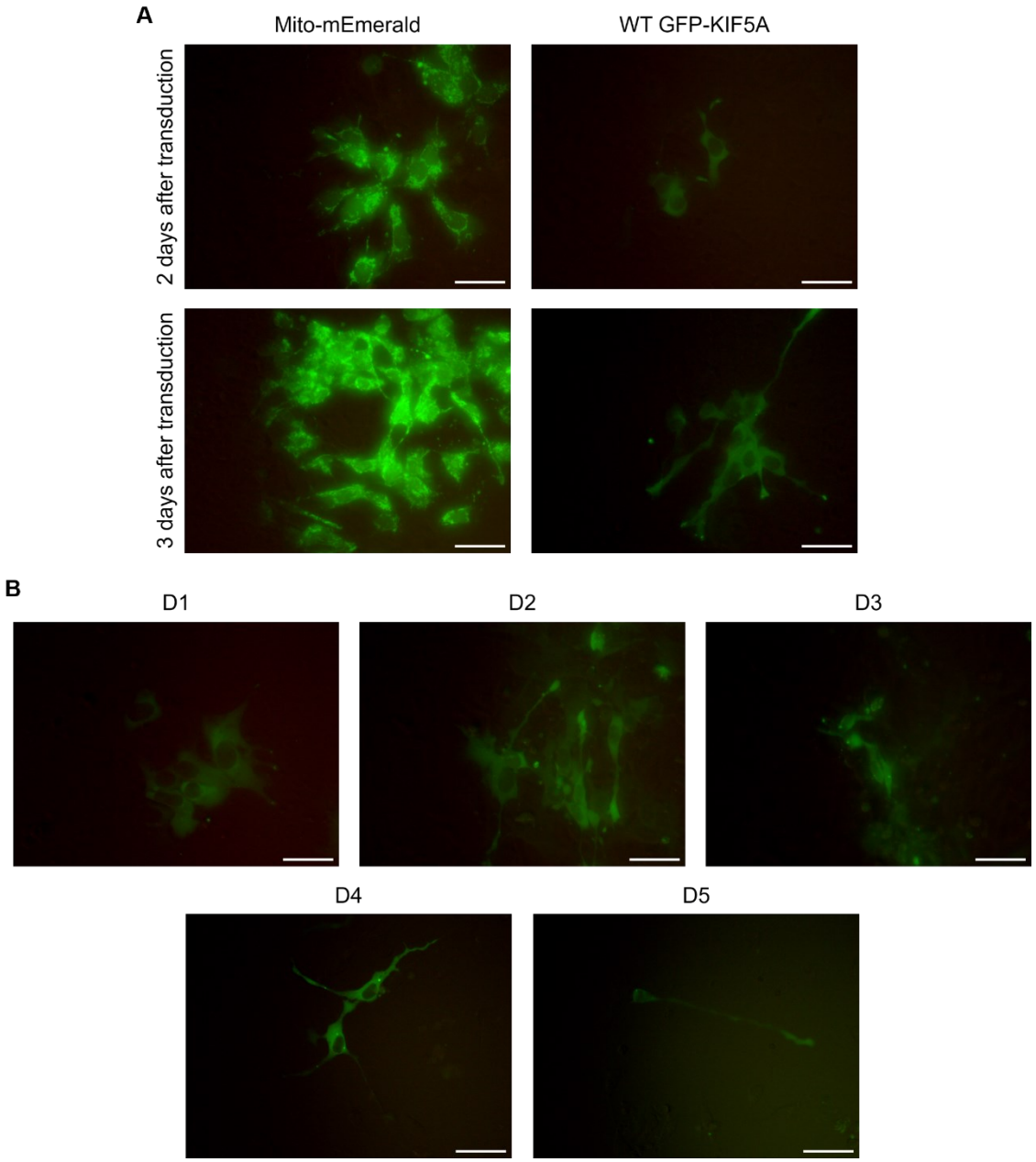

Figure 24 KIF5A overexpression in differentiating hNIL iPSCs. (A) Microscopy analysis of hNIL iPSCs transduced with Mito-mEmerald or wild type (WT) EF1α-KIF5A vectors 48 h (top panel) or 72h (bottom panel) after transduction. Scale bars 100 µm **(B)** Microscopy analysis of differentiating hNIL iPSCs transduced with WT EF1α-KIF5A (day-D). Differentiation was started 24 h after transduction (i.e., D1). Scale bars 100 µm.

Discussion

The experiments described in this Section were designed to establish a human motor neuronal model to study the effect of the five disease-linked KIF5A mutants characterised in Sections 1 and 2, with the aim of assessing bidirectional axonal transport in a context replicating MND pathophysiology better than immortalised cells. In this respect, hNIL iPSCs represented a valid candidate because they can be rapidly differentiated into i^{3}LMNs and can be efficiently transduced[284], potentially providing a good experimental platform to compare multiple KIF5A mutations in a homogeneous background in the absence of patient-derived iPSCs and bypassing time-demanding gene editing steps.

Unfortunately, the experiments described in this Section did not provide the desired outcome, since KIF5A overexpression was inexplicably very low in transduced i^{3}LMNs. The PGK and EF1α promoters were both shown to provide effective transgene overexpression in i^{3}LMNs[284], which was confirmed using the Mito-mEmerald vector as transduction control, so that the inefficiency of the system is probably not related to the chosen transfer constructs. Lentiviral transduction of hNIL iPSCs followed by differentiation was unsuccessful, too, as GFP-KIF5A levels progressively decreased with motor neuron maturation.

Loss of GFP-positive i^{3}LMNs could be due to cell death. This would be consistent with reports indicating that KIF5A mutations resulting in the enhanced anterograde motility of the protein are linked to motor neuron degeneration and that WT KIF5A overexpression has a partially toxic effect in transfected primary neurons, too[150,151]. Nonetheless, transduced hNIL iPSCs and i^{3}LMN cultures did not show clear signs of cell death, although no analyses aimed at evaluating their viability and/or mortality were performed. A second mechanism potentially explaining the progressive loss of GFP-KIF5A expression during motor neuron differentiation is related to autoregulation, which would allow to avoid potential imbalances in the equilibrium between anterograde and retrograde axonal trafficking. Since PGK and EF1α are constitutive promoters and are not normally silenced by hNIL iPSCs and i^{3}LMNs, such a putative autoregulation mechanism should limit the half-life of the KIF5A protein to avoid imbalances in the equilibrium between anterograde and retrograde axonal trafficking during neuronal commitment and maturation rather than acting on *KIF5A* transcription. The assessment of KIF5A protein levels during the various stages of hNIL iPSC differentiation into i^{3}LMNs is anyways necessary to confirm this hypothesis.

Collectively, the results of the experiments described in this Section suggest that KIF5A overexpression in hNIL iPSC-derived i^{3}LMNs is inefficient. Therefore, strategies aimed at investigating the impact of mutant KIF5A in a similar experimental setting should probably avoid

overexpression and rather rely on gene editing to introduce the mutation of interest if patient cells are not available.

Bibliography

1. Hardin, J., Bertoni, G. P. & Kleinsmith, L. J. *Becker's World of the Cell*. (Pearson Publishing, 2015).
2. Hirokawa, N. & Tanaka, Y. Kinesin superfamily proteins (KIFs): various functions and their relevance for important phenomena in life and diseases. *Exp Cell Res* **334**, 16–25 (2015).
3. Reck-Peterson, S. L., Redwine, W. B., Vale, R. D. & Carter, A. P. The cytoplasmic dynein transport machinery and its many cargoes. *Nat Rev Mol Cell Biol* **19**, 382–398 (2018).
4. Roll-Mecak, A. The tubulin code in microtubule dynamics and information encoding. *Dev Cell* **54**, 7–20 (2020).
5. Kollman, J. M., Merdes, A., Mourey, L. & Agard, D. A. Microtubule nucleation by γ-tubulin complexes. *Nat Rev Mol Cell Biol* **12**, 709–21 (2011).
6. Desai, A. & Mitchison, T. J. Microtubule polymerization dynamics. *Annu Rev Cell Dev Biol* **13**, 83–117 (1997).
7. Konietzny, A., Bär, J. & Mikhaylova, M. Dendritic actin cytoskeleton: structure, functions, and regulations. *Front Cell Neurosci* **11**, 147 (2017).
8. Hirokawa, N., Niwa, S. & Tanaka, Y. Molecular motors in neurons: transport mechanisms and roles in brain function, development, and disease. *Neuron* **68**, 610–38 (2010).
9. Vale, R. D., Reese, T. S. & Sheetz, M. P. Identification of a novel force-generating protein, kinesin, involved in microtubule-based motility. *Cell* **42**, 39–50 (1985).
10. Brady, S. T. A novel brain ATPase with properties expected for the fast axonal transport motor. *Nature* **317**, 73–75 (1985).
11. Hirokawa, N. *et al.* Kinesin associates with anterogradely transported membranous organelles in vivo. *Journal of Cell Biology* **114**, 295–302 (1991).
12. Miki, H., Okada, Y. & Hirokawa, N. Analysis of the kinesin superfamily: insights into structure and function. *Trends Cell Biol* **15**, 467–476 (2005).
13. Lawrence, C. J. *et al.* A standardized kinesin nomenclature. *Journal of Cell Biology* **167**, 19–22 (2004).
14. Hirokawa, N. *et al.* Submolecular domains of bovine brain kinesin identified by electron microscopy and monoclonal antibody decoration. *Cell* **56**, 867–878 (1989).
15. Hirokawa, N. & Noda, Y. Intracellular transport and kinesin superfamily proteins, KIFs: structure, function, and dynamics. *Physiol Rev* **88**, 1089–1118 (2008).
16. Maday, S., Twelvetrees, A. E., Moughamian, A. J. & Holzbaur, E. L. F. Axonal transport: cargo-specific mechanisms of motility and regulation. *Neuron* **84**, 292–309 (2014).
17. Terada, S. Where does slow axonal transport go? *Neurosci Res* **47**, 367–372 (2003).
18. Karki, S. & Holzbaur, E. L. F. Cytoplasmic dynein and dynactin in cell division and intracellular transport. *Curr Opin Cell Biol* **11**, 45–53 (1999).
19. Pfister, K. K. *et al.* Cytoplasmic dynein nomenclature. *Journal of Cell Biology* **171**, 411–413 (2005).
20. Kardon, J. R. & Vale, R. D. Regulators of the cytoplasmic dynein motor. *Nat Rev Mol Cell Biol* **10**, 854–865 (2009).
21. Tanaka, Y., Zhang, Z. & Hirokawa, N. Identification and molecular evolution of new dynein-like protein sequences in rat brain. *J Cell Sci* **108**, 1883–1893 (1995).
22. Rosenbaum, J. L. & Witman, G. B. Intraflagellar transport. *Nat Rev Mol Cell Biol* **3**, 813–825 (2002).
23. Pfister, K. K. *et al.* Genetic analysis of the cytoplasmic dynein subunit families. *PLoS Genet* **2**, e1 (2006).

24. May, S. R. *et al.* Loss of the retrograde motor for IFT disrupts localization of Smo to cilia and prevents the expression of both activator and repressor functions of Gli. *Dev Biol* **287**, 378–389 (2005).
25. Ha, J. *et al.* A neuron-specific cytoplasmic dynein isoform preferentially transports TrkB signaling endosomes. *Journal of Cell Biology* **181**, 1027–1039 (2008).
26. Fuhrmann, J. C. *et al.* Gephyrin interacts with dynein light chains 1 and 2, components of motor protein complexes. *Journal of Neuroscience* **22**, 5393–5402 (2002).
27. Colin, E. *et al.* Huntingtin phosphorylation acts as a molecular switch for anterograde/retrograde transport in neurons. *EMBO Journal* **27**, 2124–2134 (2008).
28. Hollenbeck, P. J. & Saxton, W. M. The axonal transport of mitochondria. *J Cell Sci* **118**, 5411–5419 (2005).
29. Johansson, M. *et al.* Activation of endosomal dynein motors by stepwise assembly of Rab7–RILP–p150Glued, ORP1L, and the receptor βIII spectrin. *Journal of Cell Biology* **176**, 459–471 (2007).
30. Saxena, S., Bucci, C., Weis, J. & Kruttgen, A. The small GTPase Rab7 controls the endosomal trafficking and neuritogenic signaling of the nerve growth factor receptor TrkA. *Journal of Neuroscience* **25**, 10930–10940 (2005).
31. Hartman, M. A. & Spudich, J. A. The myosin superfamily at a glance. *J Cell Sci* **125**, 1627–1632 (2012).
32. Tabb, J. S., Molyneaux, B. J., Cohen, D. L., Kuznetsov, S. A. & Langford, G. M. Transport of ER vesicles on actin filaments in neurons by myosin V. *J Cell Sci* **111**, 3221–3234 (1998).
33. Huang, J.-D. *et al.* Direct interaction of microtubule- and actin-based transport motors. *Nature* **397**, 267–270 (1999).
34. Ohashi, S. *et al.* Identification of mRNA/protein (mRNP) complexes containing Purα, mStaufen, fragile X protein, and myosin Va and their association with rough endoplasmic reticulum equipped with a kinesin motor. *Journal of Biological Chemistry* **277**, 37804–37810 (2002).
35. Lisé, M.-F. *et al.* Involvement of myosin Vb in glutamate receptor trafficking. *Journal of Biological Chemistry* **281**, 3669–3678 (2006).
36. Krementsov, D. N., Krementsova, E. B. & Trybus, K. M. Myosin V: Regulation by calcium, calmodulin, and the tail domain. *Journal of Cell Biology* **164**, 877–886 (2004).
37. Correia, S. S. *et al.* Motor protein–dependent transport of AMPA receptors into spines during long-term potentiation. *Nat Neurosci* **11**, 457–466 (2008).
38. Wang, Z. *et al.* Myosin Vb mobilizes recycling endosomes and AMPA receptors for postsynaptic plasticity. *Cell* **135**, 535–548 (2008).
39. Wells, A. L. *et al.* Myosin VI is an actin-based motor that moves backwards. *Nature* **401**, 505–508 (1999).
40. Osterweil, E., Wells, D. G. & Mooseker, M. S. A role for myosin VI in postsynaptic structure and glutamate receptor endocytosis. *Journal of Cell Biology* **168**, 329–338 (2005).
41. Yano, H. *et al.* BDNF-mediated neurotransmission relies upon a myosin VI motor complex. *Nat Neurosci* **9**, 1009–1018 (2006).
42. Solecki, D. J. *et al.* Myosin II motors and F-actin dynamics drive the coordinated movement of the centrosome and soma during CNS glial-guided neuronal migration. *Neuron* **63**, 63–80 (2009).
43. Mochida, S. *et al.* Myosin II is involved in transmitter release at synapses formed between rat sympathetic neurons in culture. *Neuron* **13**, 1131–1142 (1994).
44. Rex, C. S. *et al.* Myosin IIb regulates actin dynamics during synaptic plasticity and memory formation. *Neuron* **67**, 603–617 (2010).

45. Vallee, R. B., Seale, G. E. & Tsai, J.-W. Emerging roles for myosin II and cytoplasmic dynein in migrating neurons and growth cones. *Trends Cell Biol* **19**, 347–355 (2009).
46. Zhu, X.-J. *et al.* Myosin X regulates netrin receptors and functions in axonal path-finding. *Nat Cell Biol* **9**, 184–192 (2007).
47. Aizawa, H. *et al.* Kinesin family in murine central nervous system. *Journal of Cell Biology* **119**, 1287–1296 (1992).
48. Kanai, Y. *et al.* KIF5C, a novel neuronal kinesin enriched in motor neurons. *Journal of Neuroscience* **20**, 6374 (2000).
49. Brady, S. T. & Morfini, G. A. Regulation of motor proteins, axonal transport deficits and adult-onset neurodegenerative diseases. *Neurobiol Dis* **105**, 273–282 (2017).
50. Klinman, E. & Holzbaur, E. L. F. Walking forward with kinesin. *Trends Neurosci* **41**, 555–556 (2018).
51. Kull, F. J., Sablin, E. P., Lau, R., Fletterick, R. J. & Vale, R. D. Crystal structure of the kinesin motor domain reveals a structural similarity to myosin. *Nature* **380**, 550–555 (1996).
52. Funakoshi, T., Takeda, S. & Hirokawa, N. Active transport of photoactivated tubulin molecules in growing axons revealed by a new electron microscopic analysis. *Journal of Cell Biology* **133**, 1347–1353 (1996).
53. Gigant, B. *et al.* The 4 A X-ray structure of a tubulin:stathmin-like domain complex. *Cell* **102**, 809–16 (2000).
54. Gennerich, A. & Vale, R. D. Walking the walk: how kinesin and dynein coordinate their steps. *Curr Opin Cell Biol* **21**, 59–67 (2009).
55. Kawaguchi, K. & Ishiwata, S. Nucleotide-dependent single- to double-headed binding of kinesin. *Science (1979)* **291**, 667–669 (2001).
56. Asbury, C. L., Fehr, A. N. & Block, S. M. Kinesin moves by an asymmetric hand-over-hand mechanism. *Science (1979)* **302**, 2130–2134 (2003).
57. Kawaguchi, K. Energetics of Kinesin-1 stepping mechanism. *FEBS Lett* **582**, 3719–22 (2008).
58. Guydosh, N. R. & Block, S. M. Direct observation of the binding state of the kinesin head to the microtubule. *Nature* **461**, 125–128 (2009).
59. Hackney, D. D. The tethered motor domain of a kinesin-microtubule complex catalyzes reversible synthesis of bound ATP. *Proceedings of the National Academy of Sciences* **102**, 18338–18343 (2005).
60. Uemura, S. & Ishiwata, S. Loading direction regulates the affinity of ADP for kinesin. *Nat Struct Biol* **10**, 308–11 (2003).
61. Yildiz, A., Tomishige, M., Gennerich, A. & Vale, R. D. Intramolecular strain coordinates kinesin stepping behavior along microtubules. *Cell* **134**, 1030–1041 (2008).
62. DeBoer, S. R. *et al.* Conventional kinesin holoenzymes are composed of heavy and light chain homodimers. *Biochemistry* **47**, 4535–4543 (2008).
63. Diefenbach, R. J., Mackay, J. P., Armati, P. J. & Cunningham, A. L. The C-terminal region of the stalk domain of ubiquitous human kinesin heavy chain contains the binding site for kinesin light chain. *Biochemistry* **37**, 16663–16670 (1998).
64. Gyoeva, F. K., Sarkisov, D. v, Khodjakov, A. L. & Minin, A. A. The tetrameric molecule of conventional kinesin contains identical light chains. *Biochemistry* **43**, 13525–31 (2004).
65. Skoufias, D. A., Cole, D. G., Wedaman, K. P. & Scholey, J. M. The carboxyl-terminal domain of kinesin heavy chain is important for membrane binding. *Journal of Biological Chemistry* **269**, 1477–85 (1994).
66. McCart, A. E., Mahony, D. & Rothnagel, J. A. Alternatively spliced products of the human kinesin light chain 1 (KNS2) gene. *Traffic* **4**, 576–80 (2003).

67. Stenoien, D. L. & Brady, S. T. Immunochemical analysis of kinesin light chain function. *Mol Biol Cell* **8**, 675–689 (1997).
68. Coy, D. L., Hancock, W. O., Wagenbach, M. & Howard, J. Kinesin's tail domain is an inhibitory regulator of the motor domain. *Nat Cell Biol* **1**, 288–292 (1999).
69. Kaan, H. Y. K., Hackney, D. D. & Frank, K. The structure of the Kinesin-1 motor-tail complex reveals the mechanism of autoinhibition. *Science (1979)* **333**, 883–885 (2011).
70. Saxton, W. M., Hicks, J., Goldstein, L. S. B. & Raff, E. C. Kinesin heavy chain is essential for viability and neuromuscular functions in Drosophila, but mutants show no defects in mitosis. *Cell* **64**, 1093–1102 (1991).
71. Hurd, D. D. & Saxton, W. M. Kinesin mutations cause motor neuron disease phenotypes by disrupting fast axonal transport in Drosophila. *Genetics* **144**, 1075–1085 (1996).
72. Gindhart, J. G., Desai, C. J., Beushausen, S., Zinn, K. & Goldstein, L. S. B. Kinesin light chains are essential for axonal transport in Drosophila. *Journal of Cell Biology* **141**, 443–454 (1998).
73. Kimura Arimura Fukata, T. N. Y., Watanabe, H., Iwamatsu, A. & Kaibuchi, K. Tubulin and CRMP-2 complex is transported via Kinesin-1. *J Neurochem* **93**, 1371–1382 (2005).
74. Taya, S. *et al.* DISC1 regulates the transport of the NUDEL/LIS1/14-3-3 complex through Kinesin-1. *Journal of Neuroscience* **27**, 15–26 (2007).
75. Ferreira, A., Niclas, J., Vale, R. D., Banker, G. & Kosik, K. S. Suppression of kinesin expression in cultured hippocampal neurons using antisense oligonucleotides. *Journal of Cell Biology* **117**, 595–606 (1992).
76. Xia, C.-H. *et al.* Abnormal neurofilament transport caused by targeted disruption of neuronal kinesin heavy chain KIF5A. *Journal of Cell Biology* **161**, 55–66 (2003).
77. Terada, S., Kinjo, M., Aihara, M., Takei, Y. & Hirokawa, N. Kinesin-1/Hsc70-dependent mechanism of slow axonal transport and its relation to fast axonal transport. *EMBO Journal* **29**, 843–854 (2010).
78. Byrd, D. T. *et al.* UNC-16, a JNK-signaling scaffold protein, regulates vesicle transport in C. elegans. *Neuron* **32**, 787–800 (2001).
79. Toda, H. *et al.* UNC-51/ATG1 kinase regulates axonal transport by mediating motor–cargo assembly. *Genes Dev* **22**, 3292–3307 (2008).
80. Diefenbach, R. J., Diefenbach, E., Douglas, M. W. & Cunningham, A. L. The heavy chain of conventional kinesin Interacts with the SNARE proteins SNAP25 and SNAP23. *Biochemistry* **41**, 14906–14915 (2002).
81. Su, Q., Cai, Q., Gerwin, C., Smith, C. L. & Sheng, Z.-H. Syntabulin is a microtubule-associated protein implicated in syntaxin transport in neurons. *Nat Cell Biol* **6**, 941–953 (2004).
82. Cai, Q., Pan, P.-Y. & Sheng, Z.-H. Syntabulin–Kinesin-1 family member 5B-mediated axonal transport contributes to activity-dependent presynaptic assembly. *Journal of Neuroscience* **27**, 7284–7296 (2007).
83. Cai, Q., Gerwin, C. & Sheng, Z.-H. Syntabulin-mediated anterograde transport of mitochondria along neuronal processes. *Journal of Cell Biology* **170**, 959–969 (2005).
84. Glater, E. E., Megeath, L. J., Stowers, R. S. & Schwarz, T. L. Axonal transport of mitochondria requires milton to recruit kinesin heavy chain and is light chain independent. *Journal of Cell Biology* **173**, 545–557 (2006).
85. Cho, K. *et al.* Association of the kinesin-binding domain of RanBP2 to KIF5B and KIF5C determines mitochondria localization and function. *Traffic* **8**, 1722–1735 (2007).
86. Wang, X. & Schwarz, T. L. The mechanism of Ca2+-dependent regulation of kinesin-mediated mitochondrial motility. *Cell* **136**, 163–174 (2009).
87. Tanaka, Y. *et al.* Targeted disruption of mouse conventional kinesin heavy chain, kif5B, results in abnormal perinuclear clustering of mitochondria. *Cell* **93**, 1147–1158 (1998).

88. Karle, K. N., Möckel, D., Reid, E. & Schöls, L. Axonal transport deficit in a KIF5A(-/-) mouse model. *Neurogenetics* **13**, 169–179 (2012).
89. Campbell, P. D. *et al.* Unique function of Kinesin Kif5A in localization of mitochondria in axons. *Journal of Neuroscience* **34**, 14717–14732 (2014).
90. Fenton, A. R., Jongens, T. A. & Holzbaur, E. L. F. Mitochondrial adaptor TRAK2 activates and functionally links opposing kinesin and dynein motors. *Nat Commun* **12**, 4578 (2021).
91. Pilling, A. D., Horiuchi, D., Lively, C. M. & Saxton, W. M. Kinesin-1 and dynein are the primary motors for fast transport of mitochondria in Drosophila motor axons. *Mol Biol Cell* **17**, 2057–2068 (2006).
92. van Spronsen, M. *et al.* TRAK/Milton motor-adaptor proteins steer mitochondrial trafficking to axons and dendrites. *Neuron* **77**, 485–502 (2013).
93. Sainath, R. & Gallo, G. The dynein inhibitor Ciliobrevin D inhibits the bidirectional transport of organelles along sensory axons and impairs NGF-mediated regulation of growth cones and axon branches. *Dev Neurobiol* **75**, 757–777 (2015).
94. Twelvetrees, A. E. *et al.* The dynamic localization of cytoplasmic dynein in neurons is driven by kinesin-1. *Neuron* **90**, 1000–1015 (2016).
95. Nakata, T. & Hirokawa, N. Point mutation of adenosine triphosphate-binding motif generated rigor kinesin that selectively blocks anterograde lysosome membrane transport. *Journal of Cell Biology* **131**, 1039–1053 (1995).
96. Imamura, T. *et al.* Insulin-induced GLUT4 translocation involves protein kinase C-λ-mediated functional coupling between Rab4 and the motor protein kinesin. *Mol Cell Biol* **23**, 4892–4900 (2003).
97. Bananis, E. *et al.* Microtubule-dependent movement of late endocytic vesicles in vitro: requirements for dynein and kinesin. *Mol Biol Cell* **15**, 3688–3697 (2004).
98. Liu, M. *et al.* KIF5A-dependent axonal transport deficiency disrupts autophagic flux in trimethyltin chloride-induced neurotoxicity. *Autophagy* **17**, 903–924 (2021).
99. Inomata, H. *et al.* A scaffold protein JIP-1b enhances amyloid precursor protein phosphorylation by JNK and its association with Kinesin Light Chain 1. *Journal of Biological Chemistry* **278**, 22946–22955 (2003).
100. Verhey, K. J. *et al.* Cargo of kinesin identified as JIP scaffolding proteins and associated signaling molecules. *Journal of Cell Biology* **152**, 959–970 (2001).
101. Hammond, J. W., Griffin, K., Jih, G. T., Stuckey, J. & Verhey, K. J. Co-operative versus independent transport of different cargoes by Kinesin-1. *Traffic* **9**, 725–741 (2008).
102. Twelvetrees, A. E. *et al.* Delivery of GABAARs to synapses is mediated by HAP1-KIF5 and disrupted by mutant huntingtin. *Neuron* **65**, 53–65 (2010).
103. Ohashi, S. *et al.* Identification of mRNA/protein (mRNP) complexes containing Purα, mStaufen, Fragile X Protein, and Myosin Va and their association with rough endoplasmic reticulum equipped with a kinesin motor. *Journal of Biological Chemistry* **277**, 37804–37810 (2002).
104. Kanai, Y., Dohmae, N. & Hirokawa, N. Kinesin transports RNA: isolation and characterization of an RNA-transporting granule. *Neuron* **43**, 513–525 (2004).
105. Ling, S.-C., Fahrner, P. S., Greenough, W. T. & Gelfand, V. I. Transport of Drosophila Fragile X Mental Retardation Protein-containing ribonucleoprotein granules by Kinesin-1 and cytoplasmic dynein. *Proceedings of the National Academy of Sciences* **101**, 17428–17433 (2004).
106. Nakajima, K. *et al.* Molecular motor KIF5A is essential for GABA(A) receptor transport, and KIF5A deletion causes epilepsy. *Neuron* **76**, 945–961 (2012).

107. Uchida, A., Alami, N. H. & Brown, A. Tight functional coupling of kinesin-1A and dynein motors in the bidirectional transport of neurofilaments. *Mol Biol Cell* **20**, 4997–5006 (2009).
108. Rahman, A., Kamal, A., Roberts, E. A. & Goldstein, L. S. B. Defective kinesin heavy chain behavior in mouse kinesin light chain mutants. *Journal of Cell Biology* **146**, 1277–1288 (1999).
109. Fukuda, Y. *et al.* Binding and transport of SFPQ-RNA granules by KIF5A/KLC1 motors promotes axon survival. *Journal of Cell Biology* **220**, (2021).
110. Cosker, K. E., Fenstermacher, S. J., Pazyra-Murphy, M. F., Elliott, H. L. & Segal, R. A. The RNA-binding protein SFPQ orchestrates an RNA regulon to promote axon viability. *Nat Neurosci* **19**, 690–696 (2016).
111. Thomas-Jinu, S. *et al.* Non-nuclear pool of splicing factor SFPQ regulates axonal transcripts required for normal motor development. *Neuron* **94**, 931 (2017).
112. Hoerndli, F. J. *et al.* Kinesin-1 regulates synaptic strength by mediating the delivery, removal, and redistribution of AMPA receptors. *Neuron* **80**, 1421–1437 (2013).
113. Brachet, A. *et al.* A Kinesin 1-protrudin complex mediates AMPA receptor synaptic removal during long-term depression. *Cell Rep* **36**, 109499 (2021).
114. Warner, T. T. Motor neuron diseases. in *Practical Guide to Neurogenetics* 150–174 (Elsevier, 2009). doi:10.1016/B978-0-7506-5410-4.00010-4.
115. Dion, P. A., Daoud, H. & Rouleau, G. A. Genetics of motor neuron disorders: new insights into pathogenic mechanisms. *Nat Rev Genet* **10**, 769–782 (2009).
116. James, P. A. & Talbot, K. The molecular genetics of non-ALS motor neuron diseases. *Biochim Biophys Acta* **1762**, 986–1000 (2006).
117. Di Giorgio, F. P., Carrasco, M. A., Siao, M. C., Maniatis, T. & Eggan, K. Non–cell autonomous effect of glia on motor neurons in an embryonic stem cell–based ALS model. *Nat Neurosci* **10**, 608–614 (2007).
118. Cykowski, M. D. *et al.* Phosphorylated TDP-43 (pTDP-43) aggregates in the axial skeletal muscle of patients with sporadic and familial amyotrophic lateral sclerosis. *Acta Neuropathol Commun* **6**, 28 (2018).
119. Sau, D. *et al.* Mutation of SOD1 in ALS: a gain of a loss of function. *Hum Mol Genet* **16**, 1604–1618 (2007).
120. Neefjes, J. & van der Kant, R. Stuck in traffic: an emerging theme in diseases of the nervous system. *Trends Neurosci* **37**, 66–76 (2014).
121. Prior, R., Van Helleputte, L., Benoy, V. & Van Den Bosch, L. Defective axonal transport: a common pathological mechanism in inherited and acquired peripheral neuropathies. *Neurobiol Dis* **105**, 300–320 (2017).
122. Milde, S., Adalbert, R., Elaman, M. H. & Coleman, M. P. Axonal transport declines with age in two distinct phases separated by a period of relative stability. *Neurobiol Aging* **36**, 971–981 (2015).
123. Sleigh, J. N., Rossor, A. M., Fellows, A. D., Tosolini, A. P. & Schiavo, G. Axonal transport and neurological disease. *Nat Rev Neurol* **15**, 691–703 (2019).
124. Murala, S., Nagarajan, E. & Bollu, P. C. Hereditary spastic paraplegia. *Neurological Sciences* **42**, 883–894 (2021).
125. Fink, J. K. Hereditary spastic paraplegia: clinico-pathologic features and emerging molecular mechanisms. *Acta Neuropathol* **126**, 307–328 (2013).
126. de Souza, P. V. S., de Rezende Pinto, W. B. V., de Rezende Batistella, G. N., Bortholin, T. & Oliveira, A. S. B. Hereditary spastic paraplegia: clinical and genetic hallmarks. *Cerebellum* **16**, 525–551 (2017).

127. Barreto, L. C. L. S. *et al.* Epidemiologic study of Charcot-Marie-Tooth disease: a systematic review. *Neuroepidemiology* **46**, 157–165 (2016).
128. Tazir, M., Hamadouche, T., Nouioua, S., Mathis, S. & Vallat, J.-M. Hereditary motor and sensory neuropathies or Charcot–Marie–Tooth diseases: An update. *J Neurol Sci* **347**, 14–22 (2014).
129. Rossor, A. M. *et al.* Peripheral neuropathy in complex inherited diseases: an approach to diagnosis. *J Neurol Neurosurg Psychiatry* **88**, 846–863 (2017).
130. Bis-Brewer, D. M., Fazal, S. & Züchner, S. Genetic modifiers and non-Mendelian aspects of CMT. *Brain Res* **1726**, 146459 (2020).
131. McCray, B. A. & Scherer, S. S. Axonal Charcot-Marie-Tooth disease: from common pathogenic mechanisms to emerging treatment opportunities. *Neurotherapeutics* **18**, 2269–2285 (2021).
132. Cicardi, M. *et al.* Tdp-25 routing to autophagy and proteasome ameliorates its aggregation in amyotrophic lateral sclerosis target cells. *Sci Rep* **8**, 12390 (2018).
133. Philips, T. *et al.* Oligodendrocyte dysfunction in the pathogenesis of amyotrophic lateral sclerosis. *Brain* **136**, 471–482 (2013).
134. Robberecht, W. & Philips, T. The changing scene of amyotrophic lateral sclerosis. *Nat Rev Neurosci* **14**, 248–264 (2013).
135. Laferriere, F. & Polymenidou, M. Advances and challenges in understanding the multifaceted pathogenesis of amyotrophic lateral sclerosis. *Swiss Med Wkly* (2015) doi:10.4414/smw.2015.14054.
136. Kiernan, M. C. *et al.* Amyotrophic lateral sclerosis. *Lancet* **377**, 942–955 (2011).
137. Taylor, J. P., Brown, R. H. & Cleveland, D. W. Decoding ALS: from genes to mechanism. *Nature* **539**, 197–206 (2016).
138. Neumann, M. *et al.* Ubiquitinated TDP-43 in frontotemporal lobar degeneration and amyotrophic lateral sclerosis. *Science (1979)* **314**, 130–133 (2006).
139. Reid, E. *et al.* A kinesin heavy chain (KIF5A) mutation in hereditary spastic paraplegia (SPG10). *Am J Hum Genet* **71**, 1189–1194 (2002).
140. Crimella, C. *et al.* Mutations in the motor and stalk domains of KIF5A in spastic paraplegia type 10 and in axonal Charcot-Marie-Tooth type 2. *Clin Genet* **82**, 157–164 (2012).
141. Nicolas, A. *et al.* Genome-wide analyses identify KIF5A as a novel ALS gene. *Neuron* **97**, 1268-1283.e6 (2018).
142. Brenner, D. *et al.* Hot-spot KIF5A mutations cause familial ALS. *Brain* **141**, 688–697 (2018).
143. Goizet, C. *et al.* Complicated forms of autosomal dominant hereditary spastic paraplegia are frequent in SPG10. *Hum Mutat* **30**, E376–E385 (2009).
144. Kawaguchi, K. Role of Kinesin-1 in the pathogenesis of SPG10, a rare form of hereditary spastic paraplegia. *The Neuroscientist* **19**, 336–344 (2013).
145. Ebbing, B. *et al.* Effect of spastic paraplegia mutations in KIF5A kinesin on transport activity. *Hum Mol Genet* **17**, 1245–1252 (2008).
146. Dutta, M., Diehl, M. R., Onuchic, J. N. & Jana, B. Structural consequences of hereditary spastic paraplegia disease-related mutations in kinesin. *Proceedings of the National Academy of Sciences* **115**, E10822–E10829 (2018).
147. Wang, L. & Brown, A. A hereditary spastic paraplegia mutation in kinesin-1A/KIF5A disrupts neurofilament transport. *Mol Neurodegener* **5**, 52 (2010).
148. Füger, P. *et al.* Spastic paraplegia mutation N256S in the neuronal microtubule motor KIF5A disrupts axonal transport in a Drosophila HSP model. *PLoS Genet* **8**, e1003066 (2012).
149. Jennings, S. *et al.* Characterization of kinesin switch I mutations that cause hereditary spastic paraplegia. *PLoS One* **12**, e0180353 (2017).

150. Baron, D. M. *et al.* ALS-associated KIF5A mutations abolish autoinhibition resulting in a toxic gain of function. *Cell Rep* **39**, 110598 (2022).
151. Pant, D. C. *et al.* ALS-linked KIF5A ΔExon27 mutant causes neuronal toxicity through gain-of-function. *EMBO Rep* **23**, (2022).
152. Santangelo, S. *et al.* Generation of an iPSC line from a patient with spastic paraplegia type 10 carrying a novel mutation in KIF5A gene. *Stem Cell Res* **66**, 103008 (2023).
153. Pyromali, I. *et al.* New structural variations responsible for Charcot-Marie-Tooth disease: The first two large KIF5A deletions detected by CovCopCan software. *Comput Struct Biotechnol J* **19**, 4265–4272 (2021).
154. Schüle, R. *et al.* SPG10 is a rare cause of spastic paraplegia in European families. *J Neurol Neurosurg Psychiatry* **79**, 584 (2008).
155. Qiu, Y. *et al.* A novel KIF5A gene variant causes spastic paraplegia and cerebellar ataxia. *Ann Clin Transl Neurol* **5**, 1415–1420 (2018).
156. Bacquet, J. *et al.* Molecular diagnosis of inherited peripheral neuropathies by targeted next-generation sequencing: molecular spectrum delineation. *BMJ Open* **8**, e021632 (2018).
157. Grassano, M. *et al.* Systematic evaluation of genetic mutations in ALS: a population-based study. *J Neurol Neurosurg Psychiatry* **93**, 1190–3 (2022).
158. Méreaux, J.-L. *et al.* Clinical and genetic spectra of 1550 index patients with hereditary spastic paraplegia. *Brain* **145**, 1029–1037 (2022).
159. van de Warrenburg, B. P. *et al.* Clinical exome sequencing for cerebellar ataxia and spastic paraplegia uncovers novel gene-disease associations and unanticipated rare disorders. *European Journal of Human Genetics* **24**, 1460–6 (2016).
160. Carosi, L. *et al.* Hereditary spastic paraplegia: a novel mutation and expansion of the phenotype variability in SPG10. *J Neurol Neurosurg Psychiatry* **86**, 702–704 (2015).
161. Kaji, S. *et al.* Late-onset spastic paraplegia type 10 (SPG10) family presenting with bulbar symptoms and fasciculations mimicking amyotrophic lateral sclerosis. *J Neurol Sci* **364**, 45–49 (2016).
162. Elert-Dobkowska, E. *et al.* Next-generation sequencing study reveals the broader variant spectrum of hereditary spastic paraplegia and related phenotypes. *Neurogenetics* **20**, 27–38 (2019).
163. Oliveira, R., Maruta, C. & Gil-Gouveia, R. A novel KIF5A mutation identified in two-family members with spastic paraplegia type 10. *Rev Neurol (Paris)* **177**, 152–154 (2021).
164. Morais, S. *et al.* Massive sequencing of 70 genes reveals a myriad of missing genes or mechanisms to be uncovered in hereditary spastic paraplegias. *European Journal of Human Genetics* **25**, 1217–1228 (2017).
165. Collongues, N. *et al.* Novel SPG10 mutation associated with dysautonomia, spinal cord atrophy, and skin biopsy abnormality. *Eur J Neurol* **20**, 398–401 (2013).
166. Cortese, A. *et al.* Targeted next-generation sequencing panels in the diagnosis of Charcot-Marie-Tooth disease. *Neurology* **94**, e51–e61 (2020).
167. Musumeci, O. *et al.* A novel mutation in KIF5A gene causing hereditary spastic paraplegia with axonal neuropathy. *Neurological Sciences* **32**, 665–668 (2011).
168. Tessa, A. *et al.* A novel KIF5A/SPG10 mutation in spastic paraplegia associated with axonal neuropathy. *J Neurol* **255**, 1090–1092 (2008).
169. Liu, Y.-T. *et al.* Extended phenotypic spectrum of KIF5A mutations: from spastic paraplegia to axonal neuropathy. *Neurology* **83**, 612–619 (2014).
170. Nam, D. E., Yoo, D. H., Choi, S. S., Choi, B.-O. & Chung, K. W. Wide phenotypic spectrum in axonal Charcot–Marie–Tooth neuropathy type 2 patients with KIF5A mutations. *Genes Genomics* **40**, 77–84 (2018).

171. Cuchanski, M. & Baldwin, K. J. Mutation in KIF5A c.610C>T causing hereditary spastic paraplegia with axonal sensorimotor neuropathy. *Case Rep Neurol* **10**, 165–168 (2018).
172. He, J. *et al.* Whole-exome sequencing identified novel KIF5A mutations in Chinese patients with amyotrophic lateral sclerosis and Charcot-Marie-Tooth type 2. *J Neurol Neurosurg Psychiatry* **91**, 326–328 (2020).
173. Neveling, K. *et al.* A post-hoc comparison of the utility of Sanger sequencing and exome sequencing for the diagnosis of heterogeneous diseases. *Hum Mutat* **34**, 1721–1726 (2013).
174. Orsucci, D. *et al.* Hereditary spastic paraparesis in adults. A clinical and genetic perspective from Tuscany. *Clin Neurol Neurosurg* **120**, 14–19 (2014).
175. Jerath, N. U., Grider, T. & Shy, M. E. Progressive lower extremity weakness and axonal sensorimotor polyneuropathy from a mutation in KIF5A (c.611G>A;p.Arg204Gln). *Case Rep Genet* **2015**, 1–5 (2015).
176. Lee, H. *et al.* Hereditary spastic paraplegia with axonal sensorimotor polyneuropathy in a Korean family caused by pathogenic variant of KIF5A (c.611G>A). *Journal of Clinical Neurology* **16**, 347 (2020).
177. 100, 000 Genomes Project Pilot Investigators *et al.* 100,000 Genomes pilot on rare-disease diagnosis in health care - Preliminary report. *New England Journal of Medicine* **385**, 1868–1880 (2021).
178. Dellatte, J., Lievens, I. & Wang, F. C. Could some mutations of the KIF5A gene be responsible for a dominant CMT2 phenotype? (Case report). *Acta Neurol Belg* (2023) doi:10.1007/s13760-023-02248-4.
179. Fukuoka, M. *et al.* Preliminary report for Epilepsia Open: A case of West syndrome with severe global developmental delay and confirmed KIF5A gene variant. *Epilepsia Open* **6**, 230–234 (2021).
180. Lynch, D. S. *et al.* Hereditary spastic paraplegia in Greece: characterisation of a previously unexplored population using next-generation sequencing. *European Journal of Human Genetics* **24**, 857–863 (2016).
181. Perić, S. *et al.* Phenotypic and genetic heterogeneity of adult patients with hereditary spastic paraplegia from Serbia. *Cells* **11**, 2804 (2022).
182. Iqbal, Z. *et al.* Targeted high throughput sequencing in hereditary ataxia and spastic paraplegia. *PLoS One* **12**, e0174667 (2017).
183. Citrigno, L. *et al.* Kinesins in neurological inherited diseases: a novel motor-domain mutation in KIF5A gene in a patient from Southern Italy affected by hereditary spastic paraplegia. *Acta Neurol Belg* **118**, 643–646 (2018).
184. Andréasson, M. *et al.* Altered CSF levels of monoamines in hereditary spastic paraparesis 10. *Neurol Genet* **5**, e344 (2019).
185. López, E. *et al.* Identification of two novel KIF5A mutations in hereditary spastic paraplegia associated with mild peripheral neuropathy. *J Neurol Sci* **358**, 422–427 (2015).
186. Muglia, M. *et al.* A novel KIF5A mutation in an Italian family marked by spastic paraparesis and congenital deafness. *J Neurol Sci* **343**, 218–220 (2014).
187. Dohrn, M. F. *et al.* Frequent genes in rare diseases: panel-based next generation sequencing to disclose causal mutations in hereditary neuropathies. *J Neurochem* **143**, 507–522 (2017).
188. de Fuenmayor-Fernández de la Hoz, C. P. *et al.* Adult-onset distal spinal muscular atrophy: a new phenotype associated with KIF5A mutations. *Brain* **142**, e66–e66 (2019).
189. Blair, M. A., Ma, S. & Hedera, P. Mutation in KIF5A can also cause adult-onset hereditary spastic paraplegia. *Neurogenetics* **7**, 47–50 (2006).
190. Fichera, M. *et al.* Evidence of kinesin heavy chain (KIF5A) involvement in pure hereditary spastic paraplegia. *Neurology* **63**, 1108–1110 (2004).

191. Hsu, Y. *et al.* Mutation spectrum of Charcot-Marie-Tooth disease among the Han Chinese in Taiwan. *Ann Clin Transl Neurol* **6**, 1090–1101 (2019).
192. Panwala, T. F., Garcia-Santibanez, R., Vizcarra, J. A., Garcia, A. G. & Verma, S. Childhood-onset hereditary spastic paraplegia (HSP): a case series and review of literature. *Pediatr Neurol* **130**, 7–13 (2022).
193. Rinaldi, F. *et al.* A novel mutation in motor domain of KIF5A associated with an HSP/axonal neuropathy phenotype. *J Clin Neuromuscul Dis* **16**, 153–158 (2015).
194. Giordani, G. M. *et al.* Clinical and molecular characterization of a large cohort of childhood onset hereditary spastic paraplegias. *Sci Rep* **11**, 22248 (2021).
195. Lo Giudice, M. *et al.* A missense mutation in the coiled-coil domain of the KIF5A gene and late-onset hereditary spastic paraplegia. *Arch Neurol* **63**, 284–287 (2006).
196. Jia, X. *et al.* Genome sequencing uncovers phenocopies in primary progressive multiple sclerosis. *Ann Neurol* **84**, 51–63 (2018).
197. Guinto, C. O. *et al.* A novel mutation in KIF5A in a Malian family with spastic paraplegia and sensory loss. *Ann Clin Transl Neurol* **4**, 272–275 (2017).
198. Pandya, B. U., Margolin, E. A. & Micieli, J. A. Nuclear DNA mutation in KIF5A causing autosomal dominant phenotypic Leber hereditary optic neuropathy. *Journal of Neuro-ophthalmology* (2022) doi:10.1097/WNO.0000000000001699.
199. Saez-Atienzar, S. *et al.* Identification of a pathogenic intronic KIF5A mutation in an ALS-FTD kindred. *Neurology* **95**, 1015–1018 (2020).
200. Nakamura, R. *et al.* Genetic and functional analysis of KIF5A variants in Japanese patients with sporadic amyotrophic lateral sclerosis. *Neurobiol Aging* **97**, 147.e11-147.e17 (2021).
201. Gu, X. *et al.* Mutation screening of the KIF5A gene in Chinese patients with amyotrophic lateral sclerosis. *J Neurol Neurosurg Psychiatry* **90**, 245–246 (2019).
202. Zhang, K. *et al.* Mutation analysis of KIF5A in Chinese amyotrophic lateral sclerosis patients. *Neurobiol Aging* **73**, 229.e1-229.e4 (2019).
203. Tunca, C. *et al.* Revisiting the complex architecture of ALS in Turkey: Expanding genotypes, shared phenotypes, molecular networks, and a public variant database. *Hum Mutat* **41**, (2020).
204. Dulski, J., Strongosky, A. J., Al-Shaikh, R. H. & Wszolek, Z. K. Expanding the spectrum of KIF5A mutations — Case report of a large kindred with familial ALS and overlapping syndrome. *Amyotroph Lateral Scler Frontotemporal Degener* 1–4 (2023) doi:10.1080/21678421.2022.2164204.
205. Naruse, H. *et al.* Splice-site mutations in KIF5A in the Japanese case series of amyotrophic lateral sclerosis. *Neurogenetics* **22**, 11–17 (2021).
206. Faruq, M. *et al.* Intrafamilial variable spastic paraplegia/ataxia/ALS phenotype linked to a novel KIF5A mutation. *Clin Genet* **96**, 271–273 (2019).
207. Hartl, F. U., Bracher, A. & Hayer-Hartl, M. Molecular chaperones in protein folding and proteostasis. *Nature* **475**, 324–332 (2011).
208. Kampinga, H. H. & Craig, E. A. The HSP70 chaperone machinery: J proteins as drivers of functional specificity. *Nat Rev Mol Cell Biol* **11**, 579–592 (2010).
209. Balch, W. E., Morimoto, R. I., Dillin, A. & Kelly, J. W. Adapting proteostasis for disease intervention. *Science (1979)* **319**, 916–919 (2008).
210. Hoffmann, J. H., Linke, K., Graf, P. C. F., Lilie, H. & Jakob, U. Identification of a redox-regulated chaperone network. *EMBO Journal* **23**, 160–168 (2004).
211. Valastyan, J. S. & Lindquist, S. Mechanisms of protein-folding diseases at a glance. *Dis Model Mech* **7**, 9–14 (2014).

212. Kerscher, O., Felberbaum, R. & Hochstrasser, M. Modification of proteins by ubiquitin and ubiquitin-like proteins. *Annu Rev Cell Dev Biol* **22**, 159–180 (2006).
213. Pickart, C. M. & Eddins, M. J. Ubiquitin: structures, functions, mechanisms. *Biochim Biophys Acta Mol Cell Res* **1695**, 55–72 (2004).
214. Chau, V. *et al.* A multiubiquitin chain is confined to specific lysine in a targeted short-lived protein. *Science (1979)* **243**, 1576–1583 (1989).
215. Murata, S., Yashiroda, H. & Tanaka, K. Molecular mechanisms of proteasome assembly. *Nat Rev Mol Cell Biol* **10**, 104–115 (2009).
216. Alberti, S., Esser, C. & Höhfeld, J. BAG-1 – a nucleotide exchange factor of Hsc70 with multiple cellular functions. *Cell Stress Chaperones* **8**, 225–231 (2003).
217. Klionsky, D. J. *et al.* Guidelines for the use and interpretation of assays for monitoring autophagy (4th edition). *Autophagy* **17**, 1–382 (2021).
218. Tooze, S. A., Abada, A. & Elazar, Z. Endocytosis and autophagy: exploitation or cooperation? *Cold Spring Harb Perspect Biol* **6**, a018358 (2014).
219. Li, W., Li, J. & Bao, J. Microautophagy: lesser-known self-eating. *Cellular and Molecular Life Sciences* **69**, 1125–1136 (2012).
220. Cuervo, A. M. & Wong, E. Chaperone-mediated autophagy: roles in disease and aging. *Cell Res* **24**, 92–104 (2014).
221. Sica, V. *et al.* Organelle-specific initiation of autophagy. *Mol Cell* **59**, 522–539 (2015).
222. Loos, B., du Toit, A. & Hofmeyr, J.-H. S. Defining and measuring autophagosome flux — concept and reality. *Autophagy* **10**, 2087–2096 (2014).
223. Matsunaga, K. *et al.* Autophagy requires endoplasmic reticulum targeting of the PI3-kinase complex via Atg14L. *Journal of Cell Biology* **190**, 511–521 (2010).
224. Cicchini, M., Karantza, V. & Xia, B. Molecular pathways: autophagy in cancer—A matter of timing and context. *Clinical Cancer Research* **21**, 498–504 (2015).
225. Itakura, E. & Mizushima, N. Characterization of autophagosome formation site by a hierarchical analysis of mammalian Atg proteins. *Autophagy* **6**, 764–776 (2010).
226. Zhong, Y. *et al.* Distinct regulation of autophagic activity by Atg14L and Rubicon associated with Beclin 1–phosphatidylinositol-3-kinase complex. *Nat Cell Biol* **11**, 468–476 (2009).
227. Galluzzi, L. *et al.* Molecular definitions of autophagy and related processes. *EMBO Journal* **36**, 1811–1836 (2017).
228. Stolz, A., Ernst, A. & Dikic, I. Cargo recognition and trafficking in selective autophagy. *Nat Cell Biol* **16**, 495–501 (2014).
229. Arndt, V. *et al.* Chaperone-assisted selective autophagy is essential for muscle maintenance. *Current Biology* **20**, 143–148 (2010).
230. Pankiv, S. *et al.* p62/SQSTM1 binds directly to Atg8/LC3 to facilitate degradation of ubiquitinated protein aggregates by autophagy. *Journal of Biological Chemistry* **282**, 24131–24145 (2007).
231. Cristofani, R. *et al.* A crucial role for the protein quality control system in motor neuron diseases. *Front Aging Neurosci* **12**, 191 (2020).
232. Cristofani, R. *et al.* Inhibition of retrograde transport modulates misfolded protein accumulation and clearance in motoneuron diseases. *Autophagy* **13**, 1280–1303 (2017).
233. Dice, J. F. Altered degradation of proteins microinjected into senescent human fibroblasts. *Journal of Biological Chemistry* **257**, 14624–14627 (1982).
234. Kaushik, S. & Cuervo, A. M. Chaperone-mediated autophagy: a unique way to enter the lysosome world. *Trends Cell Biol* **22**, 407–417 (2012).
235. Agarraberes, F. A. & Dice, J. F. A molecular chaperone complex at the lysosomal membrane is required for protein translocation. *J Cell Sci* **114**, 2491–2499 (2001).

236. Ferreira, J. V. *et al.* STUB1/CHIP is required for HIF1A degradation by chaperone-mediated autophagy. *Autophagy* **9**, 1349–1366 (2013).
237. Cuervo, A. M. & Dice, J. F. Age-related decline in chaperone-mediated autophagy. *Journal of Biological Chemistry* **275**, 31505–31513 (2000).
238. Cuervo, A. M. & Dice, J. F. A receptor for the selective uptake and degradation of proteins by lysosomes. *Science (1979)* **273**, 501–503 (1996).
239. Bandyopadhyay, U., Sridhar, S., Kaushik, S., Kiffin, R. & Cuervo, A. M. Identification of regulators of chaperone-mediated autophagy. *Mol Cell* **39**, 535–547 (2010).
240. Salvador, N., Aguado, C., Horst, M. & Knecht, E. Import of a cytosolic protein into lysosomes by chaperone-mediated autophagy depends on its folding state. *Journal of Biological Chemistry* (2000) doi:10.1074/jbc.M001394200.
241. Kaushik, S. & Cuervo, A. M. The coming of age of chaperone-mediated autophagy. *Nat Rev Mol Cell Biol* **19**, 365–381 (2018).
242. Mijaljica, D., Prescott, M. & Devenish, R. J. Microautophagy in mammalian cells: revisiting a 40-year-old conundrum. *Autophagy* **7**, 673–682 (2011).
243. Sahu, R. *et al.* Microautophagy of cytosolic proteins by late endosomes. *Dev Cell* **20**, 131–139 (2011).
244. Uytterhoeven, V. *et al.* Hsc70-4 deforms membranes to promote synaptic protein turnover by endosomal microautophagy. *Neuron* **88**, 735–748 (2015).
245. Bjørkøy, G. *et al.* p62/SQSTM1 forms protein aggregates degraded by autophagy and has a protective effect on huntingtin-induced cell death. *Journal of Cell Biology* **171**, 603–614 (2005).
246. Ichimura, Y. *et al.* Structural basis for sorting mechanism of p62 in selective autophagy. *Journal of Biological Chemistry* **283**, 22847–22857 (2008).
247. Johansen, T. & Lamark, T. Selective autophagy mediated by autophagic adapter proteins. *Autophagy* **7**, 279–296 (2011).
248. Mizushima, N. *et al.* A protein conjugation system essential for autophagy. *Nature* **395**, 395–398 (1998).
249. Parzych, K. R. & Klionsky, D. J. An overview of autophagy: morphology, mechanism, and regulation. *Antioxid Redox Signal* **20**, 460–473 (2013).
250. Jain, A. *et al.* p62/SQSTM1 is a target gene for transcription factor NRF2 and creates a positive feedback loop by inducing antioxidant response element-driven gene transcription. *Journal of Biological Chemistry* **285**, 22576–22591 (2010).
251. Sardiello, M. *et al.* A gene network regulating lysosomal biogenesis and function. *Science (1979)* **325**, 473–477 (2009).
252. Myeku, N. & Figueiredo-Pereira, M. E. Dynamics of the degradation of ubiquitinated proteins by proteasomes and autophagy. *Journal of Biological Chemistry* **286**, 22426–22440 (2011).
253. Cohen-Kaplan, V., Ciechanover, A. & Livneh, I. Stress-induced polyubiquitination of proteasomal ubiquitin receptors targets the proteolytic complex for autophagic degradation. *Autophagy* **13**, 759–760 (2017).
254. Munch, D. *et al.* Autophagy deficiency leads to accumulation of ubiquitinated proteins, ER stress, and cell death in Arabidopsis. *Autophagy* **10**, 1579–1587 (2014).
255. Korolchuk, V. I., Mansilla, A., Menzies, F. M. & Rubinsztein, D. C. Autophagy inhibition compromises degradation of ubiquitin-proteasome pathway substrates. *Mol Cell* **33**, 517–527 (2009).
256. Hirokawa, N., Noda, Y., Tanaka, Y. & Niwa, S. Kinesin superfamily motor proteins and intracellular transport. *Nat Rev Mol Cell Biol* **10**, 682–696 (2009).

257. Nakano, J., Chiba, K. & Niwa, S. An ALS-associated KIF5A mutant forms oligomers and aggregates and induces neuronal toxicity. *Genes to Cells* **27**, 421–435 (2022).
258. Menéndez-Benito, V., Verhoef, L. G. G. C., Masucci, M. G. & Dantuma, N. P. Endoplasmic reticulum stress compromises the ubiquitin–proteasome system. *Hum Mol Genet* **14**, 2787–2799 (2005).
259. Cashman, N. R. *et al.* Neuroblastoma × spinal cord (NSC) hybrid cell lines resemble developing motor neurons. *Developmental Dynamics* **194**, 209–221 (1992).
260. Pareyson, D., Saveri, P., Sagnelli, A. & Piscosquito, G. Mitochondrial dynamics and inherited peripheral nerve diseases. *Neurosci Lett* **596**, 66–77 (2015).
261. Soustelle, L. *et al.* ALS-associated KIF5A mutation causes locomotor deficits associated with cytoplasmic inclusions, alterations of neuromuscular junctions and motor neuron loss. *Journal of Neuroscience* (2023) doi:10.1523/JNEUROSCI.0562-23.2023.
262. Farías, G. G., Guardia, C. M., De Pace, R., Britt, D. J. & Bonifacino, J. S. BORC/kinesin-1 ensemble drives polarized transport of lysosomes into the axon. *Proceedings of the National Academy of Sciences* **114**, E2955–E2964 (2017).
263. Liu, X. & Klionsky, D. J. Regulation of autophagic lysosome reformation by kinesin 1, clathrin and phosphatidylinositol-4,5-bisphosphate. *Autophagy* **14**, 1–2 (2018).
264. Pino, M. G. *et al.* Heterogeneous splicing patterns resulting from KIF5A variants associated with amyotrophic lateral sclerosis. *Hum Mol Genet* (2023) doi:10.1093/hmg/ddad134.
265. Rich, K. A. *et al.* Impaired motor unit recovery and maintenance in a knock-in mouse model of ALS-associated Kif5a variant. *Neurobiol Dis* **182**, 106148 (2023).
266. Duis, J. *et al.* KIF5A mutations cause an infantile onset phenotype including severe myoclonus with evidence of mitochondrial dysfunction. *Ann Neurol* **80**, 633–637 (2016).
267. Rydzanicz, M. *et al.* KIF5A de novo mutation associated with myoclonic seizures and neonatal onset progressive leukoencephalopathy. *Clin Genet* **91**, 769–773 (2017).
268. DaRe, J. T., Vasta, V., Penn, J., Tran, N.-T. B. & Hahn, S. H. Targeted exome sequencing for mitochondrial disorders reveals high genetic heterogeneity. *BMC Med Genet* **14**, 118 (2013).
269. Randall, T. S., Moores, C. & Stephenson, F. A. Delineation of the TRAK binding regions of the Kinesin-1 motor proteins. *FEBS Lett* **587**, 3763–3769 (2013).
270. Pant, D. C. *et al.* ALS-linked KIF5A ΔExon27 mutant causes neuronal toxicity through gain-of-function. *EMBO Rep* **n/a**, e54234 (2022).
271. Riggs, C. L., Kedersha, N., Ivanov, P. & Anderson, P. Mammalian stress granules and P bodies at a glance. *J Cell Sci* **133**, (2020).
272. Kedersha, N. *et al.* Stress granules and processing bodies are dynamically linked sites of mRNP remodeling. *Journal of Cell Biology* **169**, 871–884 (2005).
273. Markmiller, S. *et al.* Context-dependent and disease-specific diversity in protein interactions within stress granules. *Cell* **172**, 590-604.e13 (2018).
274. Van Treeck, B. *et al.* RNA self-assembly contributes to stress granule formation and defining the stress granule transcriptome. *Proceedings of the National Academy of Sciences* **115**, 2734–2739 (2018).
275. Li, Y., Shin, D. & Kwon, S. H. Histone deacetylase 6 plays a role as a distinct regulator of diverse cellular processes. *FEBS Journal* **280**, 775–793 (2013).
276. Kedersha, N. & Anderson, P. Stress granules: sites of mRNA triage that regulate mRNA stability and translatability. *Biochem Soc Trans* **30**, 963–969 (2002).
277. Khong, A. *et al.* The stress granule transcriptome reveals principles of mRNA accumulation in stress granules. *Mol Cell* **68**, 808-820.e5 (2017).
278. Wolozin, B. & Ivanov, P. Stress granules and neurodegeneration. *Nat Rev Neurosci* **20**, 649–666 (2019).

279. Fischer, J. W., Busa, V. F., Shao, Y. & Leung, A. K. L. Structure-mediated RNA decay by UPF1 and G3BP1. *Mol Cell* **78**, 70-84.e6 (2020).
280. Sormanni, P. & Vendruscolo, M. Protein solubility predictions using the CamSol method in the study of protein homeostasis. *Cold Spring Harb Perspect Biol* **11**, (2019).
281. Takahashi, K. *et al.* Induction of pluripotent stem cells from adult human fibroblasts by defined factors. *Cell* **131**, 861–872 (2007).
282. Hu, B.-Y. & Zhang, S.-C. Differentiation of spinal motor neurons from pluripotent human stem cells. *Nat Protoc* **4**, 1295–1304 (2009).
283. Zeng, H. *et al.* Specification of region-specific neurons including forebrain glutamatergic neurons from human induced pluripotent stem cells. *PLoS One* **5**, e11853 (2010).
284. Fernandopulle, M. S. *et al.* Transcription factor-mediated differentiation of human iPSCs into neurons. *Curr Protoc Cell Biol* **79**, e51 (2018).
285. Zhang, Y. *et al.* Rapid single-step induction of functional neurons from human pluripotent stem cells. *Neuron* **78**, 785–798 (2013).
286. Busskamp, V. *et al.* Rapid neurogenesis through transcriptional activation in human stem cells. *Mol Syst Biol* **10**, (2014).
287. Wang, C. *et al.* Scalable production of iPSC-derived human neurons to identify tau-lowering compounds by high-content screening. *Stem Cell Reports* **9**, 1221–1233 (2017).
288. Li, M. *et al.* Optimal promoter usage for lentiviral vector-mediated transduction of cultured central nervous system cells. *J Neurosci Methods* **189**, 56–64 (2010).
289. Norrman, K. *et al.* Quantitative comparison of constitutive promoters in human ES cells. *PLoS One* **5**, e12413 (2010).
290. Qin, J. Y. *et al.* Systematic comparison of constitutive promoters and the doxycycline-inducible promoter. *PLoS One* **5**, e10611 (2010).
291. Restani, L. *et al.* Botulinum neurotoxins A and E undergo retrograde axonal transport in primary motor neurons. *PLoS Pathog* **8**, e1003087 (2012).
292. Matsuzaki, F., Shirane, M., Matsumoto, M. & Nakayama, K. I. Protrudin serves as an adaptor molecule that connects KIF5 and its cargoes in vesicular transport during process formation. *Mol Biol Cell* **22**, 4602–4620 (2011).